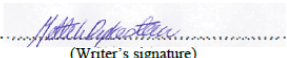




University of
Stavanger

Faculty of Science and Technology

MASTER'S THESIS

Study program/ Specialization: Master in Risk Management Offshore Safety	Spring semester, 2013 Open / Restricted Access
Writer: Mette Kahrs Dykesteen	 (Writer's signature)
Faculty supervisor: Jan Roar Bakke (University of Stavanger)	
External supervisor(s): Kees van Wingerden and Trygve Skjold (GexCon)	
Title of thesis: Re-Visiting the Piper Alpha Accident	
Credits (ECTS): 30 sp	
Key words: FLACS simulation Piper Alpha Accident Gas Explosion Accident Investigation Technical Safety	Pages: 94 + enclosure: 50 Stavanger, 14.06.2013 Date/ year

Abstract

The main objective of this thesis has been to re-visit the Piper Alpha accident using the latest version of the FLACS simulation code. In 1988/89 simulations of the gas explosion in the C Module of Piper Alpha were performed by Jan Roar Bakke and Idar Storvik at Christian Michelsen Institute, in conjunction with the investigation after the accident. For these simulations the computer code FLACS was used [1, 2]. In this thesis, the same simulation cases have been looked into, and the results obtained have then been compared to the results from the previous findings in 1988/89.

The continuous development of computer technology contributes to better and more accurate analysis tools. For assessing the consequences of gas explosions, FLACS is a well known tool. Improvements in the implementation of FLACS have contributed to increasingly more accurate calculations; becoming more and more consistent with practical experiments.

Explosion loads are determined by several factors, among other;

- Geometry
- Obstructions
- Ventilation
- Wind conditions

The new FLACS code allows for a more complex model than the code used for the previous studies, and also for adding effect of wind and ventilation. Therefore, in this thesis the effect of increasing degree of obstruction/congestion and the impact of natural ventilation inside the C Module on the Piper Alpha Platform is discussed. Various scenarios for the leakage dispersion, where leak rate, leak direction and leak position have been varied, are also presented.

A total of 21 cases have been simulated in this thesis. The first 15 scenarios that have been simulated in relation to this thesis, are based on the simulations carried out in 1988/89. Further, 6 new cases are defined based on the first 15 cases, and it is for these last 6 simulations that the effects of wind and leak dispersion has been taken into account.

The sources for modelling the geometry have not been unambiguous in this thesis; the modelling is based on model photographs and exterior photos of the platform.

The continuous development of the FLACS numerical model is illustrated through the first 5 simulation cases in this thesis. For these cases the approximately same geometry model has been generated and used for the same scenarios as those performed in the simulations in 1988/89.

The results for the next 10 simulation cases, 11-20, shows that the generated overpressure for a gas explosion in a partly confined area is dependent on the congestion inside the area, as well as the structure and equipment on the outside, and that increased congestion/obstruction increases the overpressure. The new simulations confirmed the findings from the 1988/89 simulations regarding the gas composition and the size of the gas cloud; condensate gives higher overpressure than natural gas for the same geometry and ignition location, and a gas cloud covering 50% of the volume gives a larger explosion than a gas cloud covering 30% of the volume.

In this thesis, it was also shown that the generated overpressure were higher for ignition near the wall vs. ignition in the centre of the module, for the same cloud composition and dimension.

The 6 last cases illustrates the impact of natural ventilation, leak rate, leak direction and leak position. It was found that a leak rate in the same direction as the natural ventilation at the leakage position inside the module, generated smaller gas clouds than that of a leakage direction in the opposite direction of the natural ventilation. The latter one gave too large gas clouds compared to what was expected.

It was observed that the effect of altering the leakage position by just 0.5 metre in the X-direction had a huge impact on the generated overpressure, and so had the leak rate. An increased leak rate ($2.7 \frac{kg}{s}$ vs. $1.7 \frac{kg}{s}$) led to increased overpressure.

Problem description

Computational fluid dynamics (CFD) is a branch of fluid mechanics that uses numerical methods and algorithms to solve and analyse problems that involve fluid flow, with or without chemical reactions. Many of the hazards encountered in the society, and especially in the process industries, involve accident scenarios where fluid flow in complex, large-scale, three-dimensional (3D) geometries play a key role. FLACS is a specialized CFD toolbox developed especially to address process safety applications such as [3]:

- Dispersion of flammable or toxic gas
- Gas and dust explosions
- Propagation of blast and shock waves
- Pool and jet fires

The thesis shall provide a re-simulation of the Piper Alpha accident that happened on 6th of July 1988. In 1988/89 there was an investigation in relation to the accident, where simulations using FLACS-86 and FLACS-89 were performed by Jan Roar Bakke and Idar Storvik to illustrate the chain of events [1, 2].

The motivation for this project is to see if a newer version of the FLACS code (FLACS v.10.0), a more complex geometry model, and inclusion of wind and dispersion simulations will have an impact on the simulated overpressure and perhaps shed a new light on the exact conditions during the accident. The aim is to compare the results from 1988/89 to the ones obtained in the present thesis, as well as to investigate new simulation cases which are based on the simulation outputs from the re-simulations, and an evaluation of these.

A short comparison of the FLACS versions is presented, and it is shown that both changes in the numerical code in the FLACS versions as well as changes to the model system will have an impact on the simulation output.

The project represents the final work of my Master's degree in Risk Management at the University of Stavanger, and is done in collaboration with GexCon AS.

Acknowledgements

I would like to thank my supervisor at the University of Stavanger, Jan Roar Bakke, and my external supervisors, Kees van Wingerden and Trygve Skjold at GexCon, for giving me the opportunity to write this thesis and for presenting the problem description, as well as providing valuable assistance, guidance and discussions during my work with this thesis.

I would also like to thank Josué Quilliou, Helge Hestetraet and Lars Erling Leirvåg at GexCon AS for valuable inputs for modelling and simulations in FLACS, and Bob Brewerton for providing input regarding anticipated congestion in the C Module.

Contents

Problem description	v
Acknowledgements	vii
1 Introduction	1
1.1 Background and purpose	1
1.2 Previous/ other work	2
1.3 Litterature	2
1.4 Basic Concepts and Definitions	3
1.5 Structure of the report	6
2 Background	9
2.1 The Piper Alpha Accident	9
2.2 Layout of the Piper Alpha Platform	12
2.3 The gas detection system at Piper Alpha	14
3 Theory	15
3.1 Nature of Gas Explosions	15
3.2 The FLACS Codes	18
3.2.1 Development of the FLACS Codes	18
3.2.2 Simulations for gas explosions in FLACS	20
3.2.3 Impacts on explosion simulations	20
4 Scope of Work	25
4.1 Re-simulation of the previous simulated cases	25
4.2 New simulation cases	25
4.2.1 Wind tunnel tests	25
4.3 Hypothesis	26
4.3.1 Impact on results due to new FLACS code	26
4.3.2 Impact on results due to more detailed geometry	27
4.3.3 Impact on results due to ventilation and dispersion	27

5	Simulation Cases	29
5.1	Simulation cases 1-20	29
5.2	Input for the simulation cases	33
5.2.1	Location of ignition point	35
5.2.2	Gas cloud location	37
5.3	Simulation cases 21-26	38
5.3.1	Input for the simulation cases 21-26	39
6	Results and Discussion	43
6.1	Simulation Results and Observations	43
6.2	Impact of changes in the FLACS code	44
6.3	Effect of geometry and structure	47
6.4	Effect of the location of ignition point	51
6.5	Effect of gas cloud composition and dimension	52
6.6	Peak pressure	54
6.7	The firewalls	54
6.8	Discussion of the new simulation cases	56
6.8.1	Ventilation scenario	57
6.8.2	Dispersion scenario	57
6.8.3	Explosion scenario	65
6.8.4	Peak pressure new cases	70
6.8.5	Firewalls	70
7	Conclusion and Recommendations	75
7.1	Conclusion	75
7.2	Future work	77
A	Limitations and assumptions	79
B	Model pictures	81
C	Simulation output	85
C.1	Pressure plots	85
C.2	Gas cloud sizes	101
C.2.1	Dispersion	101
C.2.2	Explosion	103
C.3	Gas detector readings	117
C.4	Firewalls	122
	Bibliography	127

List of Figures

2.1	<i>The Piper Alpha Platform before the accident [4].</i>	9
2.2	<i>The Piper Alpha Platform after the accident [5].</i>	11
2.3	<i>The Piper Alpha Platform as seen from east and west side [6].</i>	12
2.4	<i>Generated FLACS model for the production deck at Piper Alpha.</i>	13
3.1	<i>Event tree showing typical consequences of accidental releases of combustible gas or evaporating liquid into the atmosphere. Illustration from the Gas Explosion Handbook [7].</i>	15
3.2	<i>Positive feedback loop causing flame acceleration due to turbulence. Illustration from the Gas Explosion Handbook [7].</i>	17
3.3	<i>Turbulence generation in a channel due to repeated obstacles during a gas explosion. Illustration from [7].</i>	21
5.1	<i>Model picture of the old geometry of the C Module used for simulation cases 1-5.</i>	30
5.2	<i>Model picture of the simplified geometry of the C Module used for simulation cases 6-10. Right side wall (B/C) and roof removed for illustration.</i>	31
5.3	<i>Model picture of the detailed geometry of the C Module used for simulation cases 11-15. Right side wall (B/C) and roof removed for illustration.</i>	31
5.4	<i>Model picture of the geometry of the whole platform used for simulation cases 16-26.</i>	32
5.5	<i>Location of monitor points for simulation cases 6-26.</i>	33
5.6	<i>Location of ignition point for the simulation cases 1, 4, 6, 9, 11, 14, 16 and 19.</i>	36
5.7	<i>Location of ignition point for the simulation cases 2, 3, 7, 8, 12, 13, 17 and 18.</i>	36
5.8	<i>Location of ignition point for the simulation cases 5, 10, 15 and 20.</i>	37
5.9	<i>Gas cloud location and extension for the simulation cases 1-3, 6-8, 11-13 and 16-18.</i>	37
5.10	<i>Gas cloud location and extension for the simulation cases 4, 9, 14 and 19.</i>	38

5.11	<i>Gas cloud location and extension for the simulation cases 5, 10, 15 and 20.</i>	38
5.12	<i>Figure showing the position of the first leak source (010701, 010702, 010704 and 010705). The illustration also shows the size of the gas cloud at the time of ignition (after a 40 seconds release) for 010701.</i>	40
5.13	<i>Figure showing the position of the second leak source (010703 and 010706). The illustration also shows the size of the gas cloud at the time of ignition (after a 40 seconds release) for 010706.</i>	41
6.1	<i>Maximum pressures at Monitor Points 1-8 for the simplified geometry of the C Module (See Simulation case 10 in Table 5.2)</i>	46
6.2	<i>Maximum pressures at Monitor Points 1-8 for the detailed geometry of the C Module (See Simulation case 15 in Table 5.2)</i>	49
6.3	<i>Maximum pressures at Monitor Points 1-8 for the geometry of the whole platform (See Simulation case 20 in Table 5.2)</i>	50
6.4	<i>Explosion pressure for natural gas, propane and methane in air. Illustration from Gas Explosion Handbook [7].</i>	53
6.5	<i>Panel porosity for simulation case 10.</i>	55
6.6	<i>Panel porosity for simulation case 15.</i>	55
6.7	<i>Panel porosity for simulation case 20.</i>	56
6.8	<i>Flow pattern inside the C Module which illustrates the ventilation due to added wind, after 60 seconds.</i>	57
6.9	<i>Illustration of the gas cloud that sinks to the floor with a flow in the positive Z-direction.</i>	58
6.10	<i>Illustration of the gas cloud generated after 40 seconds of leakage, for a leak direction in the negative Z-direction, positive Z-direction and negative Z-direction for respectively upper left, upper right and bottom left illustrations.</i>	59
6.11	<i>Vector gradient for the leakage in simulation case 010701 after 40 seconds.</i>	60
6.12	<i>Vector gradient for the leakage in simulation case 010706 after 40 seconds.</i>	61
6.13	<i>The generated gas cloud after 40 seconds of leakage for dispersion simulation case 010706. Illustrates the amount of fuel within its flammable range (LFL and UFL).</i>	62
6.14	<i>Evolution of the cloud size.</i>	63
6.15	<i>Simulation case 010701. Left side: Gas detector pattern for the alarms in the C Module, right side: Gas detector pattern for the alarms in zone C3.</i>	64
6.16	<i>Simulation case 010701. Left side: Gas detector pattern for the alarms in zone C4, lower right side: Gas detector pattern for the alarms in zone C5.</i>	64
6.17	<i>The generated gas cloud after 40 seconds of leakage for dispersion simulation case 010701. Illustrates the amount of fuel within its flammable range (LFL and UFL).</i>	66

6.18	<i>Figure illustrating the gas cloud for simulation case 010701 with time after ignition. The amount of fuel within its flammable range (LFL and UFL) is decreasing with time.</i>	67
6.19	<i>Maximum pressures at Monitor Points 1-8 for the new simulation cases. The last case did not result in an ignition. (See Simulation cases 21-26 in Table 5.6).</i>	69
6.20	<i>Panel porosity for simulation case 21 (See Table 5.6.)</i>	70
6.21	<i>Ignition region, gas cloud size and richness for simulation case 26 at the time of ignition.</i>	72
B.1	<i>The gas detectors and zones in the C Module. Illustration taken from the Cullen report [8].</i>	81
B.2	<i>Plan view of the production deck at the Piper Alpha Platform. Illustration taken from the Cullen report [8].</i>	82
B.3	<i>Location of gas detector monitor points for the dispersion simulation cases.</i>	83
B.4	<i>Location of the C/B and C/D firewalls.</i>	83
C.1	<i>Maximum pressures at Monitor Points 1-8 for the simplified geometry of the C Module for simulation cases 6 and 7 (See Simulation cases 6-10 in Table 5.2)</i>	86
C.2	<i>Maximum pressures at Monitor Points 1-8 for the simplified geometry of the C Module for simulation cases 8 and 9 (See Simulation cases 6-10 in Table 5.2)</i>	87
C.3	<i>Maximum pressures at Monitor Points 1-8 for the detailed geometry of the C Module for simulation cases 11 and 12 (See Simulation cases 11-15 in Table 5.2)</i>	89
C.4	<i>Maximum pressures at Monitor Points 1-8 for the detailed geometry of the C Module for simulation cases 13 and 14 (See Simulation cases 11-15 in Table 5.2)</i>	90
C.5	<i>Maximum pressures at Monitor Points 1-8 for the geometry of the whole platform for simulation cases 16 and 17 (See Simulation cases 16-20 in Table 5.2)</i>	92
C.6	<i>Maximum pressures at Monitor Points 1-8 for the geometry of the whole platform for simulation cases 18 and 19 (See Simulation cases 16-20 in Table 5.2)</i>	93
C.7	<i>Maximum pressures at Monitor Points 1-8 for simulation case 21 (Table 5.6).</i>	95
C.8	<i>Maximum pressures at Monitor Points 1-8 for simulation case 22 (Table 5.6).</i>	96
C.9	<i>Maximum pressures at Monitor Points 1-8 for simulation case 23 (Table 5.6).</i>	97
C.10	<i>Maximum pressures at Monitor Points 1-8 for simulation case 24 (Table 5.6).</i>	98
C.11	<i>Maximum pressures at Monitor Points 1-8 for simulation case 25 (Table 5.6).</i>	99

C.12	<i>The gas cloud generation for dispersion simulation case 010704 at 4 different time steps.</i>	101
C.13	<i>Vector gradient for the leakage in simulation case 010702 after 40 seconds.</i>	102
C.14	<i>Vector gradient for the leakage in simulation case 010703 after 40 seconds.</i>	102
C.15	<i>Vector gradient for the leakage in simulation case 010704 after 40 seconds.</i>	103
C.16	<i>Vector gradient for the leakage in simulation case 010705 after 40 seconds.</i>	103
C.17	<i>Generated gas cloud at 4 different time steps for simulation case 16 (Table 5.2).</i>	105
C.18	<i>Generated gas cloud at 4 different time steps for simulation case 16 (Table 5.2).</i>	106
C.19	<i>Generated gas cloud at 4 different time steps for simulation case 18 (Table 5.2).</i>	107
C.20	<i>Generated gas cloud at 4 different time steps for simulation case 19 (Table 5.2).</i>	108
C.21	<i>Generated gas cloud at 4 different time steps for simulation case 20 (Table 5.2).</i>	109
C.22	<i>Generated gas cloud at time of ignition for simulation cases 21-25 (Table 5.6).</i>	111
C.23	<i>Generated gas cloud at time of ignition for simulation cases 26 (Table 5.6).</i>	112
C.24	<i>Generated gas cloud at 4 different time steps for simulation case 22 (Table 5.6).</i>	113
C.25	<i>Generated gas cloud at 4 different time steps for simulation case 23 (Table 5.6).</i>	114
C.26	<i>Generated gas cloud at 4 different time steps for simulation case 24 (Table 5.6).</i>	115
C.27	<i>Generated gas cloud at 4 different time steps for simulation case 25 (Table 5.6).</i>	116
C.28	<i>Simulation case 010702. Left side: Gas detector pattern for the alarms in the C Module, right side: Gas detector pattern for the alarms in zone C3.</i>	117
C.29	<i>Simulation case 010702. Left side: Gas detector pattern for the alarms in zone C4, lower right side: Gas detector pattern for the alarms in zone C5.</i>	117
C.30	<i>Simulation case 010703. Left side: Gas detector pattern for the alarms in the C Module, right side: Gas detector pattern for the alarms in zone C3.</i>	118
C.31	<i>Simulation case 010703. Left side: Gas detector pattern for the alarms in zone C4, lower right side: Gas detector pattern for the alarms in zone C5.</i>	118

C.32	<i>Simulation case 010704. Left side: Gas detector pattern for the alarms in the C Module, right side: Gas detector pattern for the alarms in zone C3.</i>	119
C.33	<i>Simulation case 010704. Left side: Gas detector pattern for the alarms in zone C4, lower right side: Gas detector pattern for the alarms in zone C5.</i>	119
C.34	<i>Simulation case 010705. Left side: Gas detector pattern for the alarms in the C Module, right side: Gas detector pattern for the alarms in zone C3.</i>	120
C.35	<i>Simulation case 010705. Left side: Gas detector pattern for the alarms in zone C4, lower right side: Gas detector pattern for the alarms in zone C5.</i>	120
C.36	<i>Simulation case 010706. Left side: Gas detector pattern for the alarms in the C Module, right side: Gas detector pattern for the alarms in zone C3.</i>	121
C.37	<i>Simulation case 010706. Left side: Gas detector pattern for the alarms in zone C4, lower right side: Gas detector pattern for the alarms in zone C5.</i>	121
C.38	<i>Panel porosity for simulation cases 6 and 7.</i>	122
C.39	<i>Panel porosity for simulation cases 8 and 9.</i>	122
C.40	<i>Panel porosity for simulation cases 11 and 12.</i>	123
C.41	<i>Panel porosity for simulation cases 13 and 14.</i>	123
C.42	<i>Panel porosity for simulation cases 16 and 17.</i>	124
C.43	<i>Panel porosity for simulation cases 18 and 19.</i>	124
C.44	<i>Panel porosity for simulation case 22.</i>	125
C.45	<i>Panel porosity for simulation case 23.</i>	125
C.46	<i>Panel porosity for simulation case 24.</i>	126
C.47	<i>Panel porosity for simulation case 25.</i>	126

List of Tables

5.1	<i>Coordinates of the C Module position in the FLACS geometry model, and the simulation volume used for the simulation cases 16-26.</i>	29
5.2	<i>Input for the simulation cases 1-20.</i>	34
5.3	<i>Gas cloud compositions (volume %).</i>	35
5.4	<i>Ignition source locations for simulation cases 1-20.</i>	35
5.5	<i>Leak positions for the dispersion simulation cases 010701-010706.</i> . .	39
5.6	<i>Input for the dispersion simulations.</i>	40
5.7	<i>Gas cloud compositions (volume %).</i>	41
5.8	<i>Ignition source locations for the simulation cases 21-26.</i>	41
6.1	<i>Maximum pressures at Monitor Points 1-8 for the simulation cases 1-10 (Table 5.2 in Chapter 5). [1, 2]</i>	44
6.2	<i>Maximum pressures at Monitor Points 1-8 for the simulation cases 11-20 (Table 5.2 in Chapter 5).</i>	47
6.3	<i>The impact of ignition source location illustrated by the simulation cases 16 and 17 (See Table 5.2 and 5.4, Chapter 5).</i>	51
6.4	<i>The impact of gas cloud dimension illustrated by the simulation cases 16 and 19 (See Table 5.2, Chapter 5).</i>	52
6.5	<i>The impact of gas cloud composition illustrated by the simulation cases 17 and 18 (See Table 5.2 and 5.3, Chapter 5).</i>	53
6.6	<i>Time for peak pressures (approximately) for the simulation cases 1-20 (Table 5.2 in Chapter 5).</i>	54
6.7	<i>Maximum pressures at Monitor Points 1-8 for the simulation cases 21-25 (Table 5.6 in Chapter 5).</i>	68
6.8	<i>Time after ignition for peak pressures (approximately) for the simulation cases 21-26 (Table 5.6 in Chapter 5).</i>	70

Chapter 1

Introduction

On the night of July 6, 1988 at around 10 o'clock pm, an explosion occurred in the C Module on the production deck of Piper Alpha. The platform was located about 200 km north-east of Aberdeen. 167 out of 228 men died in the explosions and following fire [9]. There was an investigation of the initial explosion that occurred on the Piper Alpha platform, and simulations of the explosion were performed in FLACS in 1988/89 to predict the overpressure that might have been generated by the initial explosion in the C Module [1, 2, 8].

This thesis describes the work done, and the results obtained, from performing a re-simulation of the accidental gas explosion. Emphasis is put on the impact of a good representation of the geometry and realistic conditions on explosion loads. In Chapter 5.3, 6 new cases are defined based on the re-simulations of the cases from 1988/89 [1, 2]. In the latter cases, the effects of wind and leak dispersion are also evaluated.

This chapter contains general information on the background of the thesis, previous work that has been performed and the literature study for this thesis. Limitations and assumptions for the project are given in Appendix A.

1.1 Background and purpose

During the investigation of the Piper Alpha accident in 1988/89, simulations to predict the generated overpressure during the explosion were performed. The parameter inputs were based on witness statements, photographs from the accident, and testimonies from the trial. The simulations from 1988/89 simulated possible scenarios as an aid to the investigation after the accident [1, 2]. The simulations were used as supporting evidence in the inquiry.

The main goal of this thesis is to perform a re-simulation of the scenarios simulated in 1988/89. The results of these re-simulations will then serve as a basis for new realistic scenarios to be simulated, to see if these can better illustrate the accident on Piper Alpha at 6th of July 1988.

The following factors are considered:

- New version of the FLACS numerical code
- Natural ventilation inside the C Module
- More details in the geometry model
- More experience on the field of gas explosions

The Cullen report [8] is a report from the public inquiry of the Piper Alpha accident. In this report it is concluded that the most likely scenario for the leakage, and the following explosions and fire, is that it started in the C Module from a blind flange on Condensate Pump A.

The motivation for re-simulating the previous simulated cases with the simplified geometry, is to have a basis for discussion of the effect of a more complex geometry as well as to address some of the differences between the FLACS codes. For the simulation cases in 1988, FLACS-86 was used, and for the simulations in 1989 a modified FLACS code was used (FLACS-89) [1, 2]. In this thesis the differences between the FLACS codes are referred to as differences between the FLACS-86 and FLACS v10.0 codes. Reusing the results obtained in 1988/89 as the foundation for evaluating the impact of added details in the geometry would have illustrated the point, but by re-doing the cases a better foundation is established.

1.2 Previous/ other work

In 1993 new simulations were performed to predict the overpressure that might have been generated by the initial explosion in Module C. This simulation was performed by Jan Roar Bakke on behalf of Paull & Williamsons, Solicitors [10].

Wind tunnel tests conducted by BMT Fluid Mechanics Ltd., at their wind tunnel at Teddington, were performed in relation to the investigation after the accident [8].

1.3 Litterature

For this thesis, emphasis is put on the following litterature:

- The Public Inquiry into the Piper Alpha Disaster [8]
- Simulation of Gas Explosions in Module C, Piper Alpha [1]
- Gas Explosion Simulation in Piper Alpha Module C using FLACS [2]

and the following course litterature:

- Gas Explosion Handbook [7]
- FLACS User's Manual [3]

Other inputs to form a picture of the layout of the Piper Alpha and the explosion effects have been the book "Fire in the Night - The Piper Alpha Disaster" and relevant articles [11, 12, 13, 14, 15].

The Piper Alpha Documentary part 1 and 2 [16, 17], and various input from my supervisors have also been important input to better understand the extent of the accident.

The course 'Technical Safety' at the University of Stavanger, and the FLACS user course held at GexCon in February 2013 have been important for understanding the theory and for the correct use of FLACS simulation code.

The main limitation in this study has been the background information. The geometry modelling is based on model photographs, little exact information was available in the form of e.g. drawings. The conclusions made in the Cullen report, regarding the gas detector alarms, the pressure from the explosion among others are based on witness observations [8].

1.4 Basic Concepts and Definitions

This appendix contains a list of selected basic concepts and definitions used in the thesis.

Blast or Blast wave This is the rapid change in air pressure that propagates away from the region of an explosion. A sharp jump in pressure is known as a shock wave and a slow rise is known as a compression wave. Weak pressure waves propagate with the speed of sound and shock waves always travel supersonically, faster than the speed of sound. A blast wave is produced by an explosion because the explosive event displaces the surrounding air rapidly [18]

Burning rate The amount of fuel consumed by the combustion process per unit time [7]

Burning velocity Velocity of the flame front with respect to the unburned gas immediately ahead of the flame [7]

Burning speed This is the speed with which a smooth (laminar) flame advances into a stationary mixture of reactants. Burning speeds in hydrocarbon fuels mixed with air are typically less than $0.5 \frac{m}{s}$. The burning speed is a function of the concentration of the fuel, temperature, and pressure of the mixture [18]

Combustion The burning of gas, liquid, or solid in which fuel is oxidized, involves heat release and often light emission [7]

Confined gas explosion Explosion within tanks, process equipment, pipes, closed rooms etc. [7]

Congestion The amount and location of equipment and structure [7]

Deflagration This is a propagating flame that moves sub-sonically (the flame speed is less than the speed of sound) in a mixture of fuel and oxidizer [18]

Detonation This is a supersonic combustion wave. Detonations in gases propagate with velocities that range from 5 to 7 times the speed of sound in the reactants. For hydrocarbon fuels in air, the detonation velocity can be up to $1800 \frac{m}{s}$. The ideal detonation speed, known as the Chapman-Jouguet velocity, is a function of the reactant composition, initial temperature and pressure [18]

Explosion There is no fixed definition of an explosion. Events that are described as explosions include a rupturing water boiler, a flash of light created by an electrical short circuit, detonation of a high explosive, deflagration of a tank containing an explosive fuel-air mixture, or the shock wave, fireball, and debris cloud produced by a thermonuclear detonation [18]. An explosion could be defined as an event leading to a rapid increase of pressure. [7]

Equivalence ratio Ratio of fuel to oxidizer divided by the same ratio at stoichiometric conditions [18]

Expansion ratio Ratio of burned gas volume to initial volume for a low-speed (constant pressure) flame. Expansion is responsible for flame-induced flow [18]

Fire This is a flame that is produced over a stationary fuel source such as a liquid hydrocarbon pool or solid such as wood [18]

Flame This is a thin zone of combustion in which diffusion plays a dominant role. Flames in hydrocarbon fuels and air are less than 0.1 mm thick for stoichiometric mixtures [18]

Flame acceleration Rapid increase in flame speed due to generation of large and small eddies - turbulence - as flow ahead of flame passes over objects or through orifices [18]

Flame speed This is the speed with which a flame, possibly turbulent, appears to move relative to a stationary observer. The flame speed can be much larger than the burning velocity due to expansion of the combustion products, instability, and turbulent deformation of the flame. Flame speeds of $10-100 \frac{m}{s}$ are commonly observed for hydrocarbon-air mixtures and it is possible under exceptional circumstances to have speeds up to $1000 \frac{m}{s}$ [18]

Flammability A fuel-air mixture is flammable when combustion can be started by an ignition source. The main fact is the proportions or composition of the fuel-air mixture. A mixture that has less than a critical amount of fuel, known as the Lean or Lower Flammability Limit (LFL), or greater than a critical amount of fuel, known as the rich or Upper Flammability Limit (UFL), will not be flammable. Flammability limits are not absolute, but depend on the type and strength of the ignition source. Studies on flammability limits of

hydrocarbon fuels have shown that the stronger the source of the ignition stimulus, the leaner the mixture that can be ignited. Flammability limits also depend on the type of atmosphere (for example, limits are much wider in oxygen than in air), the pressure, and the temperature of atmosphere [18]

Flammability limits Flammability limits refer to the range of compositions, for fixed temperature and pressure, within which an explosive reaction is possible when an external ignition source is introduced. This can happen even when the mixture is cold [18]

Fuel-air mass ratio This is the ratio of the mass of fuel to the mass of air in the reactants. The fuel-air ratio is a method of measuring the composition of a potentially flammable mixture [18]

Lean mixture This is a mixture containing less than the stoichiometric amount of fuel, equivalence ratio less than unity. Combustion of a lean mixture will result in excess oxidizer remaining in the products [18]

Gas explosion A process where combustion of a premixed gas cloud, i.e., fuel-air or fuel/ oxidizer is causing a rapid increase of pressure [7]

MOL Main Oil Line

Minimum Ignition Energy This is the lowest possible energy that will result in the ignition of a flammable mixture by an electrical discharge. The minimum ignition energy depends on the composition of the mixture [18]

Overpressure This is the pressure in excess of the ambient value that is created by the explosion process. The peak overpressure associated with deflagrations inside closed vessels can be as high as 10 times the initial pressure [18]

Partly confined gas explosion Occurs when a fuel is accidentally released, mixed with air and ignited inside a building which is partly open [7]

Pressure Stress which is exerted uniformly in all directions [7]

PSV Pressure Safety Valve

PTW Permit to Work

Rich mixture This is a mixture containing more than the stoichiometric amount of fuel, equivalence ratio greater than unity. Combustion of a rich mixture will result in partial oxidation of the fuel and the products will contain, in addition to CO_2 and C_2O , H_2 and CO for hydrocarbon fuels [18]

Sonic point The point at which the flow velocity is equal to the speed of sound. When this is applied to detonations, the velocity is computed relative to leading shock front. The elementary Chapman-Jouguet condition is that the sonic point occurs at the end of the reaction zone when the products are in equilibrium [18]

Stoichiometric composition The stoichiometric composition is defined as the composition where the amounts of fuel and oxygen (air) are in balance so that there is no excess of fuel or oxygen after the chemical reaction has been completed [7]

Stoichiometric ratio The proportions of fuel and oxidizer that will result in optimal combustion are known as a stoichiometric ratio. [18]

Turbulence Turbulent flow is characterized by an irregular random fluctuation imposed on mean flow velocity [7]

1.5 Structure of the report

The simulations presented in this thesis are based on the leakage that according to the Cullen report occurred in the C Module. A model of the C Module is reconstructed in FLACS v10.0, as similar as possible to the one used for the simulations in 1988/89. The modelling is based on photographs of the model used among other things for the wind tunnel tests [6].

It is important to emphasise that all of the modelling work in this thesis is not based on detailed drawings, but based on interpretation of model photographs of the 4 modules, and pictures and videos of the whole platform. No details for the structure and smaller equipment on the platform have been given. The available drawings only illustrate the placement of the main equipment. To represent the smaller equipment inside the modules (piping, cable gates, structure etc.) the present work has assumed an anticipated congestion. The anticipated congestion is based on inputs from drawings, P&ID's (Piping and Instrumentation Diagram), equipment lists, MTO (Material Take Off) lists etc., and also on experience from previous work and discussions among engineers with different academic background.

The model used in 1988/89 for the simulation purposes is shown in Fig. 5.1. Based on this picture, a geometry model has been reconstructed for the simulation cases 6-10, and more details are implemented on this model for the simulation cases 11-20. The simulation cases are presented in Chapter 5.

The work in this project has primarily consisted of the following activities:

Background Chapter 2 presents a short summary of the accident at Piper Alpha, including the layout of the platform and the observed pattern for the gas detector alarms.

Theory Chapter 3 gives a short introduction to the nature of gas explosions, the FLACS code and main parameters that influence the simulated overpressure of a gas explosion

Scope of Work In Chapter 4 a presentation of the work that has been performed in this thesis is given. Hypothesis for what can be expected to be observed from the new simulations are also presented.

Simulation Cases Chapter 5 presents the simulation cases for this thesis, and the modelling pictures of the geometry models.

Results and Discussion In Chapter 6 the results from the simulations and a discussion of these are presented.

Conclusion and Recommendations Chapter 7 summarizes the main conclusions from the re-simulations and from the new simulation cases, and presents a brief introduction to future work in relation to the new simulation cases.

Appendix The appendices include limitations and assumptions for this thesis, model pictures and additional simulation outputs.

Chapter 2

Background

In this chapter a short introduction to the accident, in addition to the layout of the platform and the gas detection system is given [8, 19, 20].

2.1 The Piper Alpha Accident

The Piper Alpha Platform was owned by Occidental Petroleum, and located about 200 km north-east of Aberdeen. It was originally built as an oil production platform, and started the production at the end of 1976. At a later time it was rebuilt to produce gas as well [9].



Figure 2.1: *The Piper Alpha Platform before the accident [4].*

In the days leading up to the accident, maintenance work was carried out at the platform. Occidental planned to carry out major construction, maintenance and upgrade works in the late '80s, and this was a part of that effort. On the morning of July 6, a permit to work (PTW) on the pressure safety valve (PSV) 504 on condensate pump A in the C Module was carried out (Fig. B.2). By the end of the day shift, the work had not been finished and the PSV was replaced by a

blind flange, only tightened by hand. This was noted on the PTW. The location of the valve, about 4.5-6 meters above the floor of the C Module, was different from the pump, and scaffolding was needed for the work to be performed. This made it difficult to see that the flange had been removed.

At about 21:45, on the night shift, condensate pump B tripped. This was caused by a blockage in the gas compression system pipework due to accumulation of hydrates, which they had experienced problems with earlier that day. Repeated attempts to restart pump B failed, and the operators only had a few minutes to decide what to do; if the system was stopped for a longer period the power supply would fail.

At handover from day to night shift, no oral message that pump A was out of operation was given, and the PTW was not physically delivered to the shift supervisor, instead it was placed on a desk in the control room, from where it later disappeared. The PTWs were checked, but the PTW for the PSV 504 was not found. The only PTW for pump A that was found, was one regarding general overhaul which had not yet begun. It was therefore decided to try to start pump A.

At 21:55 condensate pump A was switched on, and for this the operator had to push the button twice. At the first push, within a second or two, the condensate was forced into the pipeline and up towards the blind flange. The steel bolts on the flange were not tight enough to withstand the overpressure due to the moving condensate, and gas leaked out at a high pressure. Six gas alarms were triggered, including the high level gas alarm, see Chapter 2.3.

The mixture that was created from the leakage was flammable, and came in contact with an ignition source. Most likely an electro-static spark. The release of liquid condensate under pressure produced an electrostatic charged jet of liquid droplets, and the cloud was ignited in seconds. The initial explosion was on the production deck which hosted 4 modules; Modules A-D, (see Chapter 2.2 and Fig. 2.4).

The explosion was characterized as an explosion of a cloud of flammable gas, shortly followed by a major fire in the B Module. One of the witnesses described the smoke and flames coming from the west face south of the crane pedestal. First, it was a grey smoke issuing from the west end of C Module, and then a few seconds later a thick black smoke and large flames coming out of the west end of B Module. Another witness described a vapour mist, orange with a hint of pink, which could be seen just to the right of the crane pedestal. The mist persisted for a few seconds, before an explosion was heard, and flames were blown by the wind northwards and upwards, giving it an oval appearance.

During the explosion, most of the emergency systems failed, including the fire water system. The fire fighting system on Piper Alpha was automatic, and was driven by both diesel and electric pumps. On the night of the disaster the system had been set to manual due to diving operations, which was normal procedure whenever divers were in the water. During the initial explosion, the electric pumps were destroyed.

Both Tartan and the Claymore platforms continued to feed the Piper Alpha

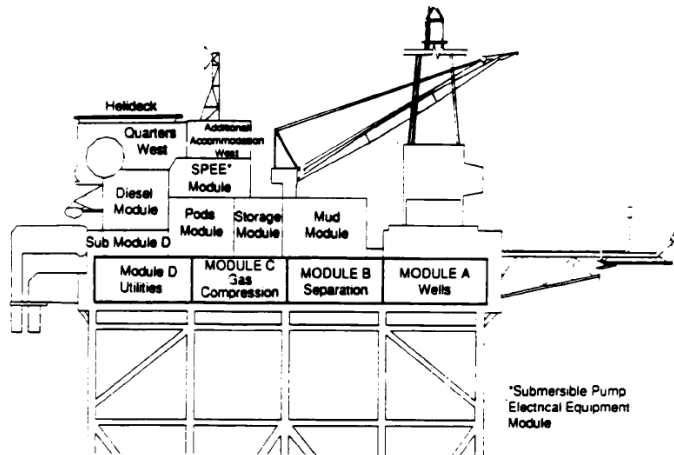
platform with oil after the initial explosion. If it had not been for this, the fire would have burned out.

About 2 hours after the initial explosion, the Piper Alpha platform was completely destroyed.

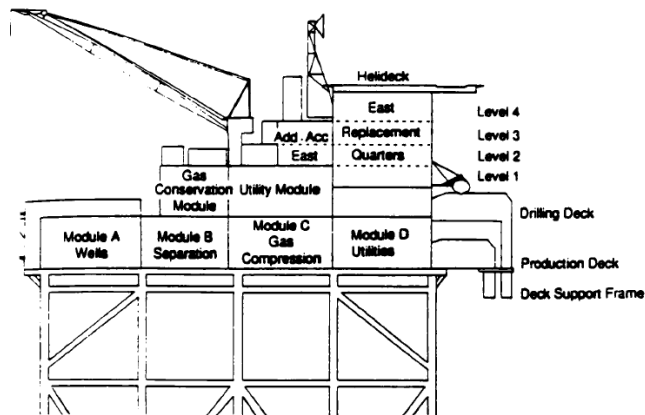


Figure 2.2: *The Piper Alpha Platform after the accident [5].*

2.2 Layout of the Piper Alpha Platform



The Piper Alpha platform: west elevation (simplified).



The Piper Alpha platform: east elevation (simplified).

Figure 2.3: *The Piper Alpha Platform as seen from east and west side [6].*

Fig. 2.4 shows the generated FLACS model of the production deck, as based on model photographs, drawings and included anticipated congestion [6].

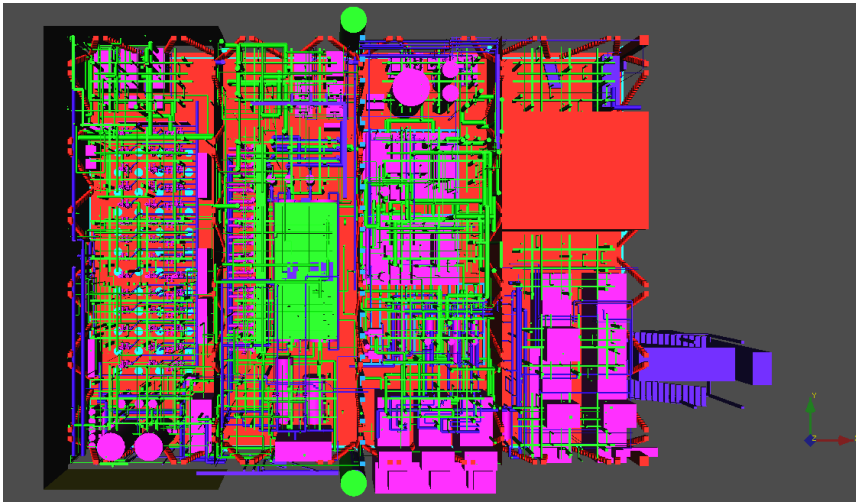


Figure 2.4: *Generated FLACS model for the production deck at Piper Alpha.*

The platform was orientated 43 degrees counter-clockwise from true north, and was anchored to the seabed by four corner legs. The production level was situated at 84 ft level (25.6 m), and consisted of four modules; A, B, C and D.

Module A was the well head module. It was located at the south end of the platform, and it contained well heads, water injection system, de-oxygenation towers and booster pumps. Its floor was on the 84 ft level and its roof at the 107 ft level (32.6 m).

Module B was the production module hosting the two main production separators. These were located in the centre of the module. It also contained four main oil line (MOL) pumps at the west end of the module, a test separator to the east of the production separators, and four gas coolers.

Module C was the gas compression module where some of the gas processing took place. It consisted of three centrifugal compressors in the eastern end. The ventilation intakes were also located on the eastern face, and the ventilation air was drawn in outside the east face of Module C towards the south side of the compressor. A gas detector on one of the centrifugal compressors would not trip the compressor if it only detected enough gas for a low alarm but would trip if the gas level reached the level required for a high alarm. It also hosted the centrifugal compressor skid, fresh-water pumps and coolers, fresh-water circulating system, and two reciprocating compressors.

Module D was the power generation and utilities module and contained the control room, the main generators, the switchgear and other utility systems.

Both the western and the eastern ends of Modules A, B and C were open. The opening at the east end of Module C was restricted by the centrifugal compressors, see Fig. 5.3. These open ends allowed access for personnel and also natural ventilation of the modules. The south face of Module A was also open, and so was the east and eastern half of the north face of Module D. Modules A, B, C and D were

each divided by firewalls. During the explosion the C/D firewall suffered severe damage towards the east and centre of the module, but the sections of both the B/C and C/D firewalls at the extreme west end apparently survived.

All of the modules were approximately the same dimension; 15m wide, 7.5m high and 45.5m long.

2.3 The gas detection system at Piper Alpha

Main hydrocarbon fuels at Piper Alpha were oil, gas and condensate. In the C Module there was methane and condensate (propane). For detection of methane gas leaks, gas detectors were installed in the roof of the module, and only one detector was placed at floor level. This detector was placed in the east end of the module. The gas leak at Piper Alpha came from condensate, which has a higher density than air. Because of the higher density, the condensate will first sink and cover the floor.

The location of gas alarms in C Module is shown in Fig. B.1 in Appendix B. All the detectors pointed downwards. The C Module was divided into 5 zones; C1 (west of module), C2 (east of module), C3, C4 and C5 (latter three were related to the centrifugal compressor compartments).

Witness observations indicated that the first alarm to be set off was the low level gas alarm in C Module, on C centrifugal compressor (zone C3). A further set of gas alarms followed; 3 low gas and 1 high gas. The 3 low gas alarms were for C Module East (zone C2) and for A and B centrifugal compressors (Zones C5 and C4); the high gas alarm was for one of the centrifugal compressors.

Chapter 3

Theory

3.1 Nature of Gas Explosions¹

Combustion of a gaseous fuel in air can occur in two different modes; one is the fire, where fuel and oxygen is mixed during the combustion process, and for the other case the fuel and air (or another oxidizer) is premixed. For the premixed case the fuel concentration must be within the flammability limits. In general, the premixed situation allows the fuel to burn faster, i.e. more fuel is consumed per unit time.

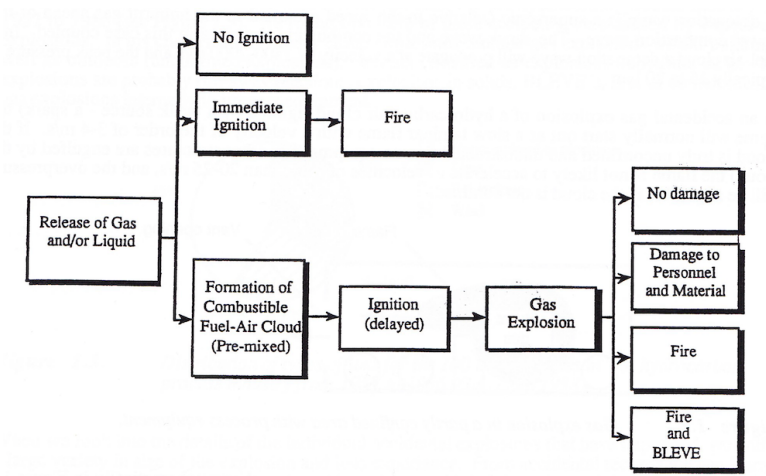


Figure 3.1: *Event tree showing typical consequences of accidental releases of combustible gas or evaporating liquid into the atmosphere. Illustration from the Gas Explosion Handbook [7].*

¹The information given in this section is based on The Gas Explosion Handbook [7]

Fig. 3.1 shows what can happen if combustible gas or evaporating liquid is accidentally released into the atmosphere. If the gas cloud is within the flammability limits and there is an ignition source, it may ignite. Ignition is dependent on the energy of the ignition source, fuel concentration and fuel type.

In case of an immediate ignition, a fire will develop, as shown in Fig. 3.1. If a large flammable premixed fuel-air cloud is formed and ignites, a serious explosion may result. A premixed fuel-air mixture will only burn as long as the fuel concentration is between Upper Flammability Level (UFL) and Lower Flammability Level (LFL).

With a strong ignition source, the gas cloud will be ignited when the edge of the cloud reaches the ignition source. If the ignition source is weak, however, the source may fail to ignite the cloud in the early phase of the dispersion process or ignite only a small part of the cloud. The time from release start to ignition can be from a few seconds and up to tens of minutes.

When a cloud is ignited the flame can propagate in two different modes through the flammable parts of the cloud; deflagration or detonation. The most common of these is the deflagration mode where the burning velocity typically is in the order of 1 to $1000 \frac{m}{s}$. For a detonation wave the burning velocity will be in the order of $1500-2000 \frac{m}{s}$.

For a deflagration wave, both the flame speed and the explosion pressure will strongly depend on the gas cloud size and the location of the ignition source as well as the geometrical conditions (congestion and confinement) within the cloud. Two mechanisms are governing the pressure build-up in partly confined gas clouds for deflagration;

- Flame acceleration due to enhanced burning due to turbulence generated by flow past obstacles
- Venting providing pressure relief or reducing the effect of the feedback mechanism

The feedback mechanism is illustrated by Fig. 3.2. The two mechanisms have competing effects; while the first one will increase the explosion pressure, the latter one will reduce the pressure. In most accidental explosions a combination of these two effects determines the pressure build-up.

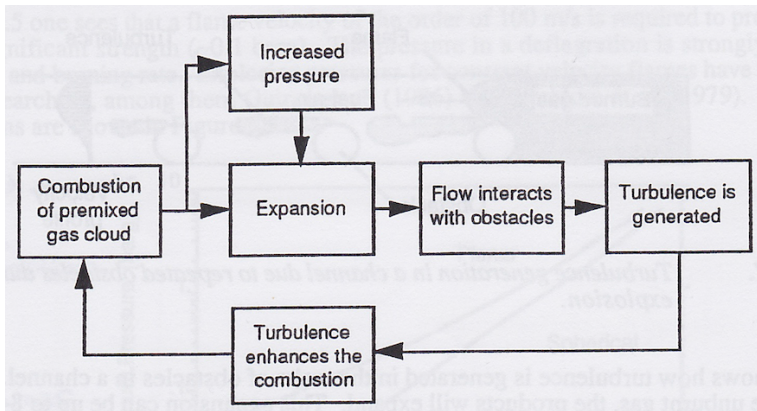


Figure 3.2: *Positive feedback loop causing flame acceleration due to turbulence. Illustration from the Gas Explosion Handbook [7].*

In an accident situation the combustible gas cloud in an obstructed and/or partly confined volume may only fill a part of the volume at the time of ignition. The filling ratio is an important parameter, but in some situations 30-50% filling ratio may cause the same explosion pressure as a 100% filled compartment. The reason for this is that during an explosion the gas that burns will expand and push the unburned gas ahead of the flame. Thereby air or fuel-air outside the flammable range is pushed out of the compartment. But when a cloud is only filling a portion of the enclosure, the explosion pressure will be much more sensitive to the ignition location. Other factors gas explosions may be very sensitive to are:

- Type of fuel and oxidizer
- Size and fuel concentration of the combustible cloud
- Location of ignition point
- Strength of ignition source
- Size, location and type of explosion vent areas
- Location and size of structural elements and equipment
- Mitigation schemes

Source of leakage can be characterized as a jet release or a diffuse release, i.e. evaporating pool. The jet release will have a high momentum and establish a strong flow field due to additional air entrainment. The evaporating pool will act as a diffuse release source and the wind forces and buoyancy will control the dispersion process. The flow velocities will be much lower than for the jet release.

3.2 The FLACS Codes²

The FLACS code is a three-dimensional gas explosion and gas dispersion simulation tool, which can be used to describe the release itself, the following dispersion process, water spray dilution, and gas and dust explosions in the case of an ignition. For this project the FLACS code has been used to simulate the gas explosion, and for the last 6 cases also the natural ventilation inside the module and the dispersion of the leakage.

The numerical code solves the 3D conservation equations for mass, momentum, enthalpy and chemical species using a finite-volume method. Turbulence is modelled by the standard k - ϵ model. The interaction between the reactive fluid flow and the surrounding geometry is taken into consideration through a distributed porosity concept. Each control volume is designated a certain area and volume blockage [22]. The numerical model takes account of the interaction between the gas flow and complex geometries such as structures, equipment and pipework, and produces quantitative information in the form of pressure-time curves. [7]

The main outcomes of the FLACS tool, i.e. the results of the calculations, are concentration-profiles and fields when considering dispersion and the primary effects of gas explosions: static overpressure profiles and fields, dynamic overpressure profiles and fields both inside the flammable cloud and at some distance from this cloud (blast effects).

Due to improvements in the understanding of the explosion process, new sub-models which describe the process better have been implemented, and have led to a continuous work in further development of the codes implemented in FLACS. Some of the differences that may have an impact on the simulation results, are highlighted below.

3.2.1 Development of the FLACS Codes³

This section describes some of the changes that are made in the FLACS code.

In this project the aim is not to study the FLACS simulation code, and therefore only the main changes are presented. Several other changes are made, such as:

- Improved thermodynamics (including more realistic chemistry)
- Improvements in the modelling of turbulence (including sub-grid turbulence energy)
- Improvements in the representation of the flame front
- Improvements in the combustion modelling (including flame folding)
- Numerical improvements

²This chapter is in high degree based on the FLACS User Manual v10.0 (2013) [3] and the Ph.D. thesis "Modelling of Turbulence and Combustion for Simulation of Gas Explosions in Complex Geometries" by Bjørn Johan Arntzen [21]

³Based on the Ph.D. thesis "Modelling of Turbulence and Combustion for Simulation of Gas Explosions in Complex Geometries" by Bjørn Johan Arntzen [21]

- Larger validation basis

The above mentioned improvements will also impact the results.

Geometry representation

The simulation volume is divided into a set of control volumes by three sets of grid planes, one in each direction. In order to have a good representation of the effect of obstacles it is important that they are well represented geometrically by the chosen grid. Large geometry objects (> 1.5 Control Volume's in size) such as walls and decks are recommended to be aligned to a grid line, to avoid undesirable situations such as "leaking corners" or larger/smaller vent areas.

The geometry is made by adding a range of simple objects to represent the geometry. In the pre-processor CASD, two types of objects can be chosen; boxes and cylinders. Boxes have a position (x, y, z) , a size (L_x, L_y, L_z) and area porosities $(\beta_x, \beta_y, \beta_z)$. Cylinders have similarly a position (x, y, z) , a diameter, d , a length, L , a direction $(\pm x, \pm y$ or $\pm z)$ and volume porosity (β_v) .

In FLACS-94, and earlier versions, cylinders were represented as boxes, with a diagonal equal to the cylinder diameter. This gave an acceptable representation of turbulence generation, but the area blockage was too small. A too small area blockage results in too high flow rates and thereby too low pressures for situations with near sonic flows (obtained with pressures above 1 barg).

Combustion modeling

The purpose of a combustion model for premixed combustion, like gas explosions, is to localize the reaction zone and convert reactants to products at a rate similar to that of a real flame in an explosion. Turbulent combustion processes are often handled by mixing controlled combustion models of eddy break-up type. The combustion process may however be described better by dividing the combustion model into two parts, a flame model and a burning velocity model.

The reaction rate described by turbulent combustion used in FLACS, before the FLACS 93 version, was the Hjertager-Magnussen (H-M) model [Hjertager (1982)]. In the referred Ph.D.-thesis [21], it is found that the burning velocity obtained with this model was far too low.

The burning velocity, U , is the velocity of the flame front with respect to the unburned gas immediately ahead of the flame. The relation between flame speed, S , and burning velocity, U , is:

$$S = U + u \quad (3.1)$$

where u is the velocity of the unburned gas just ahead of the flame. The flame speed S , is defined as velocity of the flame relative to a stationary observer i.e. the ground or another fixed frame. [7]

The problems illustrated above were corrected with a new combustion model in 1993, the β -flame model. Here the combustion modelling is divided into two parts; flame and burning velocity modelling.

Ignition in the H-M model, was modelled by assuming that at time zero, half of the flammable mixture in the ignition cell is converted to products, thus the time between ignition and peak explosion pressure will largely depend on the grid size chosen. Later studies have shown that normally this will not agree with the experimental results.

In the β -flame model, the reactants are converted to products at a rate given by flame area and burning velocity in the ignition cell. This model secures the same conversion as for the real flame and gives a good agreement between simulated and experimental time to peak pressure, independent of grid size chosen.

3.2.2 Simulations for gas explosions in FLACS

The first step of a FLACS simulation is to generate the geometry that is to be investigated. Gas cloud composition, size and location, location of ignition point, and specific output parameters have to be determined before the simulation of the gas explosion can start [7]. This can be done in the preprocessor of FLACS; CASD.

The building blocks in a CASD geometry are instances of objects that combines simple solid primitives (boxes and cylinders) by Boolean operators (unions and left differences). Each object in a CASD database is assigned a material property, illustrated by a specific color. Instances can be grouped under assemblies, which is a way to group the instances in complicated geometries. Geometry consists of at least one assembly, called the top assembly. In CASD, all geometries are stored in a database. [3]

Geometrical layout such as equipment, piping, walls etc. in the simulated geometries are represented as cylinders or boxes which are aligned with the main axes of the module. Pipes are represented as long cylinders. Beams which are not vertical or horizontal are represented by vertical or horizontal, or a combination of these, beams with blockage similar to the original beams. [7]

Walls are represented by boxes with zero width in one direction. Porosity for walls and decks is a value between 0.0 and 1.0, defining the fraction of the area available for flow. A solid wall has a porosity of 0.0 [7]. Firewalls are represented by pressure relief panels, and type can be specified in CASD. The panel is initially represented by a closed wall which opens up when the simulated explosion pressure reaches a specified value. [7]

Flowvis is the postprocessor for the CFD-code in FLACS, and is a program for visualizing results from computer aided simulations of gas explosions, gas dispersion and multi phase flow. [3]

The purpose of Flowvis is to visualize simulation results from FLACS. The results from a simulation include grid, geometry, bulk data, scenario and results. The results may be visualized by creating a presentation consisting of one or more pages, each containing one or more plots. [3]

3.2.3 Impacts on explosion simulations

As described in Section 3.1, several parameters affect the rate of flame propagation and thereby the explosion pressure. In this section a presentation of the influence

of flow regime, congestion and confinement, and the location of the ignition point has on explosion loads are given.

Flow regime

In an accidental gas explosion of a hydrocarbon-air cloud the flame will normally start out as a slow laminar flame with a velocity of the order of 3-4 $\frac{m}{s}$. In an offshore module, with equipment and other structures hindering the wave, the flame may accelerate to several hundred meters per second. When the gas is burning the temperature will increase and the gas will expand by a factor of up to 8 or 9. The unburned gas is therefore pushed ahead of the flame and a turbulent flow field is generated. When the flame propagates into a turbulent flow field, the effective burning rate will increase and the flow velocity and turbulence ahead of the flame increases further. This strong positive feedback mechanism is causing flame acceleration and high explosion pressures and in some cases transition to detonation. Reynolds number, Re , is used to determine whether the flow regime is laminar or turbulent [7], and is defined by

$$Re = \frac{uL}{\mu} \quad (3.2)$$

where u = flow velocity, L =characteristic dimension of the geometry, and μ =kinematic viscosity.

The turbulence will increase with increasing L (Eq. 3.2).

Congestion and confinement

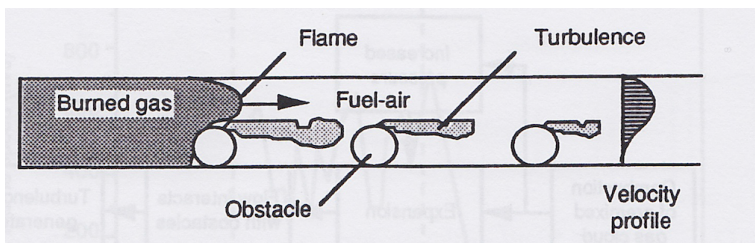


Figure 3.3: *Turbulence generation in a channel due to repeated obstacles during a gas explosion. Illustration from [7].*

Fig. 3.3 shows how turbulence is generated in the wake of obstacles in a channel. The turbulence is very important for how fast the flame can propagate in a premixed gas cloud.

The ideal gas law equation below (Eq. 3.3), illustrates the impact any of the following factors have on generation of overpressure:

- Walls
- Equipment
- Surrounding air

$$p = \frac{\rho RT}{M} \quad (3.3)$$

where p = overpressure, ρ = *density*, R =universal gas constant, T =temperature in Kelvin and M =Molar mass.

Small changes in the geometry regarding vent area and the location of the venting, can lead to order of magnitude changes in the explosion pressure. When there is sufficient venting close to the ignition point, the flame speed will be low and the turbulence generated behind the obstacles will be limited. Hence, the pressure will be low.

The flame acceleration can to some extent be avoided by venting the hot combustion products. Venting of unburned gas ahead of the flame may also contribute to a lower explosion pressure. When a deflagration propagates through a region of obstacles and then ends up in an unobstructed region the flame speed will normally drop and adjust to the new environment.

In a partly confined area with obstacles the flame may accelerate to several hundred meters per second during a gas explosion due to the wrinkling of the flame front by large eddies and the turbulent transport of heat and mass at the reaction front. This turbulence is mainly caused by the interaction of the flow with structures, pipe racks, etc. Each obstacle will generate a turbulent shear layer that will accelerate the flame up to a certain level, and smaller obstacles will generate higher pressures.

Pedersen et al. investigated the effect of vegetation, both in terms of tree species, number of branches and the presence of their foliage experimentally, on the observed flame velocity and overpressure-time development. The experiments showed that the insertion of three spruce branches with foliage enhances the maximum overpressure by a factor of 10 compared to that of an empty rig. Removing the foliage from the three branches reduces the maximum overpressure to approximately one-third of that obtained with the same configuration, needles intact [22]. This experiment indicates the importance of including small details to the geometry model.

Ignition point

Various experiments and FLACS simulations have shown that explosion pressures can be very sensitive to the location of the ignition point. In general the lowest pressure is obtained if the ignition point is:

- Close to the vent area or
- At the edge of the cloud

Repeated obstacles will generate turbulence, while venting of combustion products will reduce the turbulence generation. By igniting near the vent opening the combustion products will be vented and the flow velocity and the turbulence in the unburned mixture will be low. By igniting near a wall, away from venting area, a high flow velocity will be generated ahead of the flame which will generate turbulence by interaction with obstacles and hence support a high burning rate and cause high explosion pressures. However, if venting combustion products is not sufficient to keep the flame speed at a low level, edge ignition may cause higher explosion pressures than central ignition. The venting of hot combustion products may also influence turbulence generation and flame acceleration. If hot combustion products are vented out of a compartment, the flow and the turbulence can be reduced since the driving pressure is relieved and less gas is pushed ahead of the flame.

Wind

Experiments performed by Van Wingerden et al. [23] of gas dispersion in a 1:5 scale model of an offshore module concluded that for medium and large scale jet releases the dispersion in a module is dominated by the jet, but the actual gas concentration depends upon the ventilation, whilst for smaller release both dispersion and gas concentration are dominated by natural ventilation. It showed that the accumulation of gas inside a module in case of an accidental gas release will to some extent be dependent on the ventilation of the module. This was shown by performing tests with similar leak conditions but varying ventilation. The non-ventilated case gave very uniform gas concentrations with much higher concentrations than for the ventilated cases. For the non-ventilated case the concentration will keep on increasing as long as gas is released into the module, but for the ventilated cases the gas concentration will only increase as long as the leak rate is larger than the amount of gas which is carried away by the ventilation.

Jet release

Explosions due to non-homogeneous gas clouds filling only a part of a module are expected to give rise to lower explosion overpressure than those expected from homogeneous, stoichiometric clouds in the same module. However, turbulence generated by especially the jet release may enhance the explosion [23].

The accumulation of gas inside the module is strongly dependent on the direction of the jet release relative to the ventilation flow in the module and the possible interaction of the jet with equipment or walls. If the jet release is parallel and in the same direction as the ventilation flow, and the jet does not impact on any equipment the flammable part of the cloud, it will have a cigar shape with large concentration variations. However, when the jet interacts with obstacles, pipes or vessels, a different flow pattern is formed, completely changing the concentration pattern of the gas inside the module. Pointing the jet perpendicular to the wind direction results in a more uniform gas distribution across the entire module. The main reason for this is the fact that the jet impacts on the roof of the module, causing large vortices with dimensions in the order of several meters. [23]

Experiments performed by Wingerden et al. with varying leak rate in the same offshore module as used above, showed that the size of the cloud varied with the leak rate. Results from these experiments indicated that the overall gas concentration in the flammable part of the cloud is dictated by the release rate as well as the size of the cloud. [23]

Chapter 4

Scope of Work

4.1 Re-simulation of the previous simulated cases

FLACS-86 was used to investigate different explosion scenarios in connection with the investigation of the accident at the Piper Alpha Platform [1, 2]. In this thesis the same simulation cases are simulated with the latest version of FLACS; FLACS v10.0. The simulation cases from 1988/89 are referred to as simulation cases 1-5, and the cases that are re-simulated in this thesis are referred to as simulation cases 6-20. For the first 5 simulation cases in this thesis, the approximately same geometry as for the simulations in 1988/89 has been used, for the next 5 cases a more complex geometry was used, and then for the last cases the whole platform was used as the simulation domain. The simulation cases are presented in more detail in Chapter 5 in this thesis.

4.2 New simulation cases

Based on the results from the first 15 simulation cases, 6 new cases have been identified for the purpose of better illustrating what happened on the night of 6th of July 1988. For these last cases, wind and dispersion simulations have also been included. This will illustrate the effect wind has on the leak itself, the formation of the gas cloud which ignited, and by that on explosion loads. The observations from these simulations will further serve as a starting point for the explosion simulations, to illustrate what really happened and to see if the findings from 1988/89 were correct.

4.2.1 Wind tunnel tests¹

Especially the leak rate inputs are based on two wind tunnel tests performed by BMT Fluid Mechanics Ltd., at their wind tunnel at Teddington. The tests were performed in conjunction with the investigation of the accident. The first set of

¹The information given in this section is based on The Cullen Report [8]

experiments investigated a number of different leaks, with emphasis on leaks from the area of PSV 504 in C Module (condensate). The second set was concerned with leaks of neutrally buoyant gas.

The wind tunnel tests investigated the leaks to illustrate the set of gas alarms and their patterns in setting off alarms, see Chapter 2.3.

Only the larger leaks could give a flammable gas cloud containing the quantity of fuel evidently necessary to cause the observed explosion effects. The results from the explosion simulations in FLACS-86 indicated that a cloud containing much less than 45 kg of fuel would not give a sufficiently large explosion.

Based on the wind tunnel tests, the conclusion was that the leak occurred in 2 stages. The first jag released a swirl of vapour, at about $4 \frac{kg}{min}$. At the second push on the button, the rate increased to $110 \frac{kg}{min}$ for about 30 seconds, and around 45 kg of condensate were allowed to seep out and fill the module about 25% of the volume.

The tests point to the later, larger leak as being one of propane from position 1 (PSV 504), from a downward pointing jet or partial fan. The 2 sets of test results taken together show that the C3 low level alarm came up first only in tests with these features. Tests involving a leak of neutrally buoyant gas in any of the 4 leak positions gave the C2 rather than the C3 low level alarm first.

Preliminary to the wind tunnel tests it was necessary to establish the ventilation air flow corresponding to the conditions at Piper on the evening of 6th of July. Wind conditions were based on those recorded by the Lowland Cavalier and were taken as wind direction 207 degrees (in relation to Piper Alpha Platform) and wind velocity $8.2 \frac{m}{s}$. For these conditions the ventilation rate through the module was $46 \frac{m^3}{s}$. This corresponds to an air change rate of 39 air changes per hour and to average air velocity of $0.5 \frac{m}{s}$.

4.3 Hypothesis

4.3.1 Impact on results due to new FLACS code

As indicated in Chapter 3.2, later simulations and experiments has indicated that the old FLACS code (94 and earlier) generated higher flow rates due to too small blockage ratio, and thereby too low pressures with near sonic flows. Since none of the pressures for the simulated cases exceeded pressures of 1 barg, this is not applicable here.

It has later been showed that the combustion model used in 1989 gave too low burning velocities [21]. As seen by Eq. 3.2, lower flow velocities will reduce Reynolds number, Re. Re is a dimensionless characteristic value for determining whether a flow is laminar or turbulent; a laminar flow is given by low Re, and turbulent for high Re ($Re > 400\ 000$). It is therefore expected that the effect of turbulence was reduced for the simulations performed in 1988/89, and thus also the pressure.

For the new simulations the following results may be expected due to changes in the FLACS code:

- Higher burning velocity
- Higher flame speed (Eq. 3.1)
- Increased turbulence
- Increased explosion pressure

4.3.2 Impact on results due to more detailed geometry

The geometry models used in FLACS-86 and FLACS v10.0 are not identical, and this is expected to have an impact on the explosion loads. If the venting in the C Module used in the present thesis is other than what it was for the 1988/89 simulations, due to different geometry, this may have an impact on the explosion pressure. Venting of the unburned gas ahead of the flame may contribute to a lower pressure [7].

It is further anticipated that the explosion pressure will increase in the last 10 simulation cases, due to a more complex geometry model and additional structure on the outside of the C Module. This is assumed to have an impact on the flame propagation, the turbulence and the venting area, and also on the blocking of the flames for the last 5 cases.

In FLACS, the simulation volume, grid cell sizes and the location of monitor points are also defined. These parameters were not identically reproduced from the simulations in 1988/89, and it is therefore assumed that it will have an impact on the simulated overpressure.

Given the information stated in Chapter 3.2.3, the following might be expected for the simulation cases 11-20:

- Increased burning rate
- Increase of the flow velocity and turbulence ahead of the flame
- Increase in the simulated explosion pressure due to more obstacles, both inside and outside of the module
- Reduced venting due to more equipment will also contribute to a higher explosion pressure

4.3.3 Impact on results due to ventilation and dispersion

Ventilation is simulated for the last 6 cases; cases 21-26. The added wind will have a natural ventilation effect inside the module. It is anticipated that this will lead to an increase in the gas concentration only as long as the leak rate is larger than the amount of gas carried away by the ventilation. When these two are equal (due to lower flow rates from the leak location or that the leak has stopped) the maximum concentration in the gas cloud will be reached. After this the concentration will continuously decrease as a result of the ventilation of the module.

The dispersion of the leakage is assumed to influence the cloud composition and size. The gas cloud that is generated through the dispersion simulations will be non-homogeneous, while for the first 15 cases in this thesis the simulated gas cloud was homogeneous and stoichiometric. This is expected to contribute to a lower explosion overpressure, but the turbulence generated from the leak itself may generate a higher overpressure.

It is further anticipated that also the direction of the leakage will have an impact on the simulated explosion overpressure. A leakage in the same direction as the ventilation gradient inside the module at the position of the leakage, is assumed to result in a gas cloud with large concentration variations. With a leakage direction perpendicular to the ventilation gradient, it is expected that a more uniform gas distribution across the entire module will be generated.

Also the leak rate is anticipated to affect the simulated overpressure. The hypothesis is that a lower leak rate will give lower overpressure.

Chapter 5

Simulation Cases

This chapter presents the inputs for the simulation cases 6-20 which are a re-run of the simulations performed in 1988/89, as well as input to the new simulation cases 21-26. FLACS v10.0 has been used for the cases 6-26, with grid cells of 0.5 m in all directions. The simulation volume and the coordinates of the C Module are given in Table 5.1. Grid cells in the area outside of the module were stretched.

Table 5.1: *Coordinates of the C Module position in the FLACS geometry model, and the simulation volume used for the simulation cases 16-26.*

	X		Y		Z	
	min	max	min	max	min	max
Module C	31 m	46 m	-4.5 m	45.5 m	0 m	7.5 m
Simulation Cases						
6-15	5 m	65 m	-49.5 m	100.5 m	-10 m	15 m
16-26	-58 m	134 m	-119.5 m	207.5 m	-42 m	54 m

Other simulation outputs than those presented in this chapter, and relevant for this thesis, can be found in Appendix C.

5.1 Simulation cases 1-20

The simulation cases 1-5 are referring to the cases 1-4 performed by Bakke and Storvik in 1988 and case 1 performed by Bakke and Storvik in 1989 [1, 2]. A picture of the geometry model that was used for these simulations, is shown in Fig. 5.1. The simulation cases 6-20 are referring to the cases performed in this thesis, where 6-10 refers to the simplified geometry of the C Module shown in Fig. 5.2, cases 11-15 to the new geometry of the C Module, illustrated by Fig. 5.3, and the simulation cases 16-20 refer to the cases taking the geometry of the whole platform into account. The geometry of the whole platform is shown in Fig. 5.4.

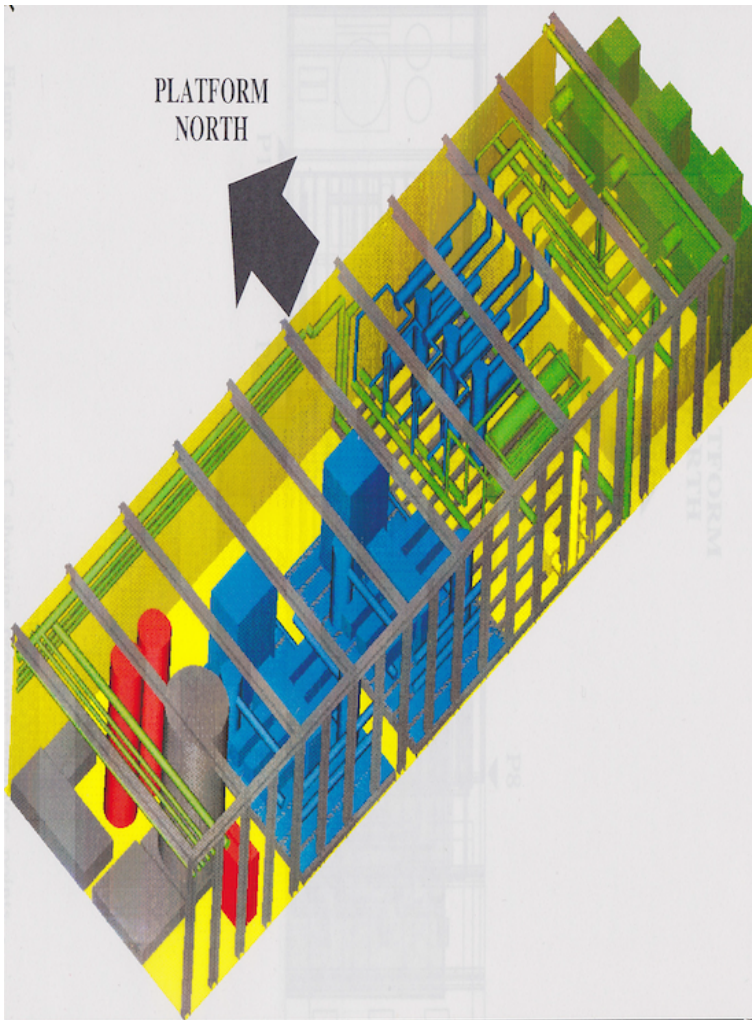


Figure 5.1: *Model picture of the old geometry of the C Module used for simulation cases 1-5.*

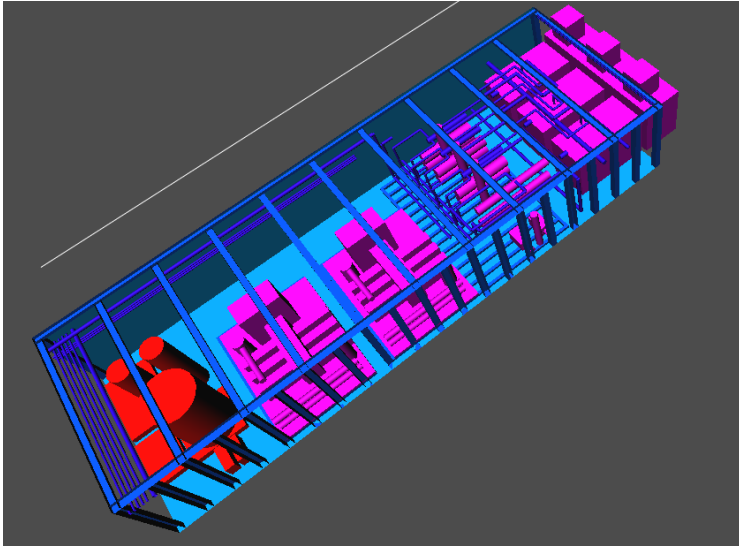


Figure 5.2: Model picture of the simplified geometry of the C Module used for simulation cases 6-10. Right side wall (B/C) and roof removed for illustration.

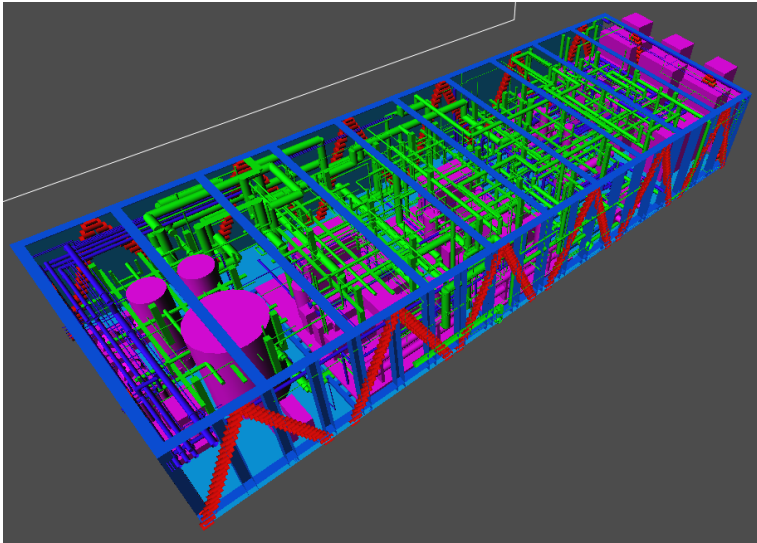


Figure 5.3: Model picture of the detailed geometry of the C Module used for simulation cases 11-15. Right side wall (B/C) and roof removed for illustration.

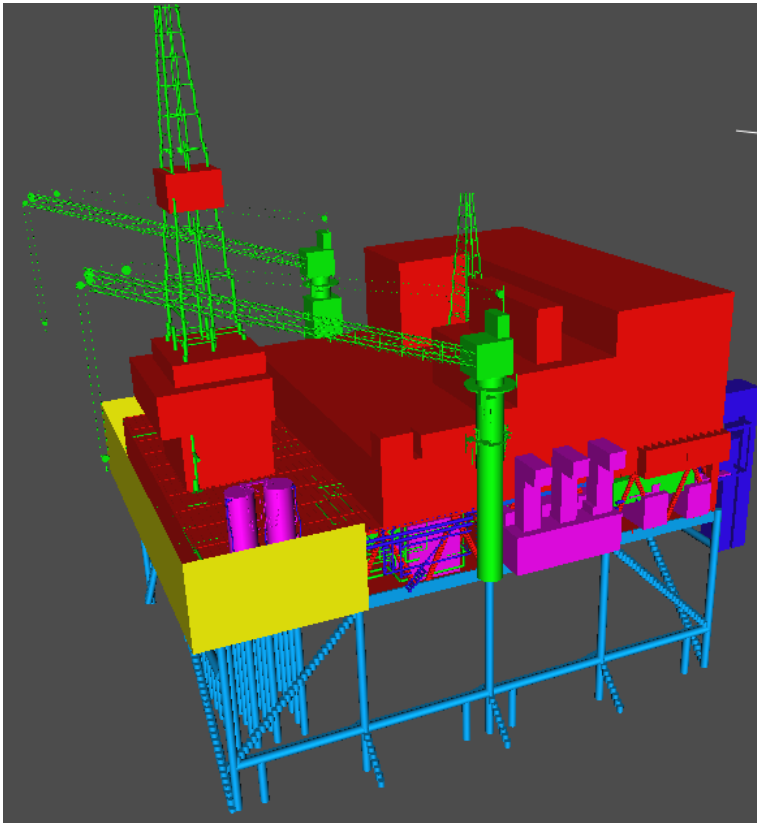


Figure 5.4: *Model picture of the geometry of the whole platform used for simulation cases 16-26.*

To monitor the simulation outputs, the same coordinates for a total of 8 monitor points have been used for the simulation cases 6-26. The monitor points are shown in Fig. 5.5. The points are evenly spaced along the two long walls of the module (C/B and C/D), and the coordinates were chosen based on the location of the monitor points that were used for the simulations in 1988/89.

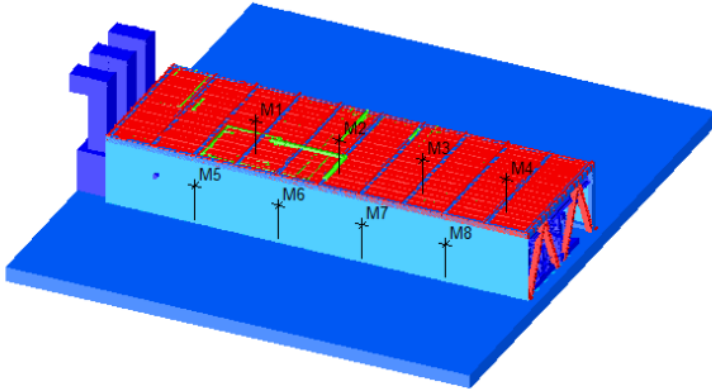


Figure 5.5: *Location of monitor points for simulation cases 6-26.*

5.2 Input for the simulation cases

This section presents the inputs for the simulation cases 6-20, as well as pictures of the geometry model that was generated in FLACS v10.0. The figures also illustrate the locations of the ignition points and the cloud locations for the simulation cases as specified in Table 5.2.

For the simulation cases 1-20, it is assumed to be zero wind speed inside the C Module. The gas clouds are assumed to be equivalent, homogeneous and stoichiometric. Pressure relief panels of type "Popout" with properties as shown in Table 5.2 are specified in FLACS v10.0, to simulate the C/B and C/D firewalls. The firewalls were made up of 2.5×1.5 metre panels bolted together [9]. Pressure relief panels were used in the geometry model to simulate if the firewalls were destroyed during the simulated explosion scenarios, and if so, the degree of destruction. For the simulation cases 6-10, the firewalls are represented as one panel each.

Table 5.2: *Input for the simulation cases 1-20.*

	Simulation Cases 1-20				
	1/ 6 / 11 / 16	2/ 7 / 12 / 17	3/ 8 / 13 / 18	4/ 9 / 14 / 19	5/ 10 / 15 / 20
Fuel type	Nat. gas	Nat. gas	Condensate	Nat. gas	Condensate
Cloud location	Eastern half	Eastern half	Eastern half	Eastern half	East
Ignition source location	Position 1	Position 2	Position 2	Position 1	Position 3
Extent of cloud	50 %	50 %	50 %	30 %	12 x 19 x 3.5 m
Overpressure failure B/ C freewall	138 mbar	138 mbar	138 mbar	138 mbar	138 mbar
Overpressure failure C/ D freewall	250 mbar	250 mbar	250 mbar	250 mbar	250 mbar
Maximum travel distance freewalls if failure	1 m	1 m	1 m	1 m	1 m

Table 5.3: *Gas cloud compositions (volume %).*

Fuel type	Natural Gas	Condensate
Methane	87.66	40.04
Propane	12.34	59.96

The gas compositions specified in Table 5.3 were used for the simulations in 1988/89 because it was not possible to simulate with the real gas composition (Table 5.7). The gas compositions in Table 5.3 were also used for the simulation cases 6-20 in this thesis.

5.2.1 Location of ignition point

Table 5.4: *Ignition source locations for simulation cases 1-20.*

Position	X	Y	Z	Description
Position 1	39.25 m	2.25 m	4.25 m	Centrifugal compressors (edge) (east end of module)
Position 2	34.7 m	18.7 m	2.2 m	Reciproc. Compressors (central) (module centre)
Position 3	33.4 m	10.3 m	0.7 m	Close to the south wall, at 1m elevation and in centre of cloud

As shown in Table 5.4, the ignition point location has been varied between three different locations. These locations are shown in Fig. 5.6-5.8.

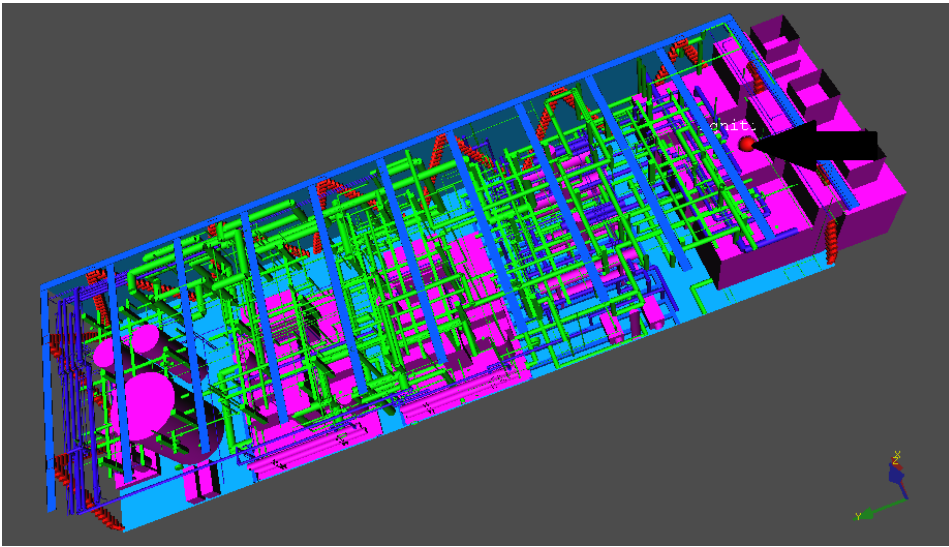


Figure 5.6: Location of ignition point for the simulation cases 1, 4, 6, 9, 11, 14, 16 and 19.

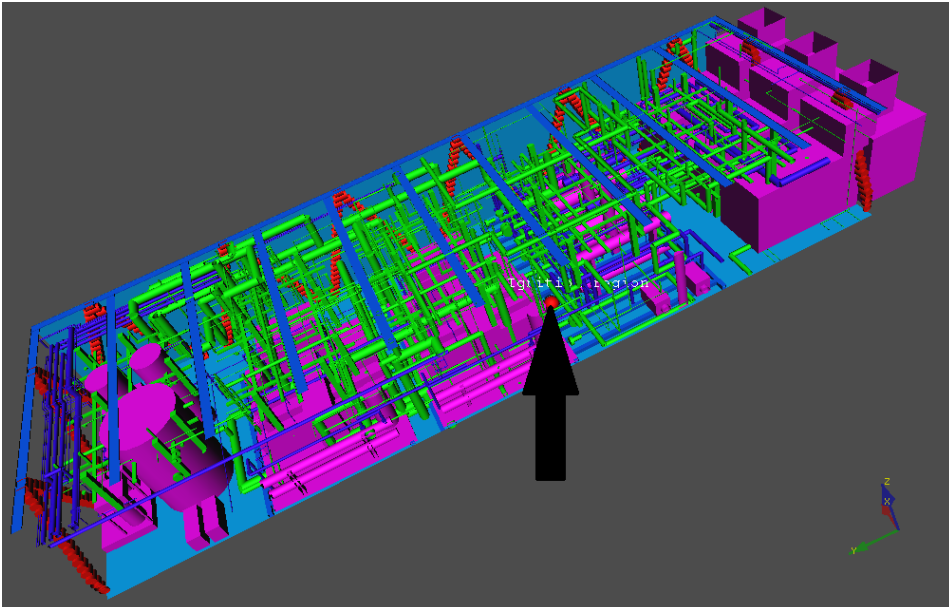


Figure 5.7: Location of ignition point for the simulation cases 2, 3, 7, 8, 12, 13, 17 and 18.

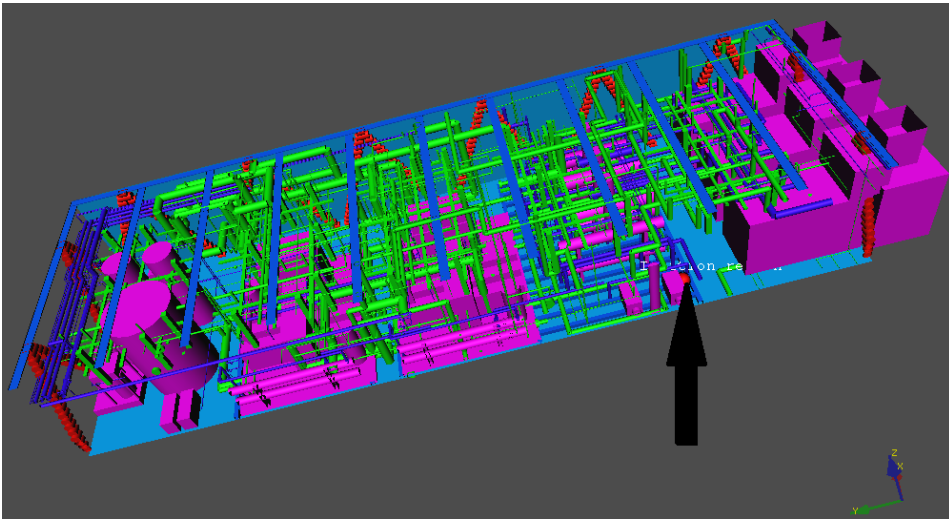


Figure 5.8: Location of ignition point for the simulation cases 5, 10, 15 and 20.

5.2.2 Gas cloud location

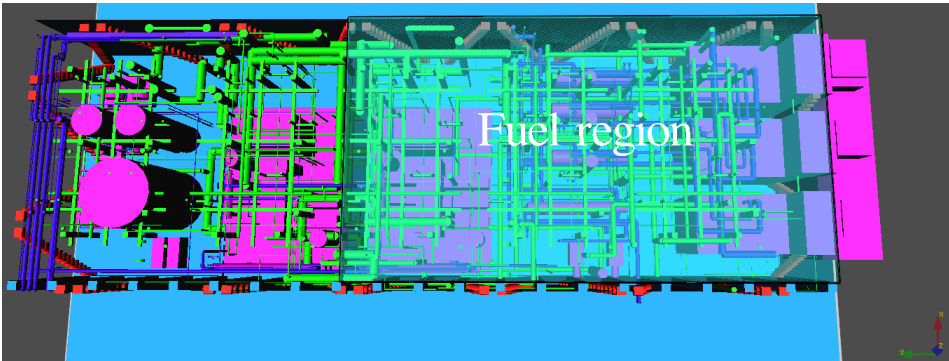


Figure 5.9: Gas cloud location and extension for the simulation cases 1-3, 6-8, 11-13 and 16-18.

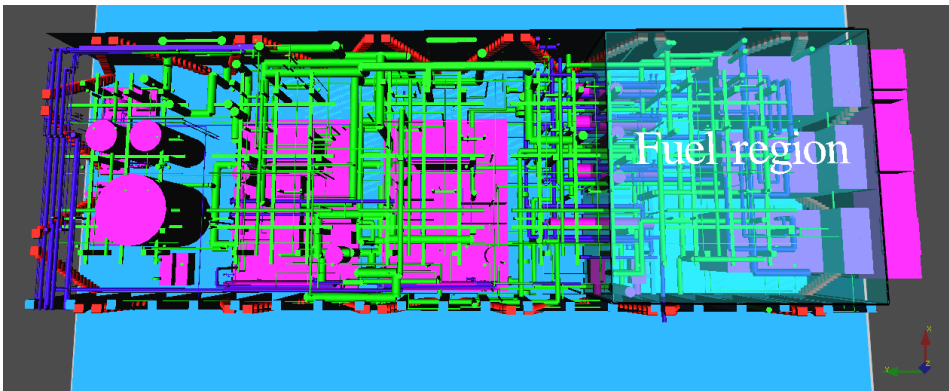


Figure 5.10: *Gas cloud location and extension for the simulation cases 4, 9, 14 and 19.*

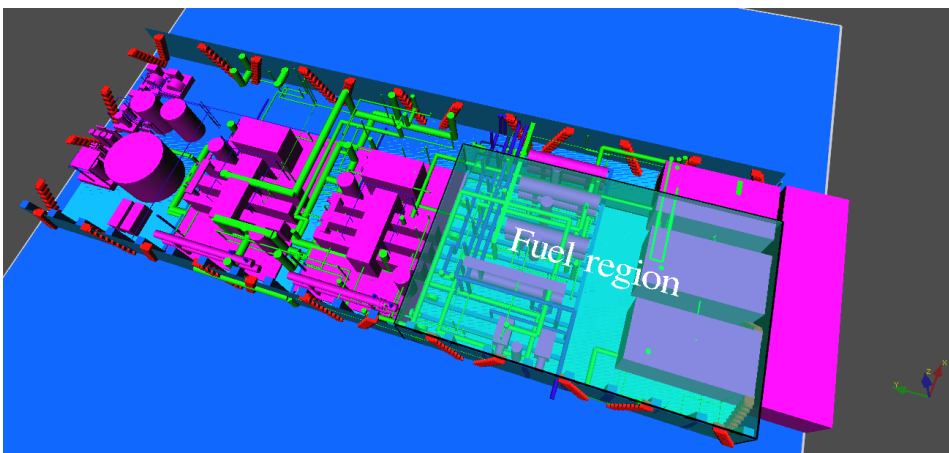


Figure 5.11: *Gas cloud location and extension for the simulation cases 5, 10, 15 and 20.*

5.3 Simulation cases 21-26

Based on the results from simulation cases 6-20, with emphasis on case 5, 10, 15 and 20, 6 new cases have been defined. The purpose of these new simulations is to improve the accuracy of the results by including parameters such as wind and dispersion of the leakage.

5.3.1 Input for the simulation cases 21-26

Input for the ventilation scenario

The following wind conditions for the ventilation scenario have been used [8]:

- Wind speed: $8.2 \frac{m}{s}$
- Wind direction relative to platform north: 207 deg

Input for the dispersion simulations

To illustrate the dispersion for possible leakage scenarios, 6 different cases were simulated in FLACS v10.0. For these 6 cases the leak rates, leak positions and ignition source locations were altered as shown in Table 5.5 and Table 5.6. The two different leak positions were only differed by 0.5 meters in the x-direction. Both positions are close to the location of the PSV 504 on Condensate Pump A. The coordinates for the two positions are given in Table 5.5, and the positions are shown in Fig. 5.12 and Fig. 5.13.

The simulation cases for the dispersion scenarios are referred to 010701-010706.

Table 5.5: *Leak positions for the dispersion simulation cases 010701-010706.*

Leak positions			
Position	X	Y	Z
Position 1	33.625 m	18.5 m	5.0 m
Position 2	34.25 m	18.5 m	5.0 m

The leak inputs for the dispersion simulation cases are shown in Table 5.6. Input for the leak hole size and the pressure was found in the Cullen report ([8]). Based on these parameters and the concluded leak rates from the wind tunnel tests, a leak rate of $1.7 \left[\frac{kg}{s} \right]$ were chosen as one of the two different leak rates that were simulated in this thesis. The second leak rate, $2.7 \left[\frac{kg}{s} \right]$, was chosen to illustrate the generated gas cloud size for a larger leak rate. For all of the cases the leak hole size was $0.0069 (m^2)$ and the pressure was 62 barg. For monitoring of the leak in relation to the gas detection pattern the monitor point coordinates shown in Fig. B.3 in Appendix B has been used. The leak was started after 60 seconds with wind simulations and lasted for 40 seconds before the ignition.

Table 5.6: *Input for the dispersion simulations.*

Simulation Cases						
	010701	010702	010703	010704	010705	010706
Leak rate $\frac{kg}{s}$	1.6512	2.7	1.6512	1.6512	1.6512	2.7
Leak position	Position 1	Position 1	Position 1	Position 1	Position 2	Position 1
Leak direction	-Y	-Y	-Z	+Z	-Y	-Z

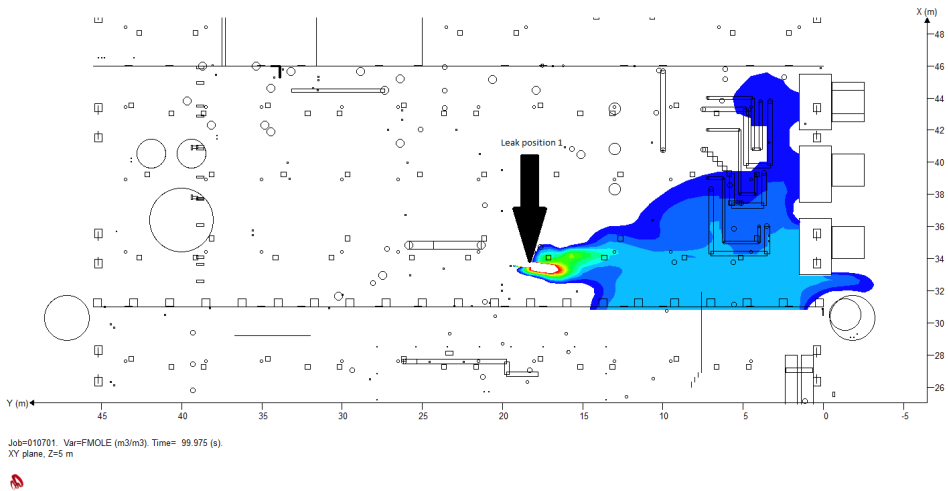


Figure 5.12: *Figure showing the position of the first leak source (010701, 010702, 010704 and 010705). The illustration also shows the size of the gas cloud at the time of ignition (after a 40 seconds release) for 010701.*

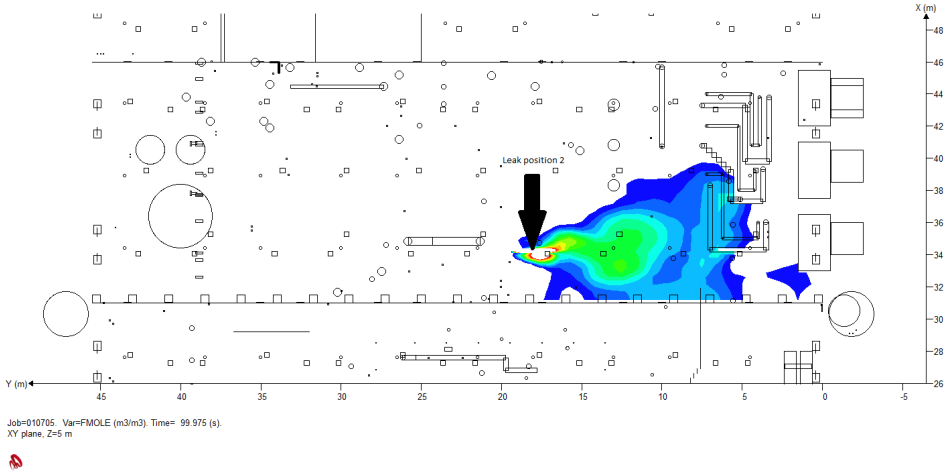


Figure 5.13: Figure showing the position of the second leak source (010703 and 010706). The illustration also shows the size of the gas cloud at the time of ignition (after a 40 seconds release) for 010706.

Input for explosion scenario

The simulation cases for explosion are referred to as simulation cases 21-26.

Table 5.7: Gas cloud compositions (volume %).

	Natural Gas	Condensate
Methane	67.75	19.86
Ethane	15.76	18.98
Propane	9.34	31.06
Butanes	1.97	17.16
Pentanes	0.45	9.94
Carbon dioxide	0.45	0.27
Nitrogen	4.23	0.46

Table 5.8: Ignition source locations for the simulation cases 21-26.

Leak positions				
Position	X	Y	Z	Simulation cases
Position 1	33.4 m	10.3 m	0.7 m	21, 22, 23
Position 2	39.25 m	2.25 m	4.25 m	24, 25
Position 3	38.75 m	3.25 m	4.25 m	26

The ignition point for the simulation cases 21-23 is ignition point location 3 (Fig. 5.8). Ignition point location 1 was used as the ignition point for the simulation cases 24-26 (Fig. 5.6).

For all of these simulation cases condensate was used as fuel type, the natural gas composition as given in Table 5.7 has not been used in this thesis. The gas composition for the condensate is also shown in Table 5.7. The ignition time was set to 40 seconds after the leakage started, i.e. at 100 seconds in FLACS v10.0 (ventilation lasted for 60 seconds before the leakage was started). Illustrations of the generated clouds at different time steps are included in Chapter 6 and in Appendix C.

Chapter 6

Results and Discussion

In this chapter the results from the simulations are presented together with a discussion of these. First a presentation of the first 15 cases are given, together with a discussion around the observed differences and the new results. Secondly, the new simulation cases are presented and discussed.

Simulation outputs are shown in this chapter and in Appendix C.

6.1 Simulation Results and Observations

The first 15 simulation cases illustrates the point that small details matter. With increasing blockage ratio (congestion and obstacles) the overpressure increases. This observation is illustrated by Fig. 6.1, 6.2 and 6.3, which shows the simulated pressures for the 8 monitor points for the simulation cases 10, 15 and 20, respectively. Pressure curves for the other cases are shown in Fig. C.1- C.6 in Appendix C.

The dispersion scenarios illustrate that when the leak direction is pointing in the positive or negative Z-direction, the mixing of the released fuel with air is very good, generating a large stoichiometric cloud. When the leak direction is in the negative Y-direction, i.e. the same direction as the wind at the location of the leakage (Fig. 6.8), the generated cloud is smaller and is located in the eastern part of the module which corresponds to the gas detector readings.

The jet releases in the Z-directions do not coincide with any of the witness observations given in the Cullen report; the cloud that is generated is too big to give a pressure like the one that was described. Also the gas detectors in other parts of the module would have given alarms, see Fig. C.28- C.37 in Appendix C. For the last dispersion case, with leakage direction in negative Z-direction and a leakage rate of $2.7 \frac{kg}{s}$, no ignition occurred. This indicates that all of the altered parameters (leak position, leak rate and ignition source location) have an impact on the occurrence of an ignition. This is further discussed in the following sections.

Another observation that can be seen from the plots, is that the pressure on the simplified geometry ("old" geometry) is lower than the pressures resulting from simulations on the approximate same geometry performed in 1988/89, which is

the opposite of the hypothesis given in Chapter 4.3. This observation is further discussed below in Chapter 6.2.

6.2 Impact of changes in the FLACS code

In the first five simulation cases of this thesis, a similar geometry to the one used for the simulation cases in 1988/89 has been used. The findings from the simulations in the present thesis are compared to the results obtained in 1988/89 to indicate the differences between the two FLACS versions; FLACS-86 and FLACS v10.0. The fact that the two geometry models used for these cases are not identical, will also influence the results. The geometry model used for simulations in 1988/89 has not been available for the re-simulations, so a new geometry model has been built in FLACS v10.0. The new geometry model is based on model pictures of the old one; no detailed drawings with dimensions and positions of the structure and equipment have been available for this work. This also applies to the locations of the monitor points.

The differences between the two geometries will impact the generated overpressure, while the differences between the location of the monitor points will also affect the simulated overpressure because it will be simulated at slightly different locations throughout the module. The pressure will change in time, so by just moving these points by small distances the simulated pressures will be different from each other. These changes makes it difficult to discuss the influence of the changes in the FLACS code itself, but due to the improvements that has been done on the numerical code (3.2.1), some of the differences is expected to be a result of this.

Table 6.1 shows the simulated maximum pressures for monitor points 1-8 for the simulations from 1988/89 [1, 2] as well as the first 5 simulation cases in this thesis.

Table 6.1: *Maximum pressures at Monitor Points 1-8 for the simulation cases 1-10 (Table 5.2 in Chapter 5). [1, 2]*

Sim. case	Maximum pressure							
	MP1	MP2	MP3	MP4	MP5	MP6	MP7	MP8
1	0.430	0.430	0.390	0.340	0.370	0.370	0.350	0.370
2	0.550	0.630	0.630	0.670	0.510	0.600	0.700	0.720
3	0.690	0.760	0.770	0.770	0.620	0.700	0.720	0.840
4	0.110	0.150	0.190	0.190	0.100	0.150	0.170	0.190
5	0.219	0.269	0.314	0.261	0.230	0.302	0.310	0.288
6	0.255	0.264	0.290	0.313	0.256	0.266	0.288	0.327
7	0.419	0.438	0.429	0.366	0.492	0.459	0.459	0.382
8	0.508	0.507	0.462	0.389	0.610	0.529	0.498	0.439
9	0.034	0.035	0.031	0.019	0.035	0.034	0.030	0.019
10	0.252	0.286	0.293	0.245	0.299	0.300	0.274	0.233

Table 6.1 illustrates that the differences between the simulated maximum pressures at the 8 monitor points throughout the module is quite similar. The pressures in 1988/89 are consistently higher than the ones in the present thesis. For the last scenario, which was the one that was concluded with was the most likely one, the pressures are quite similar, reference is made to Table 6.1.

Pressure curves for the monitor points 1-8 for the simulation case 10 are shown in Fig. 6.1, the pressure curves for cases 6-9 are shown in Fig. C.1 and Fig.C.2 in Appendix C.

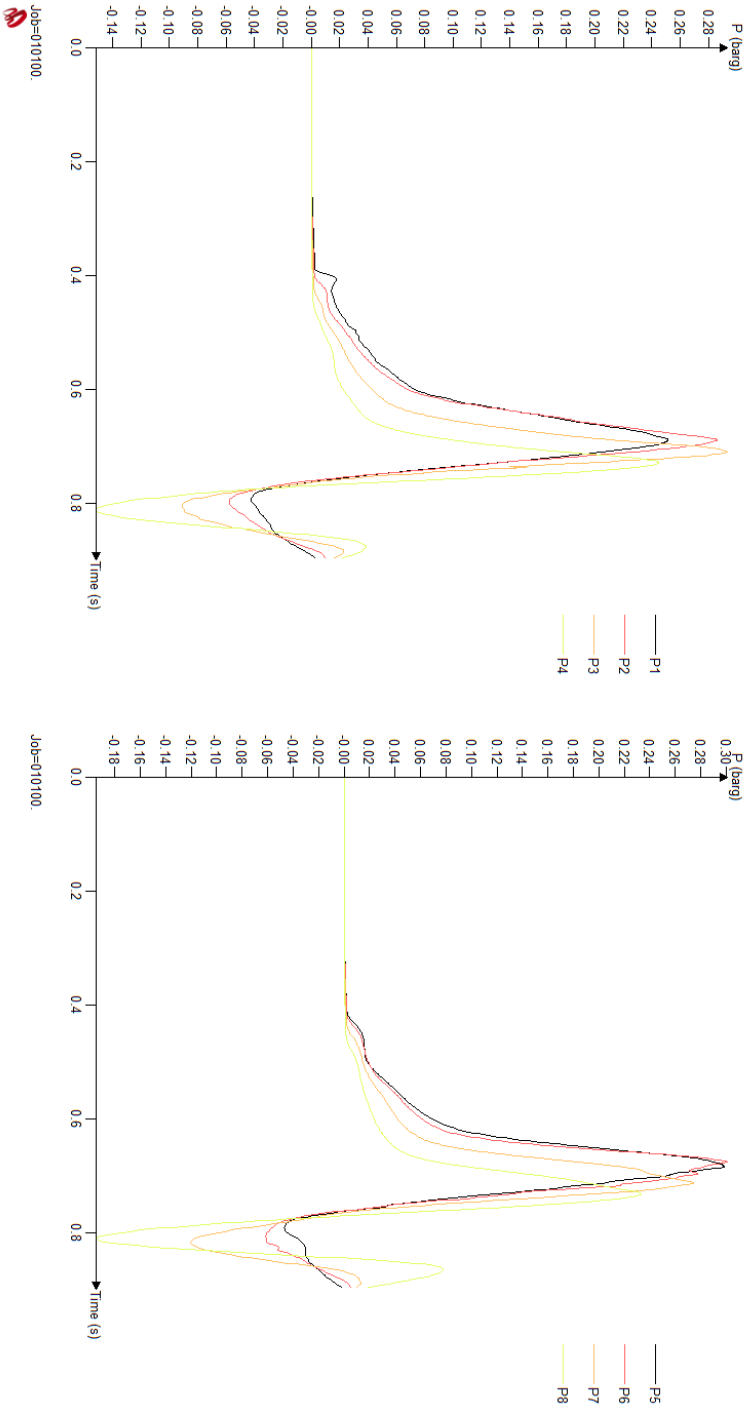


Figure 6.1: Maximum pressures at Monitor Points 1-8 for the simplified geometry of the C Module (See Simulation case 10 in Table 5.2)

As stated in Chapter 1 a complete comparison of the two FLACS versions is not a part of this thesis, but the observed differences may be due to changes in the numerical models in the FLACS versions, but also to the fact that the two geometry models and the location of the monitor points are not identical. In addition, the grid cells and the simulation volumes used in both studies, will have an impact on the results.

The impact of the geometrical model and the structure will be further discussed in Section 6.3.

6.3 Effect of geometry and structure

Simulation cases 11-15 were performed to illustrate the effect the increased amount of obstacles have on the generated overpressure inside the module. This is performed by adding more structure and equipment inside the C Module, including most of the small details. The small details added are based on both model photographs and a random piping script implemented in the FLACS v10.0 code. The inputs for this random script for piping are based on the anticipated congestion (1.5) for the C Module.

For the cases 16-20, the C Module is included as a part of the whole platform structure. This further illustrates the effect of increased congestion. By adding geometry around the module, the boundary conditions were also changed.

Table 6.2 shows the maximum pressures for the simulation cases 11-20.

Table 6.2: *Maximum pressures at Monitor Points 1-8 for the simulation cases 11-20 (Table 5.2 in Chapter 5).*

Sim. case	Maximum pressure							
	MP1	MP2	MP3	MP4	MP5	MP6	MP7	MP8
11	0.358	0.587	0.940	0.610	0.369	0.575	0.730	0.540
12	0.703	0.660	0.537	0.491	0.981	0.851	0.832	0.610
13	0.832	0.773	0.613	0.593	1.418	1.013	1.135	0.782
14	0.402	0.519	0.338	0.254	0.405	0.454	0.354	0.268
15	0.374	0.393	0.326	0.236	0.550	0.705	0.469	0.324
16	0.848	1.193	2.264	2.075	0.877	1.074	2.337	1.567
17	0.838	0.823	0.724	0.606	1.253	0.989	1.027	0.712
18	1.044	1.001	0.884	0.756	1.553	1.206	1.399	0.970
19	0.916	1.024	0.798	0.563	1.069	1.148	0.710	0.470
20	0.545	0.517	0.486	0.343	0.690	1.405	0.707	0.446

Fig. 6.2 and 6.3 shows the pressure curves for each of the monitor points for simulation cases 15 and 20, respectively. As illustrated by these figures the pressure increases with increasing amount of obstacles inside the module. The increased amount of congestion decreases the venting of the module, which generates higher

overpressure. Also, the pressure will continue to increase by adding geometry around the C Module. The geometry around, will act as walls hindering the gas to expand freely on the outside of the module. Especially, can it be seen that the pressure for MP6 for the last simulation case, is much higher for the whole platform than for the detailed geometry, which again is significantly higher than for the simplified geometry. MP6 is located on the C/D wall, near the middle, see Fig. B.3. MP6 is the monitor point that is furthest away from the ignition source location in the fuel region, and the combustion wave will have time and space to develop and to increase its flame speed due to distance and obstructions. For the monitors that are nearer the ignition source location the difference between the pressures are smaller, the flame will have had less time and distance to build up and obtain a higher velocity. The flame speed is also increasing with the amount of obstacles, and due to a shorter distance it will be less turbulence that affect the burning velocity.

For case 5, the maximum pressure was 0.314 bar for monitor point 5, while for the cases 10, 15 and 20, maximum pressures were 0.300 bar, 0.705 bar and 1.405 bar, respectively, for MP6. Case 5 and 10, have approximately the same values for the maximum pressure, but at different locations in the module. For case 5, MP5 corresponds to the east-most point at the C/D wall, while MP6 in case 10 corresponds to the next point in western direction at the C/D module. These numbers illustrate that by just adding the smaller details inside the module, the maximum pressure doubles, and by also including the geometry on the outside of the module, the maximum pressure is doubled ones more. The last number, for the whole platform, is approximately 4.5 times higher than for the simplified geometry of the C Module. This shows the effect the details in the geometry model have on explosion loads. With increasing amount of equipment inside the module, the venting area is reduced. For partly confined areas, like the area of the C Module, both size and location of the explosion vent areas are important for the generated overpressure.

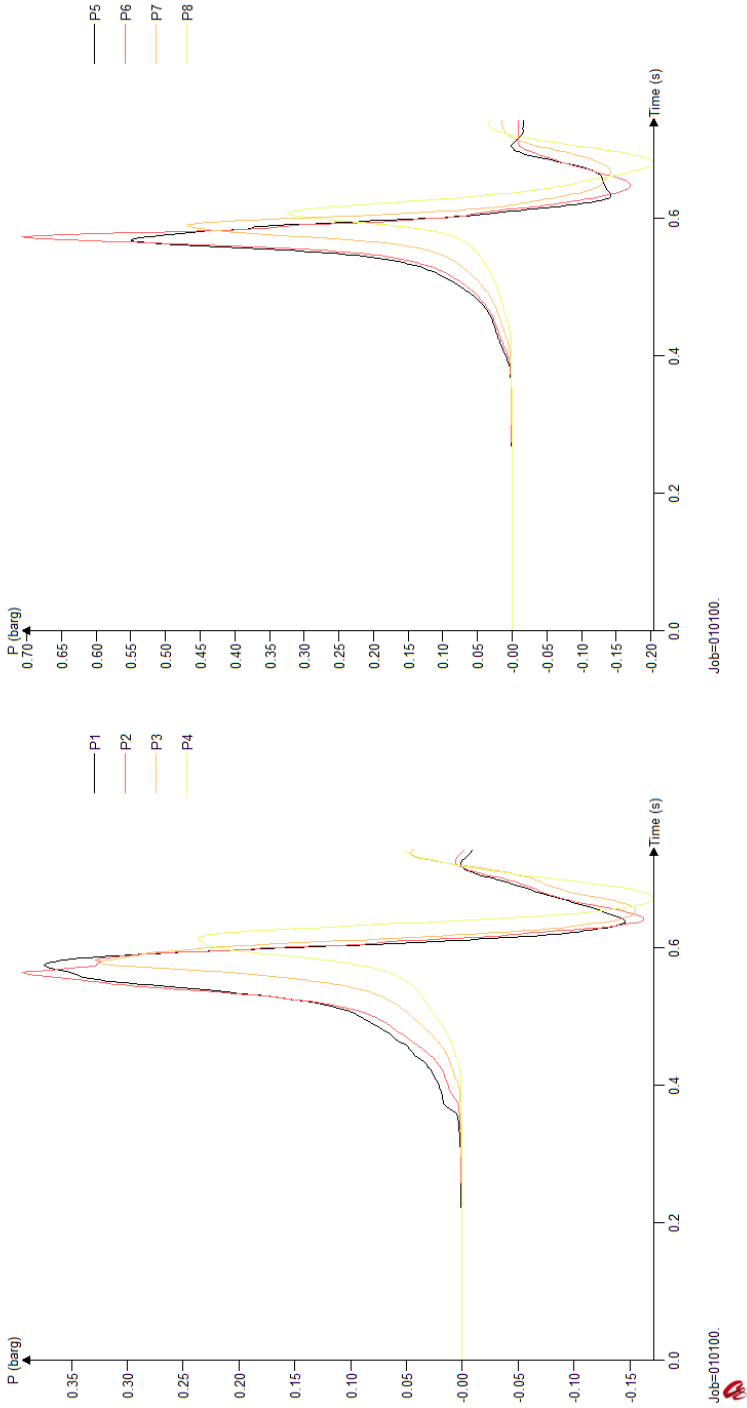


Figure 6.2: Maximum pressures at Monitor Points 1-8 for the detailed geometry of the C Module (See Simulation case 15 in Table 5.2)

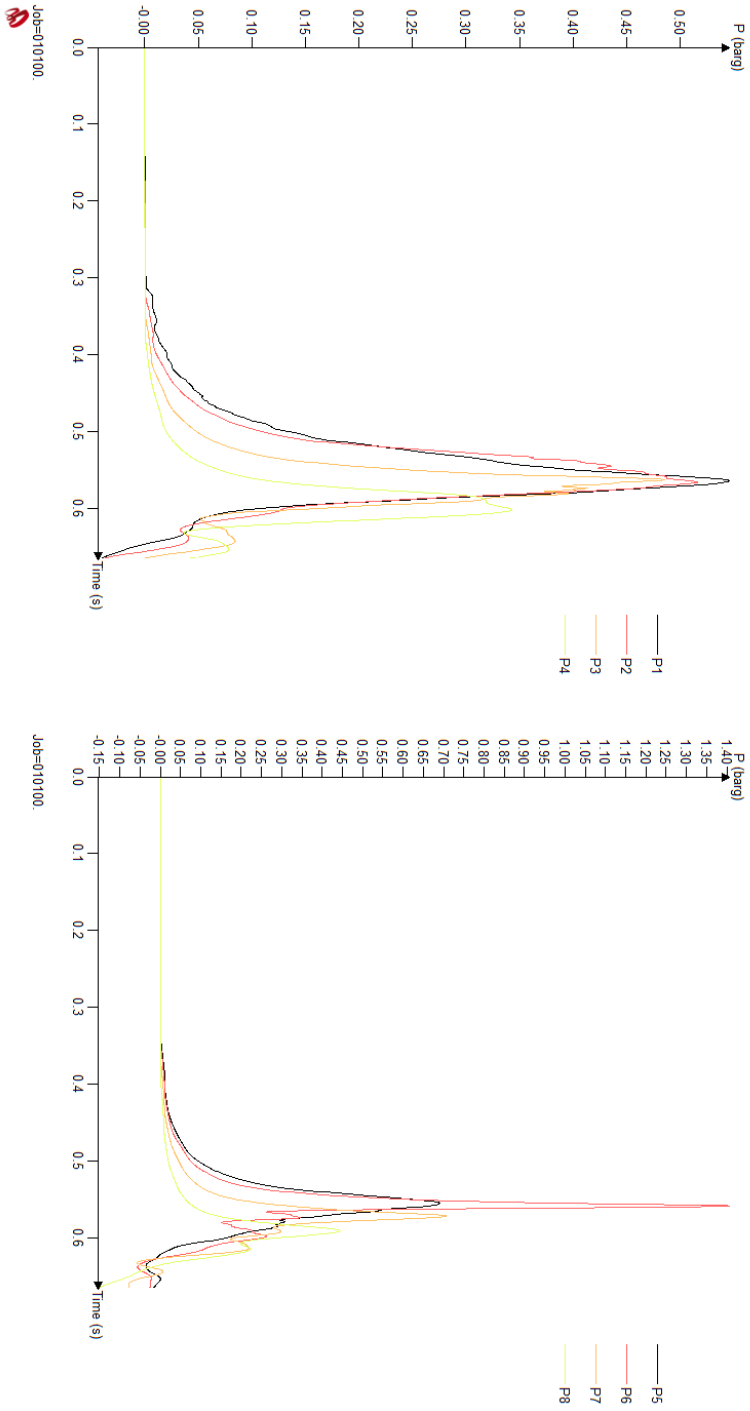


Figure 6.3: Maximum pressures at Monitor Points 1-8 for the geometry of the whole platform (See Simulation case 20 in Table 5.2)

The results from the simulation cases 6-20 all indicates that the cases 10, 15 and 20, which corresponds to simulation case 5 that were concluded with was the most likely, all is within the indicated pressure range of 0.3-0.7 bar [8]. Only MP6 for simulation case 20 is much higher than the given range.

6.4 Effect of the location of ignition point

For the discussion of the impact the location of the ignition source has on explosion loads, the cases 16 and 17 is used. The only change between these cases is the ignition source location, which is moved further into the module and down to the floor for case 17 compared to case 16. Position 2 is also closer to the C/B wall of the module.

Table 6.3: *The impact of ignition source location illustrated by the simulation cases 16 and 17 (See Table 5.2 and 5.4, Chapter 5).*

Simulation number	16	17
Ignition source location	Position 1	Position 2
Maximum pressure [barg]	2.337	1.253
Maximum pressure at	MP7	MP5
Time before maximum pressure [sec]	1.19	0.875

Both of the maximum pressures are for the C/D wall, but for simulation case 17 the maximum pressure is at the eastern part of the wall, and for 16 it is at the western part of the wall. The difference between the two pressures is approximately 1 barg, where the pressure is much higher with ignition source location at position 1 (case 16) compared to position 2 (case 17). Position 1 is at the eastern end of the module, at the centrifugal compressor, while position 2 is at module centre at the reciprocal compressor. By igniting near the wall, the pressure is significantly increased. A high flow velocity is generated ahead of the flame and generates turbulence by interaction with obstacles. In the eastern end, the flame will be pushed back by the ventilation inlets at the centrifugal compressor. Also for position 1 compared to position 2, the flame will have a longer distance to develop. The flame acceleration for a deflagration wave will increase due to enhanced burning due to turbulence generated by flow past several obstacles, reference is made to Chapter 3.1 in this thesis. With increasing temperature, the gas will expand and create a turbulent flow field, causing even higher pressures.

The peak pressure is also seen almost 0.5 seconds later for position 1 compared to position 2, which further illustrates that the pressure increases with the increased distance for the flame to accelerate on.

In the simulations performed in 1988/89 the overpressure were higher with ignition at the centre of the module, than with ignition at the end of the module. This is the opposite of what is found in the present thesis. This can be a result of the added congestion inside the C Module for the simulation cases 11-20 which will generate increased turbulence. This indicates the importance of including all of the geometry, also the small details.

6.5 Effect of gas cloud composition and dimension

For the discussion of the gas cloud dimension, the cases 16 and 19 are used. The only change between these cases is the gas cloud dimension, which are 50% of the volume of the C Module for simulation case 16 and 30% for case 19.

The impact of the gas cloud composition is illustrated by simulation cases 17 and 18, where the difference is that natural gas is used for case 17 and condensate for case 18.

Table 6.4: *The impact of gas cloud dimension illustrated by the simulation cases 16 and 19 (See Table 5.2, Chapter 5).*

Simulation number	16	19
Gas cloud dimension	50 %	30 %
Maximum pressure [<i>barg</i>]	2.337	1.148
Maximum pressure at	MP7	MP6
Time before maximum pressure [<i>sec</i>]	1.19	1.04

As seen in Table 6.4, a larger gas cloud generates a higher overpressure, it is approximately doubled when extending the dimension of the gas cloud from covering 30% of the volume of the C Module to covering 50% of the volume.

The conclusion in this thesis regarding the gas cloud dimension is the same as it was in the 1988/89 study, i.e. that a higher overpressure is generated with larger gas clouds.

Table 6.5: *The impact of gas cloud composition illustrated by the simulation cases 17 and 18 (See Table 5.2 and 5.3, Chapter 5).*

Simulation number	17	18
Gas cloud composition	Natural gas	Condensate
Maximum pressure [barg]	1.253	1.553
Maximum pressure at	MP5	MP5
Time before maximum pressure [sec]	0.875	0.770

The difference on pressure when changing the gas cloud composition is only 0.3 barg, compared to above 1 barg for the changes in ignition source location and gas dimension described above. This illustrates that the changes in ignition source location and gas dimension have a larger impact on the explosion loads than the gas composition.

The conclusion in this thesis is that condensate generates higher overpressure than natural gas, which is the same conclusion as was drawn in 1988/89.

The simulated gas composition for the two gases, are as given in Table 5.3 in Chapter 5.2. For condensate a lower content of methane is simulated with, than for natural gas. Fig 6.4 illustrates that with increasing content of methane, the overpressure is reduced. Methane is the least reactive fuel of methane and propane.

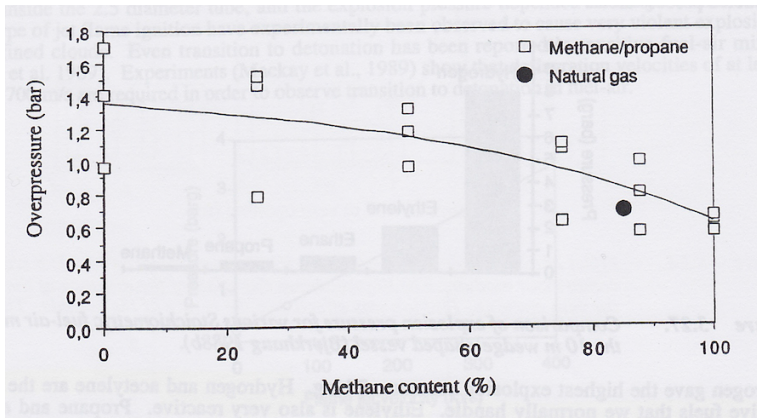


Figure 6.4: *Explosion pressure for natural gas, propane and methane in air. Illustration from Gas Explosion Handbook [7].*

6.6 Peak pressure

Table 6.6: *Time for peak pressures (approximately) for the simulation cases 1-20 (Table 5.2 in Chapter 5).*

Sim. case	Time [s]	Sim. case	Time [s]	Sim. case	Time [s]	Sim. case	Time [s]
1	1.2	6	1.0	11	0.7	16	1.05
2	1.0	7	0.9	12	0.7	17	0.7
3	1.0	8	0.7	13	0.6	18	0.6
4	1.2	9	1.9	14	0.7	19	0.9
5	0.9	10	0.7	15	0.6	20	0.6

As indicated in Table 6.6, the peak pressure for the last case (simulation case 5) that were concluded most realistic in 1988/89, are later than it is for the equivalent cases in this thesis. The peak pressure for simulation case 5 was observed at around 0.9 seconds, while for the re-simulations it was observed at 0.7, 0.6 and 0.6 seconds for the simulation cases 10, 15 and 20 respectively. The table also indicates that the general trend for the peak pressures for the re-simulations is that these are too early compared to the findings in 1988/89.

6.7 The firewalls

The inputs for the simulations in FLACS regarding the firewall porosity for maximum pressure for failure, were 0.138 barg for the C/B firewall and 0.250 bar for the C/D firewall. This is the same as was used in the simulations in 1988/89 [1, 2]. Fig.6.5- 6.7 below illustrates the panel porosity for the cases 10, 15 and 20 respectively. A 100% porosity means that the firewall was completely destroyed. The panel porosity for the other simulation cases are shown in Fig.C.38- C.43 Appendix C.

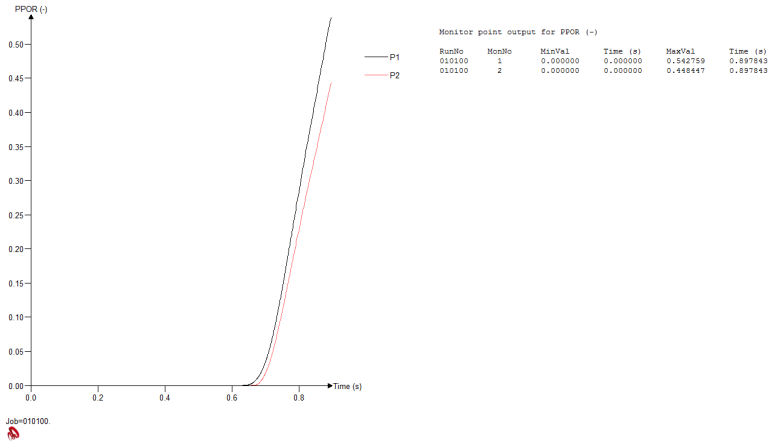


Figure 6.5: Panel porosity for simulation case 10.

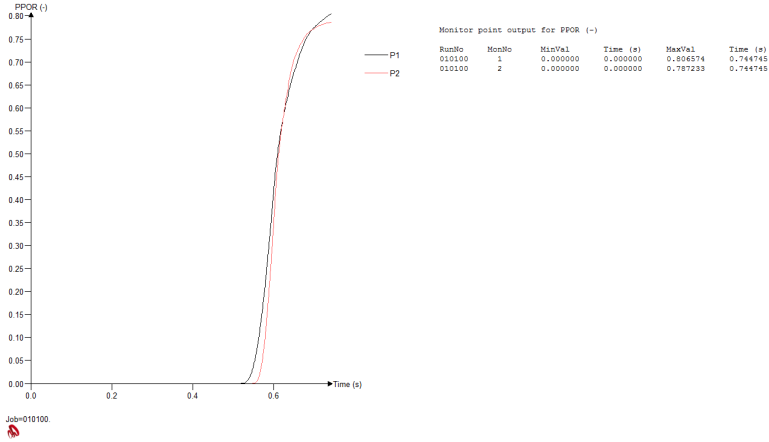


Figure 6.6: Panel porosity for simulation case 15.

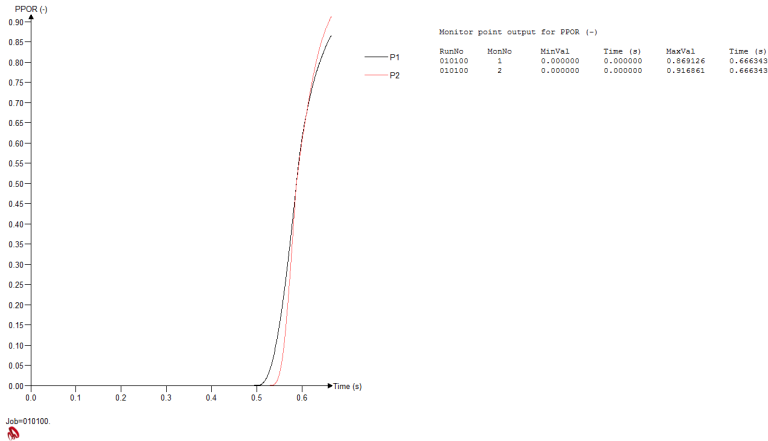


Figure 6.7: Panel porosity for simulation case 20.

In all of the cases 16-19, the porosity for both of the firewalls were approximately 100%. This indicates that the generated overpressure for the simulated scenarios are too high. Witness observations from the accident described that only the C/D firewall failed completely. For simulation case 20, the porosities were 54% for the C/B firewall and 45% for the C/D firewall. This indicates that for this simulation case, none of the firewalls were completely destroyed, but that the C/B firewall were more destroyed than the C/D firewall.

In 1988/89 the porosities of the firewalls were 20% and 40% for the C/B and C/D firewalls respectively [1, 2].

The results from these simulations also show that for simulation case 9, the firewalls did not fail. This result is the same as the result obtained in 1988/89 for the simulation case 4. The graphs also illustrate that the C/B firewall was more destroyed than the C/D firewall in all of the cases except 7, 8 and 16 where the porosity for the C/B firewall were lower than for the C/D firewall. For simulation case 13 the porosities for the two firewalls were approximately the same.

6.8 Discussion of the new simulation cases

In 1988/89 it was concluded that the generated gas cloud contained 46.1 kg of hydrocarbon within the flammable range. The cloud was assumed to be of a homogeneous and stoichiometric mixture [1, 2]. The monitored air changes per hour inside the module were 39, and it was further concluded that the leakage was of a two-staged leak; the first leak rate was $4 \frac{kg}{min}$ and the second was $100 \frac{kg}{min}$. Witnesses have described a noise, most likely the noise of the leak, lasting for approximately 30 seconds. [8]

For the final cases (case 21-26), both wind and dispersion have been included in the simulations. The results from these simulations are presented below in

Chapter 6.8.1 and Chapter 6.8.2, respectively. In Chapter 6.8.3 the results from the explosion scenarios for the last cases are presented.

6.8.1 Ventilation scenario

The wind conditions used for the simulations were as stated in Chapter 5.3. Fig. 6.8 shows the vector gradients for the ventilation inside the C module after 60 seconds. The gradients for both of the ignition point locations are pointing in the negative Y-direction. The air changes per hour calculated in the FLACS v10.0 utility program estimated the air changes per hour to be 67 for the entire module. When the simulation domain was changed to just include the centre of the module, this number increased to 87 air changes per hour. Both of these numbers indicates that the air changes per hour increase with natural ventilation of the module. The change in this value indicates that it depends strongly on where in the module the air changes per hour is monitored. Parts in the module with a strong ventilation flow pattern, as seen on Fig. 6.8 (the western half of the C Module), will give higher rates of air changes per hour than parts with a flow that is almost static (as seen in the eastern part of the module). Static flow may be due to equipment blocking for the flow. The ventilation is quite stagnant at the eastern part of the module, housing the centrifugal compressors.

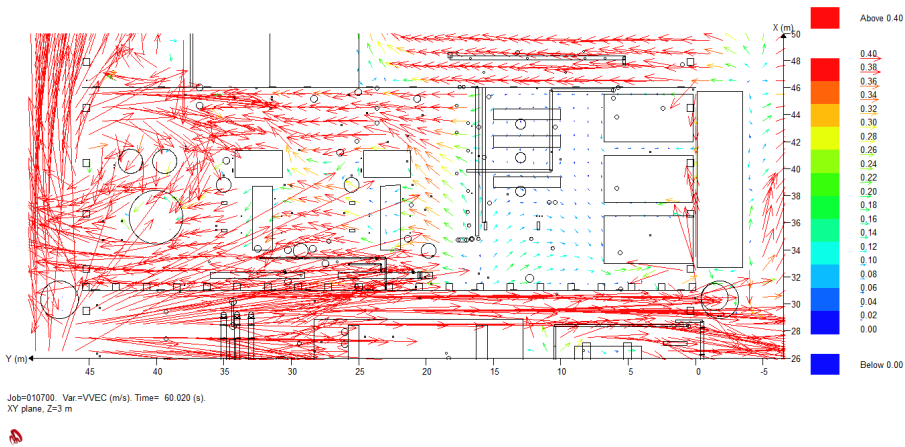


Figure 6.8: *Flow pattern inside the C Module which illustrates the ventilation due to added wind, after 60 seconds.*

6.8.2 Dispersion scenario

For the dispersion simulations different leak rates, positions and directions were simulated. The simulations with a flow direction in the Z-direction, both negative and positive, resulted in too good mixing of the fuel and air. This resulted in huge

stoichiometric clouds close to the floor. These clouds would have set off alarms in the entire module, not only in the C3-C5 zones as described in the Cullen report [8]. The leaked gas (condensate) had a higher density than air, and it will therefore first cover the floor level of the module before it raises. This is shown in Fig. 6.9, and in Fig. C.12 in Appendix C.

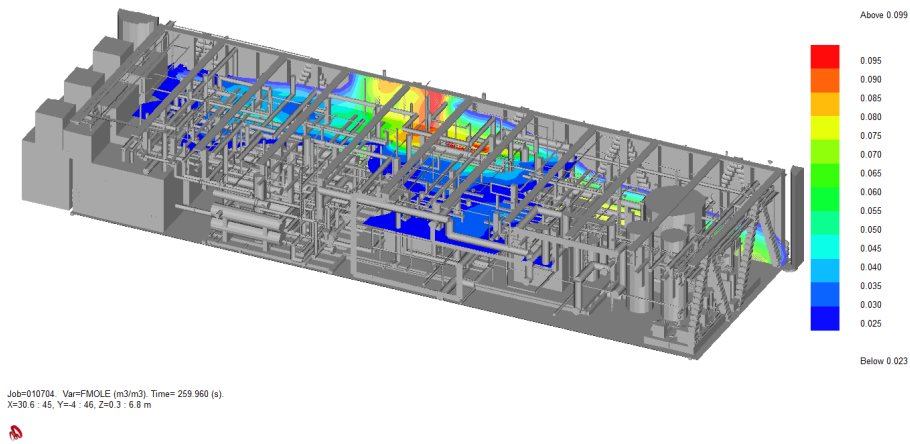


Figure 6.9: *Illustration of the gas cloud that sinks to the floor with a flow in the positive Z-direction.*

With a leak in the Z-direction, the generated overpressure would have been much higher than that experienced and concluded. Further gas explosion simulations have therefore only included the cases with a leakage direction in negative Y-direction.

The gas clouds generated by a leakage in the Z-directions are shown in Fig. 6.10 after a leakage lasting for about 40 seconds.

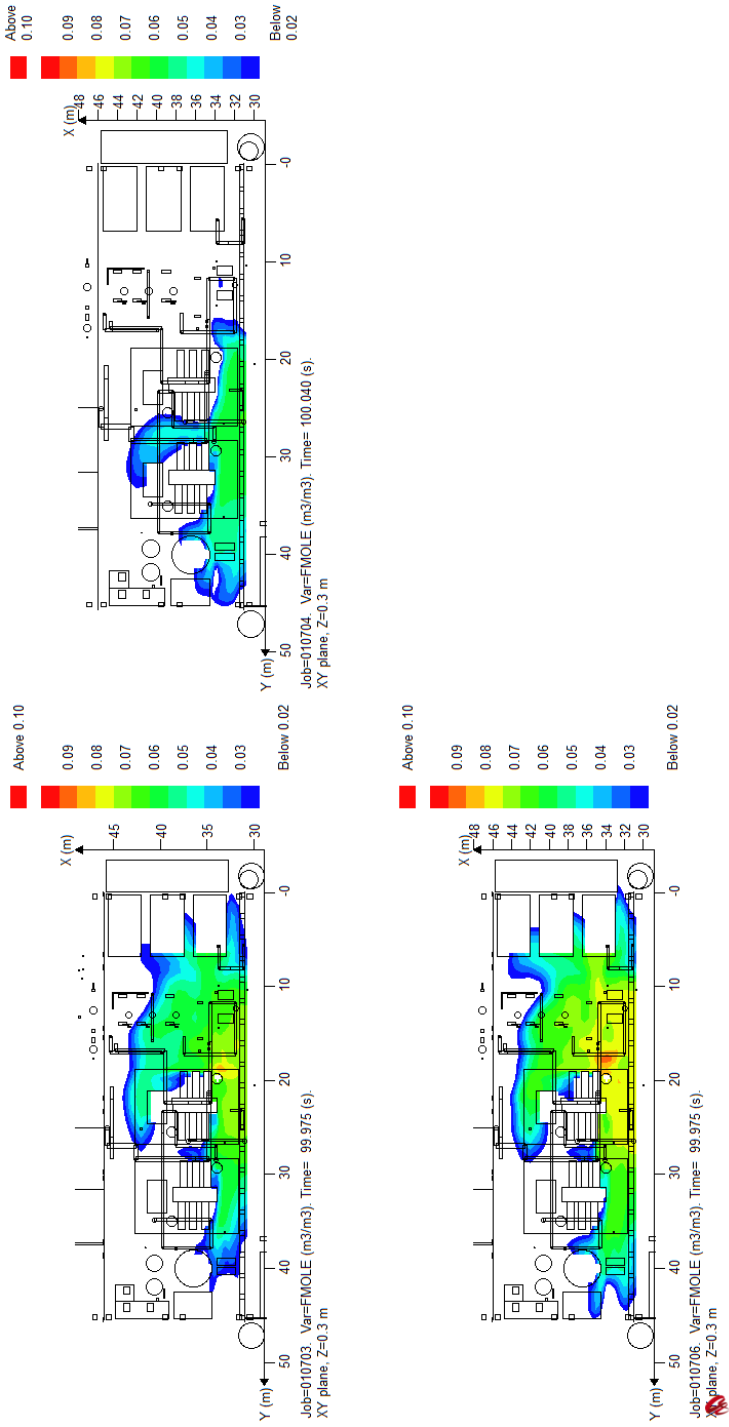


Figure 6.10: Illustration of the gas cloud generated after 40 seconds of leakage, for a leak direction in the negative Z-direction, positive Z-direction and negative Z-direction for respectively upper left, upper right and bottom left illustrations.

The observed mixing for the simulation cases 010703, 010704 and 010706, where the leak direction is in positive/negative Z-direction, is a result of the opposite directions of ventilation inside the module and the leak direction. The results are too good mixing between fuel and air, and the simulated gas clouds cover almost the entire module.

The generated flow patterns for the simulation cases 40 seconds after the leakage started are shown in Fig. 6.11 and Fig. 6.12 for the simulation cases 010701 and 010706 respectively. The flow pattern for the other cases are shown in Fig. C.13-C.16 in Appendix C.

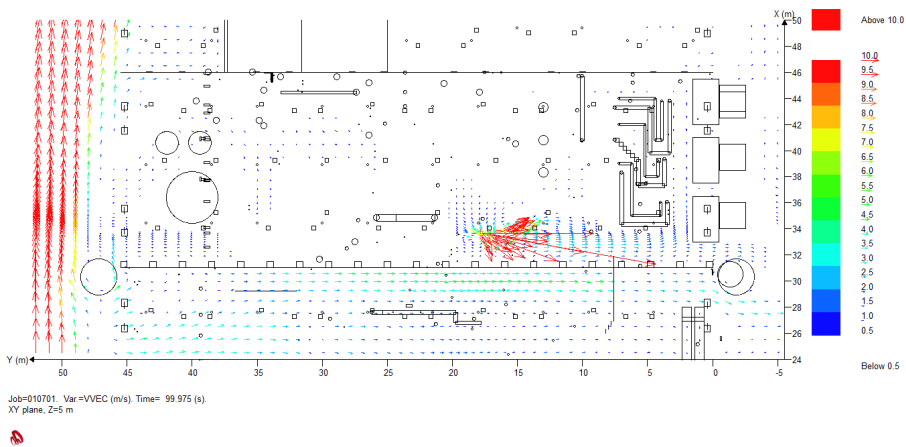


Figure 6.11: *Vector gradient for the leakage in simulation case 010701 after 40 seconds.*

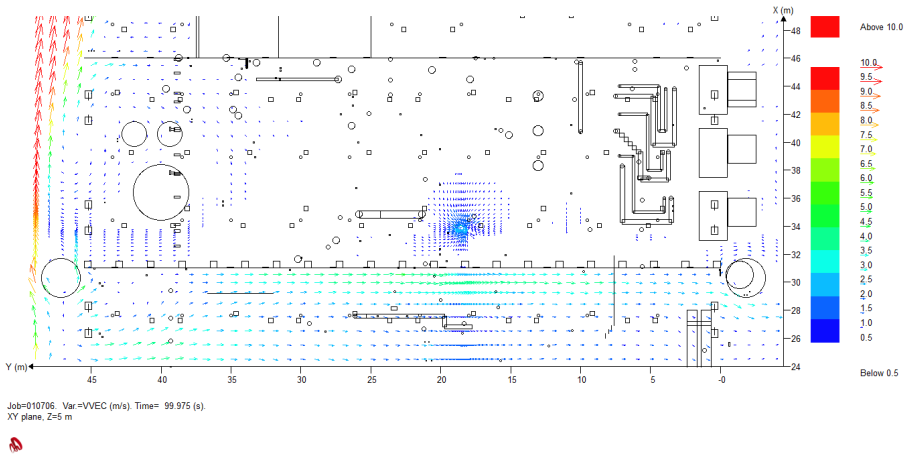


Figure 6.12: *Vector gradient for the leakage in simulation case 010706 after 40 seconds.*

Fig. 6.11 and Fig. 6.12 illustrates the differences in the mixing of fuel and air with different leak directions. For simulation case 010701, where the leak direction is in negative Y-direction, the leakage will contribute to a generated cloud of approximately the same amount of fuel within 40 seconds as that simulated in 1988/89, whereas for 010706 the generated cloud will be much larger, as seen in Fig. 6.13.

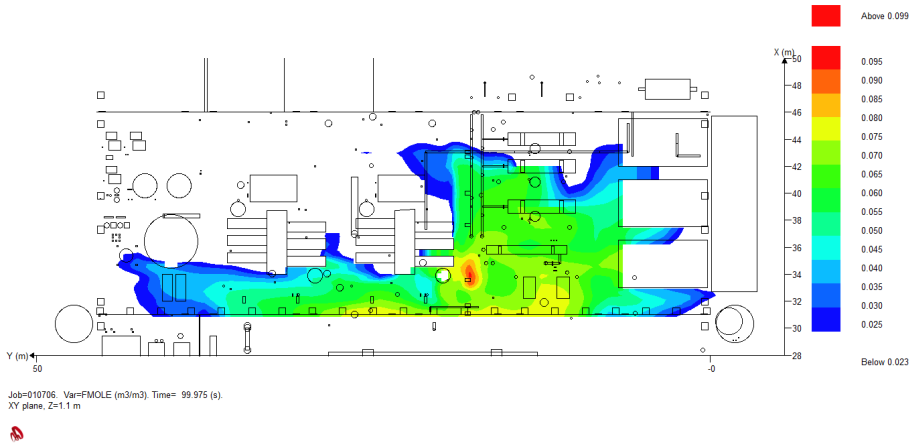


Figure 6.13: *The generated gas cloud after 40 seconds of leakage for dispersion simulation case 010706. Illustrates the amount of fuel within its flammable range (LFL and UFL).*

Fig. 6.14, illustrates the evolution of the cloud size (within the flammable range) for simulation case 010701, and as seen from this figure a flammable amount of fuel (y-axis) of approximately 50 kg is reached after around 100 seconds (x-axis). This was used as an input for the explosion scenarios so that these scenarios were started at 100 seconds, after 60 seconds of ventilation simulation and 40 seconds with leakage.

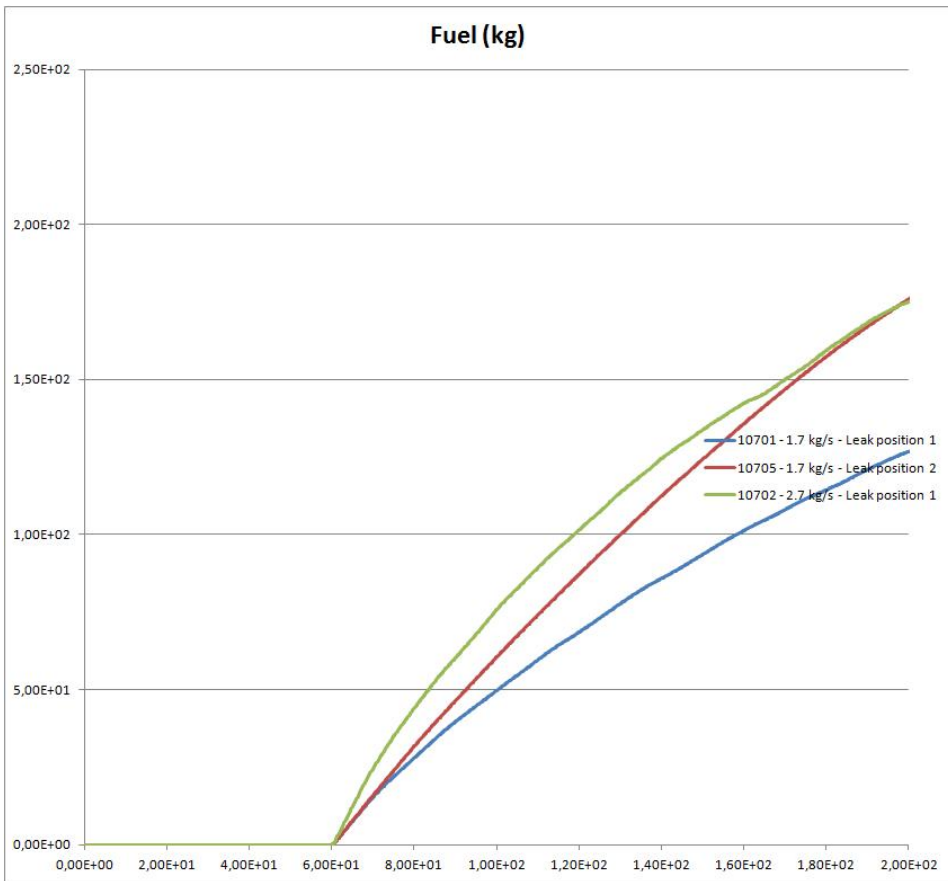


Figure 6.14: *Evolution of the cloud size.*

The dispersion simulations were also used to illustrate the gas detection pattern. The plots in Fig. 6.15- 6.16 shows the amount of fuel with time, illustrating the timing of the gas detectors by monitoring the fuel at each gas detector point.

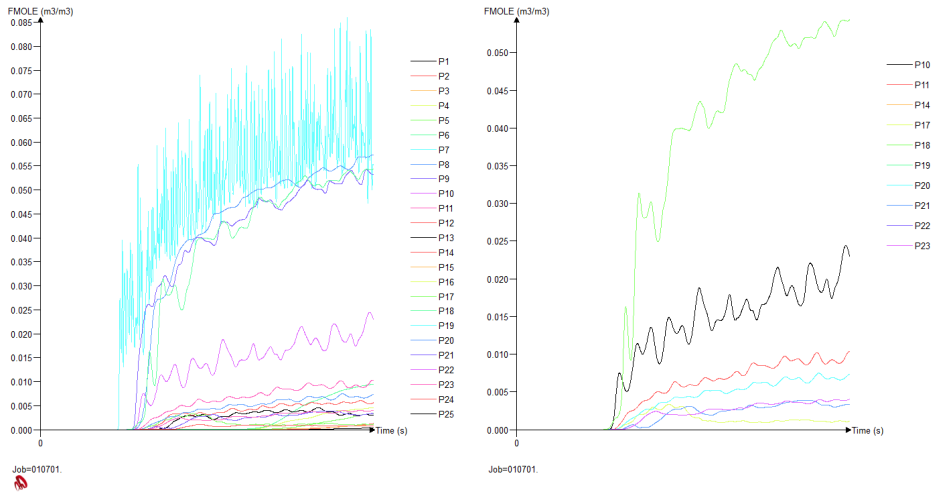


Figure 6.15: *Simulation case 010701. Left side: Gas detector pattern for the alarms in the C Module, right side: Gas detector pattern for the alarms in zone C3.*

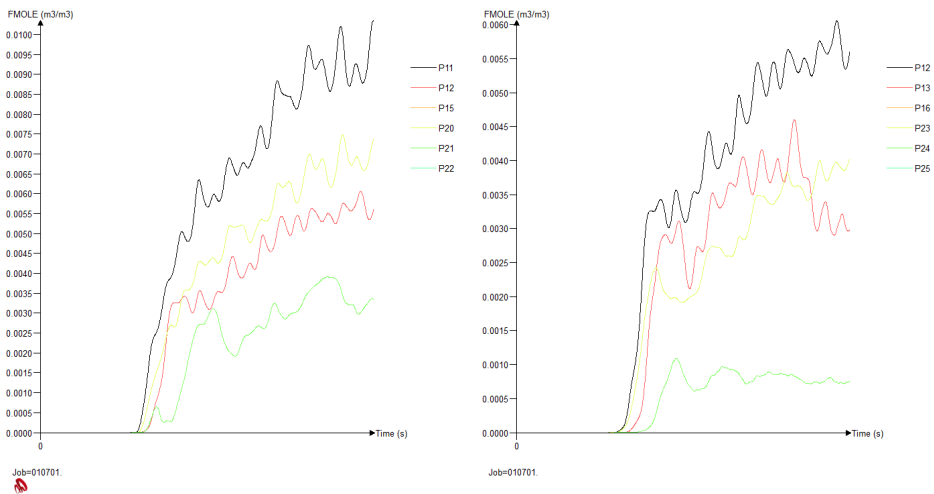


Figure 6.16: *Simulation case 010701. Left side: Gas detector pattern for the alarms in zone C4, lower right side: Gas detector pattern for the alarms in zone C5.*

The gas detector pattern for the other simulation cases (010702-010706) is shown in Fig. C.28- C.37 in Appendix C.

For the 3 cases where the clouds generated are close to the estimated amount

from 1988/89; case 010701, 010702 and 010705, case 010701 gives the best results in accordance to the gas detector alarms. Fig. 6.15- 6.16 shows the timing of the gas alarms for simulation case 010701. The witness descriptions of the gas detector pattern was presented in Chapter 3 in this thesis, and gas detectors that were observed to set off alarms were in the zones C3, C4 and C5 of the module. Gas detectors and zones are shown in Fig. B.1 in Appendix B. The curves for the simulation case 010701 are in quite good agreement with the witness descriptions of the gas alarm pattern, and the observed pattern from the wind tunnel tests [8]. The curves indicates that the alarms were first set off in the C1 and C2 zones with a couple of gas detectors in each zone, before the alarm pattern in high degree is for the zones C3-C5. This indicates that further simulations for the dispersion scenarios should be performed to optimize this pattern, but from the simulation cases that are simulated in this thesis, the observed pattern for 010701 is the best.

6.8.3 Explosion scenario

Based on the observations from the dispersion scenarios, the following of the dispersion simulation cases have been used as input for the explosion simulations:

- 010701
- 010702
- 010705

All of the above cases had leakage directions in the negative Y-direction. After 40 seconds with leakage, the 010701 case had generated a gas cloud of approximately 46 kg of fuel within the flammable range (Fig. 6.14).

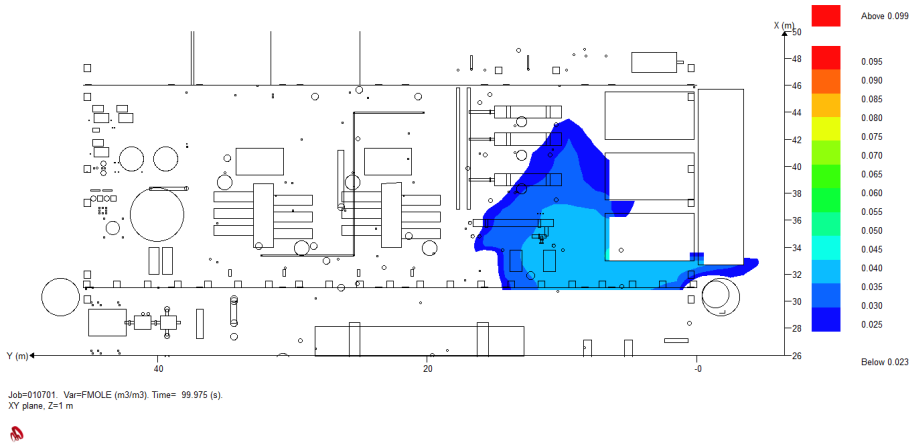


Figure 6.17: *The generated gas cloud after 40 seconds of leakage for dispersion simulation case 010701. Illustrates the amount of fuel within its flammable range (LFL and UFL).*

Fig. 6.17 illustrates the amount of fuel within flammable range for the dispersion case 010701 at the time of ignition.

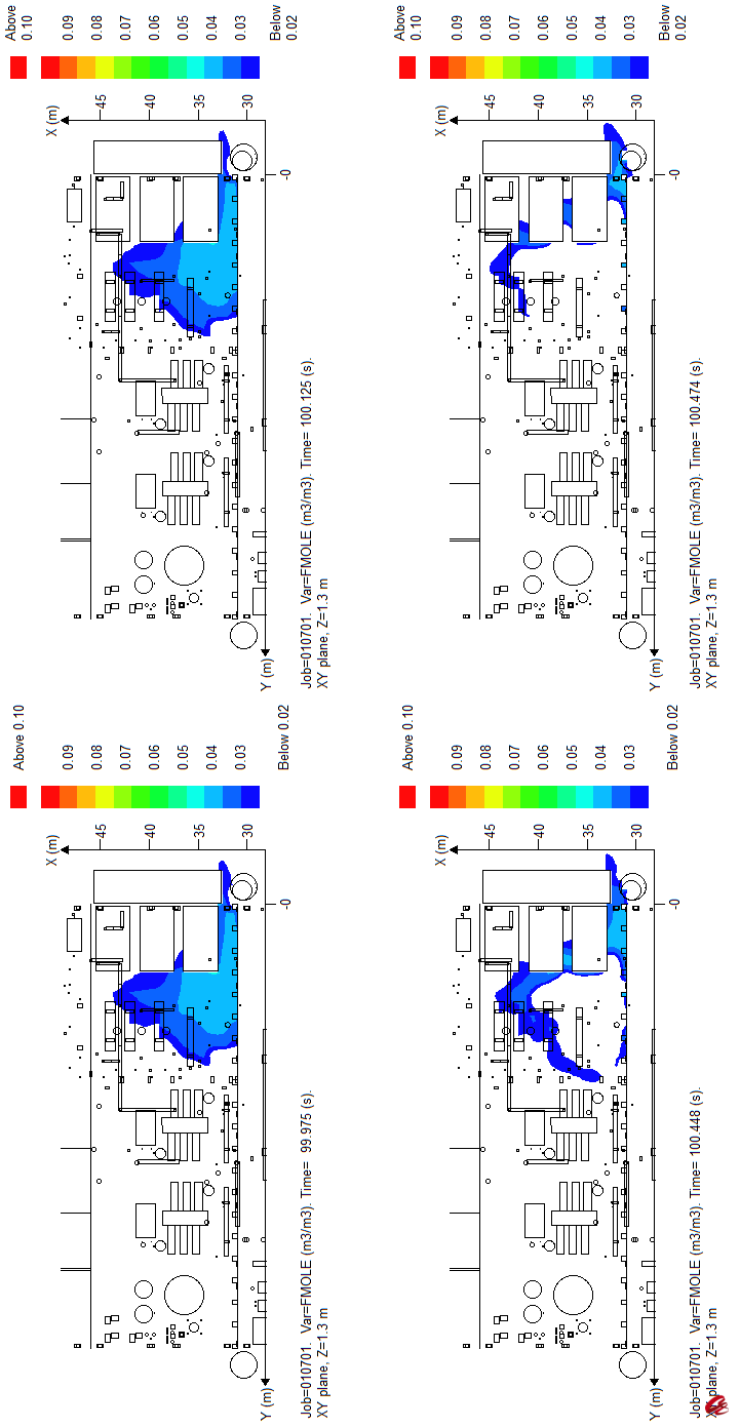


Figure 6.18: Figure illustrating the gas cloud for simulation case 010701 with time after ignition. The amount of fuel within its flammable range (LFL and UFL) is decreasing with time.

Fig. 6.18 illustrates the amount of flammable fuel at the time of ignition, and after. The figure illustrates that once the gas cloud is ignited, the gas will expand and the flame front propagates rapidly. Only the amount of fuel within the flammable range will contribute to overpressure. Further, it illustrates that the gas concentration is decreasing due to that the leak rate is lower than the amount of gas which is carried away by the ventilation (Chapter 3.2.3).

Table 6.7: *Maximum pressures at Monitor Points 1-8 for the simulation cases 21-25 (Table 5.6 in Chapter 5).*

	Maximum pressure							
Sim. case	MP1	MP2	MP3	MP4	MP5	MP6	MP7	MP8
21	0.486	0.437	0.372	0.271	0.506	0.449	0.367	0.283
22	1.152	1.045	0.816	0.588	1.220	1.104	0.836	0.637
23	0.883	0.821	0.721	0.508	1.251	1.155	1.763	0.584
24	0.315	0.429	0.330	0.211	0.281	0.275	0.282	0.188
25	0.819	1.299	0.837	0.514	0.598	0.902	0.742	0.600

The simulated overpressure for the 6 new simulation cases, show that simulation case 21 generates overpressure that is in the range of 0.3-0.7 barg. Simulation case 24 has value just below the range, while the cases 22, 23 and 25 have values above.

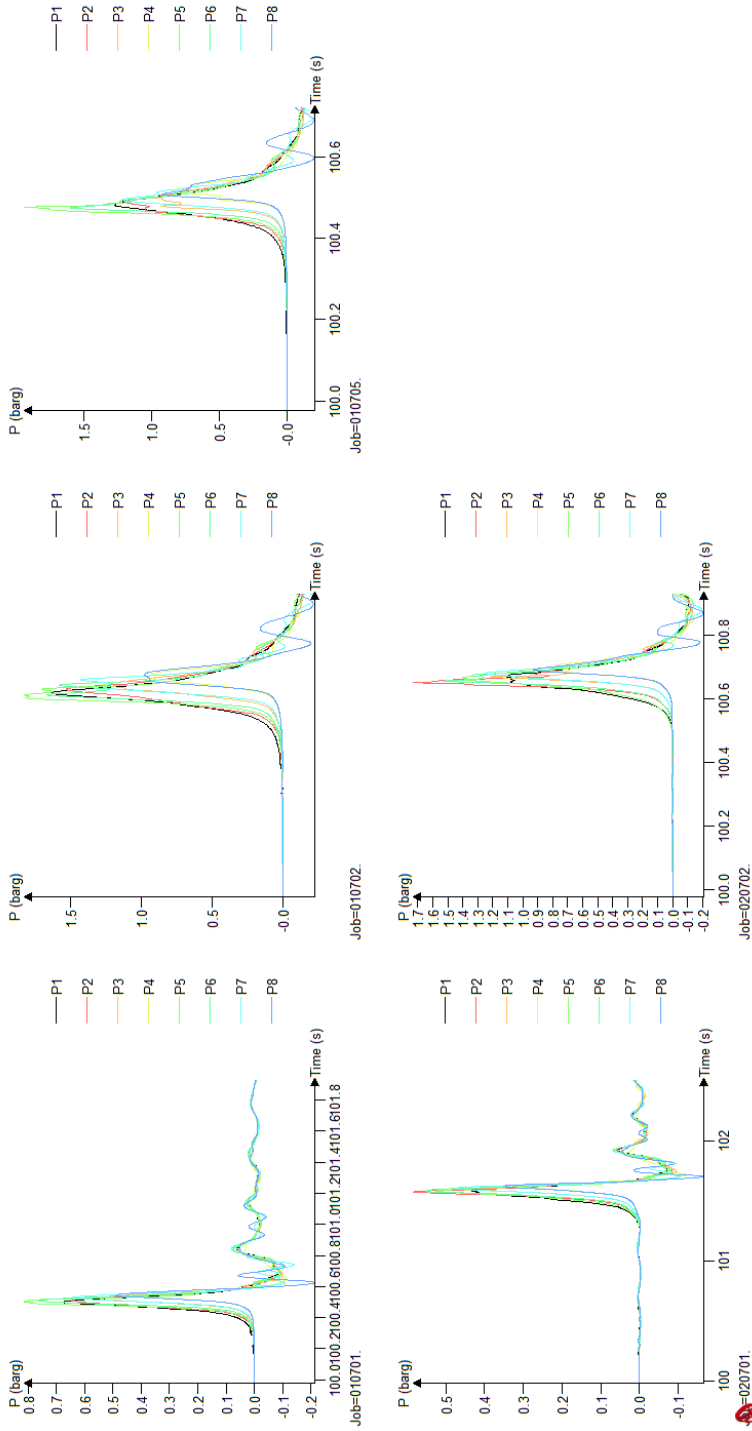


Figure 6.19: Maximum pressures at Monitor Points 1-8 for the new simulation cases. The last case did not result in an ignition. (See Simulation cases 21-26 in Table 5.6).

6.8.4 Peak pressure new cases

Table 6.8: *Time after ignition for peak pressures (approximately) for the simulation cases 21-26 (Table 5.6 in Chapter 5).*

Sim. case	Time [s]
21	0.5
22	0.45
23	0.5
24	1.6
25	0.7

Table 6.8 shows the time after ignition for the peak pressures for each of the new simulation cases. For the simulation cases 21-23 the peak pressures are around 0.5 seconds, while for simulation case 24 it is after approximately 1.6 seconds.

6.8.5 Firewalls

Fig. 6.20 shows the firewall porosities for the C/B and C/D firewalls for simulation case 21. The graphs for simulation cases 22-26 are shown in Fig. C.44- C.47 in Appendix C.

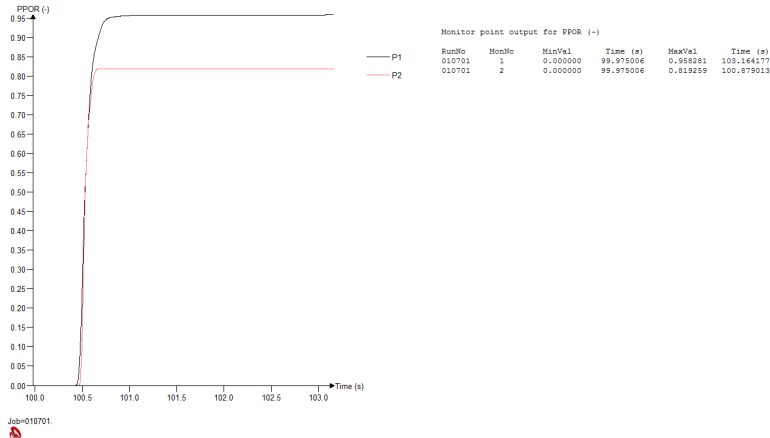


Figure 6.20: *Panel porosity for simulation case 21 (See Table 5.6.)*

For the simulation cases 21-25, the firewalls are almost completely destroyed. The porosities for the firewalls are nearly 100% for all of the cases, except simulation case 24 where the porosities are 86% and 64% for the C/B and C/D firewalls, respectively. Also, for the cases 21, 24 and 25 the C/B firewall is more destroyed than the C/D firewall. For simulation case 23 the C/D firewall has a slightly higher

porosity than the C/B firewall, and for case 22 the porosities are almost the same for the two firewalls.

Discussion of leak rate

Simulation cases 21, 23 and 24 are simulated with a leak rate of $1.7 \frac{kg}{s}$, while a leak rate of $2.7 \frac{kg}{s}$ is used for cases 22 and 25. Simulation case 26 is not considered here, as no ignition occurred. This is further discussed below in Chapter 6.8.5. As shown in Fig. 6.19 the simulated overpressure for cases 21 and 24 are lower than for the cases 22, 23 and 25. This indicates that the leak rate will have an impact on the generated overpressure; with increasing leak rate the pressures will also increase. But simulation case 23 with a low leak rate, generates a high overpressure. For this simulation case the leak direction is in the negative Z-direction. As stated above in Chapter 6.8.2, this will generate high pressures due to the really good mixing of fuel and air. The low leak rate will generate a leaner cloud than a higher leak rate. With ignition at a richer cloud the generated overpressure will be higher than with ignition at a leaner cloud.

The observations for the leak rates are in accordance with the experiments performed by Wingerden et al. [23], where it was concluded that the overall gas concentration in the flammable part of the cloud is dictated by both the release rate as well as the size of the cloud.

Discussion of ignition point location

For simulation case 26, no ignition will occur. As shown on Fig. 6.21 the ignition region at the time of ignition is on the outside of the flammable part of the simulated gas cloud. This result illustrates the impact the ignition source location has on the generated overpressure.

For simulation cases 21-23, the ignition source location is near the south wall, while for the cases 24 and 25 the location of ignition is in the middle of the C Module at the reciprocal compressors. With the ignition location near the south wall, the simulated overpressure is much higher than for ignition at the reciprocal compressors. For position 1, the flames are pushed back by the wall, and the gas is not allowed to expand freely in all directions, as it is with ignition at Position 2.

The ignition source location for simulation cases 21-23 is in the middle of the generated cloud, in contrast to the location for cases 24 and 25, where it is on the edge of the cloud. As presented in Chapter 3.2.3, the lowest pressure is in general obtained if the ignition point is close to the vent area or at the edge of the cloud. The results from the simulation cases 21-25, illustrates that lower pressures are generated with ignition at the edge of the cloud than with ignition in the middle.

For the cases 21-23, the flame will also have to travel past more obstacles and it has a longer distance to develop on, compared to the cases 24-25. This will generate turbulence and increase the burning rate and the explosion pressure.

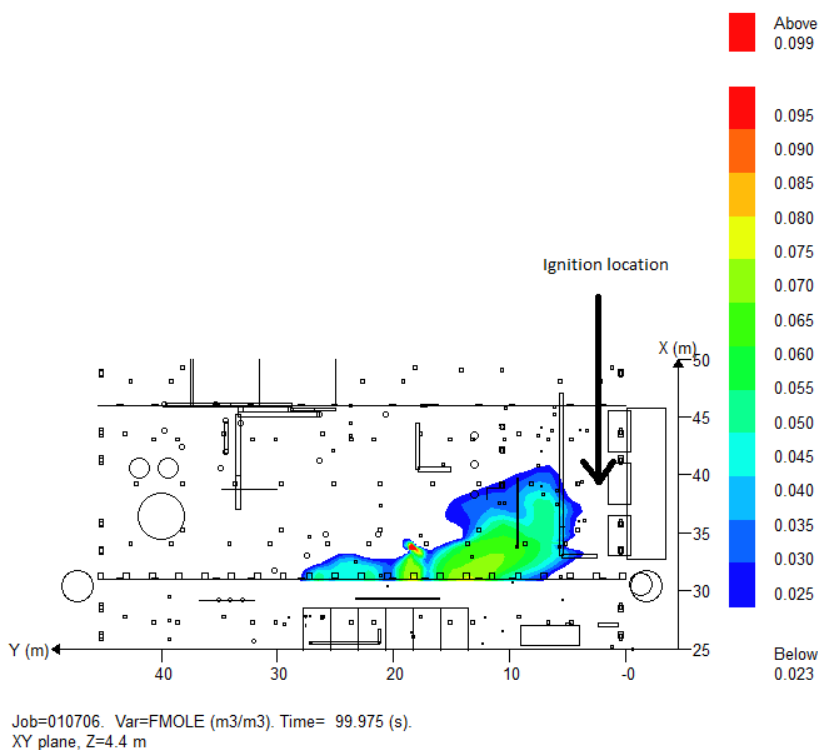


Figure 6.21: *Ignition region, gas cloud size and richness for simulation case 26 at the time of ignition.*

Discussion of leak position

Two different leak positions were used for the dispersion simulations. These are shown in Table 5.5, Fig. 5.12 and Fig. 5.13 in Chapter 5.3.1. Position 1 was used for the cases 21, 22, 24 and 25, while Position 2 was used for simulation cases 23 and 26.

The simulation cases 21 and 23 have the same leak rates, leak directions and ignition point locations. The only difference between these two cases is the leak position. The maximum pressures of simulation case 23 are approximately the double of the maximum pressures for simulation case 21. This illustrates the importance of the leak position to the generated explosion pressures. Fig. 5.12 and Fig. 5.13 in Chapter 5.3.1 illustrates the generated gas cloud size at time of ignition. From these two figures it can be seen that a larger cloud is generated for the simulation

case 21 (leak position 1) than for case 23 (leak position 2), but the cloud for case 23 is richer than for case 21. The cloud generated with leak position 2 is also richer at the location of ignition. This also illustrates that a richer cloud, given that it is in between the flammability levels, generates higher overpressure than a leaner cloud within its flammability limits.

Discussion of gas cloud size and composition

The differences between simulation cases 20 and 21 are the generated gas cloud; its composition and extension/dimension. For simulation case 20, the gas cloud is simulated with gas composition for condensate as given in Table 5.3 (Chapter 5.2), while for simulation case 21 the composition is also for condensate but as given in Table 5.7 (Chapter 5.3.1). The generated cloud for the case 20 is simulated as a homogeneous cloud of stoichiometric mixture with fuel region as shown in Fig. 5.11. For simulation case 21, the gas is generated through a dispersion simulation with a leak rate of $1.7 \frac{kg}{s}$ lasting for 40 seconds. The generated cloud for simulation case 21 is shown in Fig. 6.17.

Maximum overpressure for simulation case 21 was about 0.5 barg (MP5), while it was just above 1.4 barg (MP6) for simulation case 20. This indicates what was found in the experiments performed by Wingerden et al. ([23]); explosions due to non-homogeneous gas clouds filling only a part of a module are expected to give rise to lower explosion overpressure than those expected from homogeneous, stoichiometric clouds in the same module.

The gas composition used for case 20 consisted of 40.04 volume % methane and 59.96 volume % propane. For simulation case 21 the composition included more gases, but the amount of methane was reduced to 19.86 volume % and the amount of propane to 31.06 volume %. This illustrates the opposite of what was found in Chapter 6.8.5, that with increasing content of methane, the overpressure is reduced, and also what was shown in Fig. 6.4. But for these cases, the gas composition is not the only parameter that is changed, and therefore the discussion basis is not as good as it should be. This only indicates that the generated gas cloud extension impacts more on the explosion pressure than the gas composition, and that it would be expected that if the only parameter changed had been real versus homogeneous and stoichiometric gas cloud, the difference would have been even bigger than that illustrated in this thesis.

Chapter 7

Conclusion and Recommendations

In this chapter a conclusion to the work performed in this thesis, together with recommendations for further work is presented.

7.1 Conclusion

The goal of this thesis was to re-simulate the accident at the Piper Alpha platform, and to evaluate what would be the effect on the simulated overpressure by using the latest version of the FLACS code, and by using the added features of this code compared to the code used in the 1988/89 simulations. Such added features include allowing a more complex geometry model, and to include impact of wind and dispersion. The second aim was to define new simulation cases based on simulation of more exact conditions during the accident.

Differences between the findings from the simulations performed in 1988/89 and the results in this thesis have been highlighted. Whether these differences are due to the newer version of FLACS, the geometry model itself or the location of the monitor points, cannot be stated. Most likely it is a combination of all of these factors, in addition to the chosen grid and simulation volume in this thesis versus the simulations in 1988/89. Also, some of the differences between the FLACS codes were highlighted; improvements in the combustion modelling, thermodynamics and geometry modelling.

One observation to be made from this work is that small things matter. The increased congestion for the simulation cases 11-20 versus the simulation cases 6-10, significantly increased the simulated overpressure. The overpressure was approximately doubled when going from the simplified geometry to the detailed geometry of the C Module, and even further doubled when also including the entire platform in the simulation domain.

Simulations with ignition near the wall also resulted in significantly higher overpressure than ignition in the middle of the module. This is the opposite of what

was concluded from the simulations in 1988/89, but can be explained as follows; Ignition near a wall will generate a high flow velocity ahead of the flame which will generate turbulence by interaction with obstacles and hence support a high burning rate and cause high explosion pressures.

The conclusion in this thesis regarding the gas cloud dimension is the same as it was in the 1988/89 study, i.e. that a higher overpressure is generated with a gas cloud covering 50% of the volume compared to a gas cloud that is covering 30% of the volume. Also, the generated overpressure for the first 15 simulation cases, indicates that the overpressure for equivalent stoichiometric clouds is higher than for real non-equivalent clouds as those generated in simulation cases 21-26.

The simulations for the dispersion cases, were simulated with a low leak rate. This illustrates one of the effects wind can have on the explosion loads; it can dilute the gas cloud and contribute to lower pressures. It was further found that leak rate, leak position and leak direction will impact on the generated overpressure. The overpressure increased with increasing leak rate, and by moving the leak position the generated overpressure was significantly increased. The leak direction gave too large clouds when assuming a leakage perpendicular to the ventilation gradient at the location of the leak. Smaller clouds were generated with a leakage in the same direction as the ventilation, and these clouds were in good agreement with the concluded amount of fuel from the 1988/89 simulations.

The firewalls failed for all of the cases except simulation case 9. Simulation case 9 is equivalent to case 4 from 1988/89, and also for this case the firewalls did not fail. When including more details to the geometry and also the entire platform, the firewalls failed also for this scenario. Another finding in this thesis was that for most of the scenarios, the C/B firewall experienced a greater degree of destruction than the C/D firewall.

The results from the simulation cases 6-20 all indicates that the cases 10, 15 and 20, which corresponds to simulation case 5 of the 1988/89 study, and which was concluded to be the most likely, are all within the indicated pressure range of 0.3-0.7 barg [8]. Only MP6 for simulation case 20 is much higher than the given range. The new simulation cases 21 and 24 are also in between the given range of 0.3-0.7 barg.

Only two leak positions were simulated as part of the present study. Since only a limited amount of simulations have been performed, there is a risk that not all of the outcomes are included, and it is therefore not possible to conclude that the lowest/ highest overpressure has been found.

Simulation case 21 gives a good indication of what happened with more exact conditions, and the gas detector readings for this case was also the most accurate of the ones simulated. When simulating a real gas cloud, which will change in time, and both size and concentration will vary, a number of different simulations could be performed to account for all the time steps. These simulations could further include several different ignition points over time to map this fact. With simulation case 21 as a starting point, it is therefore recommended to use the model developed in this work to perform further simulations to better illustrate what happened.

7.2 Future work

Some further simulations of the accident could possibly result in an improvement of the actually scenario that happened. A possible way to do this, is to start with the simulation case 21 in this thesis, and simulate with several different leak positions, leak rates and ignition point locations.

This thesis also illustrated that for the scenarios simulated, the C/B firewall experienced a greater extent of destruction than the C/D firewall. Scenarios to be simulated should therefore aim at obtaining the opposite results. Also the degree of damage on the walls during the explosion is too high compared to the witness statements. This might be an indication that the generated pressures in the scenarios simulated in this thesis, are too high, and that a smaller amount of fuel was released prior to the explosion. Further work could therefore also include simulations with smaller fuel amounts.

Appendix A

Limitations and assumptions

Time frame and refinements:

- The extent of this thesis is a Master's degree of 30 academic credits
- For the purpose of comparison, the simulations are limited to the same cases as those from 1988/89 (Chapter 6)
- Simulation of additional cases, including wind and leak dispersion, are performed to get a better understanding of what happened
- The modelling of the platform became a greater part of the work than first anticipated, which results in fewer but more accurate simulations

Assumptions:

- The general dimensions and layout of equipment and piping in A-D Modules are based on drawings and model photographs [6]
- The ignition source is unknown, it was most likely an electrostatic spark [8]
- Parameters like extent of gas cloud, gas type and ignition location were varied for simulation cases 1-20, see Table 5.2
- Parameters for the cases 21-26 are based on results from the 15 first cases simulated in this thesis, and the witness statements given in the Cullen report [8]
- Properties of firewalls between the B/C Module and the C/D Module are the same as used in 1988/89, except for the end porosity which is set to 100% (completely open) [1, 2]
- Simulation gas composition for simulation cases 1-20 as used in 1988/89 [1, 2]
- For simulation cases 1-20 it is assumed that there is no wind inside the modules, no leak during the explosion and that the generated gas cloud was an equivalent, homogeneous and stoichiometric cloud

Additional assumptions for simulation cases 21-26:

- Wind conditions are as given in Chapter 5.3.1
- Leak rates, leak positions and ignition source locations that are simulated are given in Table 5.6
- The leakage source was most likely a blind flange that replaced PSV 504 on Condensate Pump A in the C Module
- Gas composition as given in Table 5.7

Appendix B

Model pictures

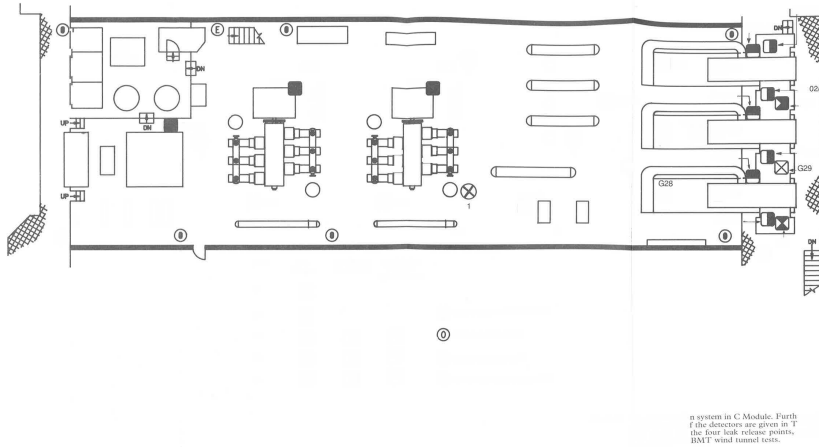


Figure B.1: *The gas detectors and zones in the C Module. Illustration taken from the Cullen report [8].*

Monitor point output for FMOLE (m3/m3)

RunNo	MonNo	MinVal	Time (s)	MaxVal	Time (s)
010701	1	0.000000	0.000000	0.000357	260.025024
010701	2	0.000000	0.000000	0.001295	260.025024
010701	3	0.000000	0.000000	0.001115	260.025024
010701	4	0.000000	0.000000	0.004516	257.475006
010701	5	0.000000	0.000000	0.003509	260.025024
010701	6	0.000000	0.000000	0.009515	260.025024
010701	7	0.000000	0.000000	0.085924	238.725006
010701	8	0.000000	0.000000	0.057371	259.125000
010701	9	0.000000	0.000000	0.054244	253.875013
010701	10	0.000000	0.000000	0.024446	256.424988
010701	11	0.000000	0.000000	0.010346	259.125000
010701	12	0.000000	0.000000	0.006059	249.375013
010701	13	0.000000	0.000000	0.004604	216.375013
010701	14	0.000000	0.000000	0.000000	0.000000
010701	15	0.000000	0.000000	0.000000	0.000000
010701	16	0.000000	0.000000	0.000000	0.000000
010701	17	0.000000	0.000000	0.003337	118.725006
010701	18	0.000000	0.000000	0.054620	260.025024
010701	19	0.000000	0.000000	0.000000	0.000000
010701	20	0.000000	0.000000	0.007483	235.275009
010701	21	0.000000	0.000000	0.003912	223.575012
010701	22	0.000000	0.000000	0.000000	0.000000
010701	23	0.000000	0.000000	0.004053	260.025024
010701	24	0.000000	0.000000	0.001094	124.575005
010701	25	0.000000	0.000000	0.000000	0.000000

Figure B.3: Location of gas detector monitor points for the dispersion simulation cases.

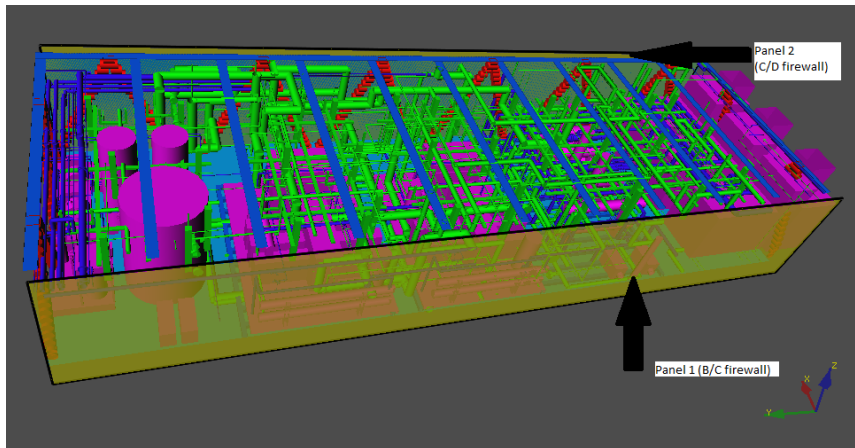


Figure B.4: Location of the C/B and C/D firewalls.

Appendix C

Simulation output

C.1 Pressure plots

Simplified Geometry

The figures below are for simulation cases 6-10, where Job Number 010101, 010102, 010103, 010104 and 010100 refers to simulation cases 6, 7, 8, 9 and 10, respectively.

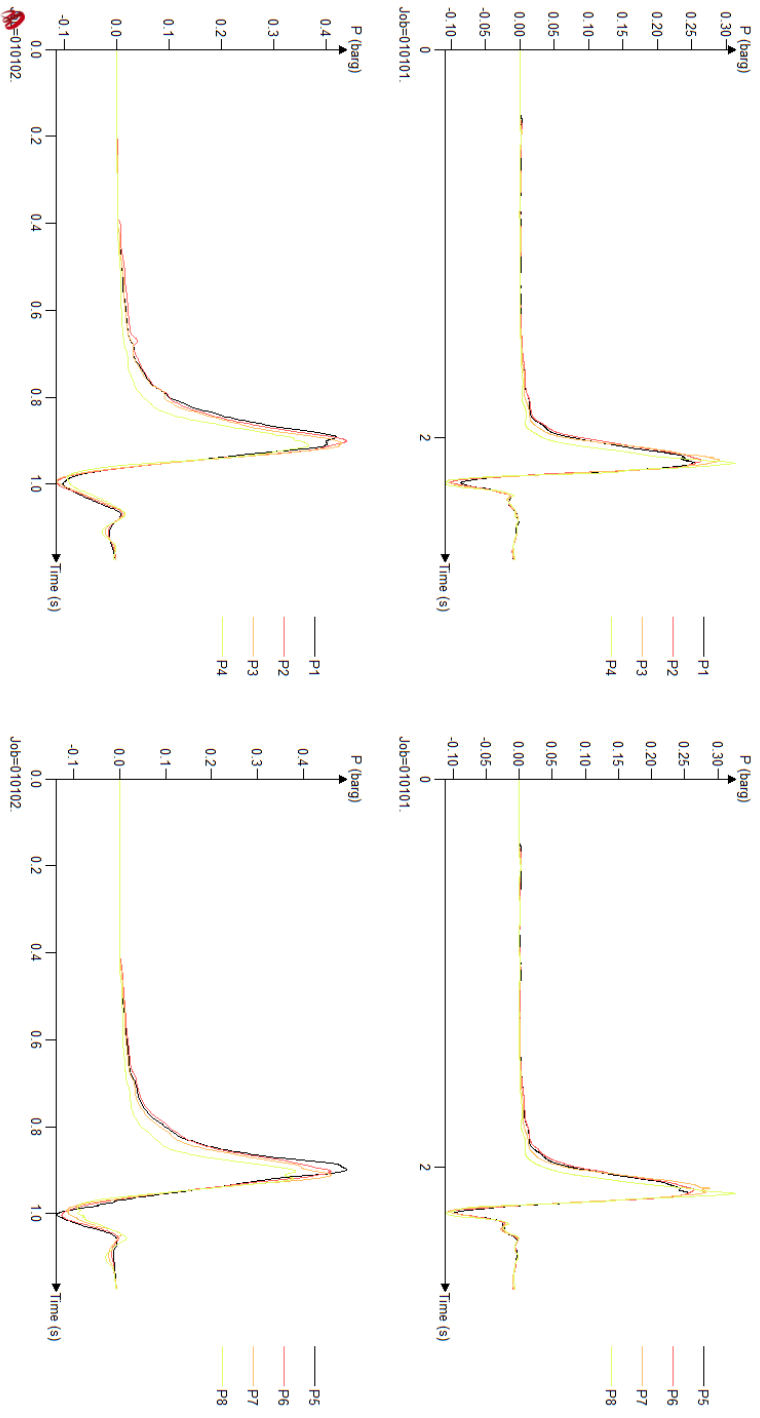


Figure C.1: Maximum pressures at Monitor Points 1-8 for the simplified geometry of the C Module for simulation cases 6 and 7 (See Simulation cases 6-10 in Table 5.2)

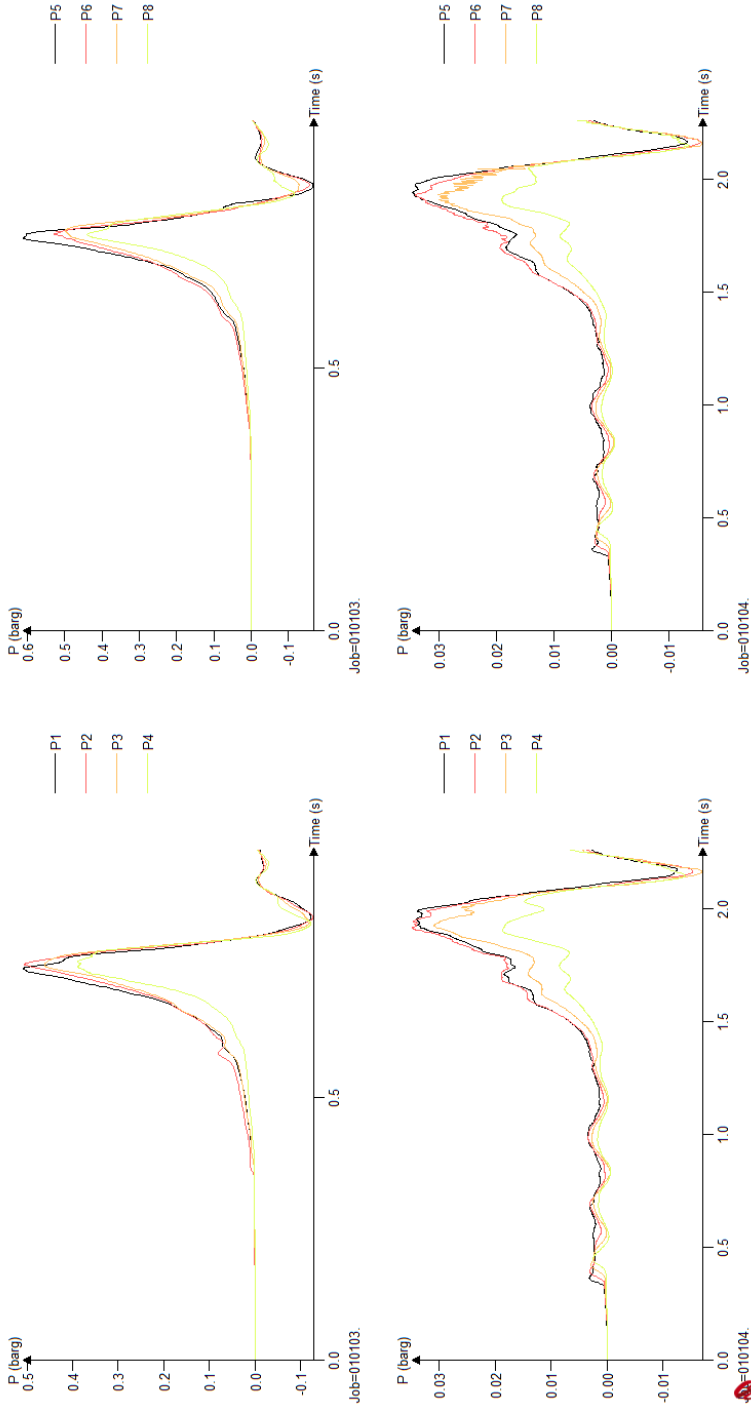


Figure C.2: Maximum pressures at Monitor Points 1-8 for the simplified geometry of the C Module for simulation cases 8 and 9 (See Simulation cases 6-10 in Table 5.2)

Detailed Geometry

The figures below are for simulation cases 11-15, where Job Number 010101, 010102, 010103, 010104 and 010100 refers to simulation cases 11, 12, 13, 14 and 15, respectively.

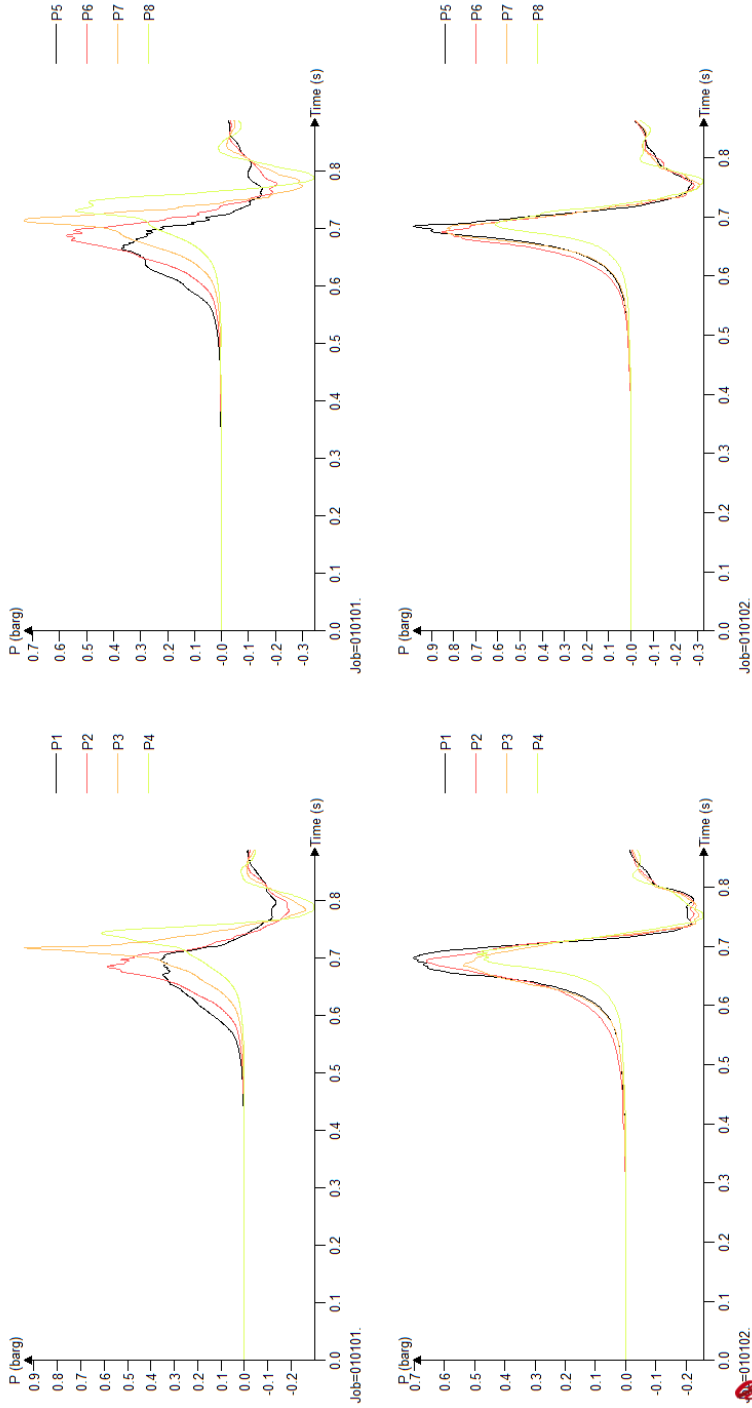


Figure C.3: Maximum pressures at Monitor Points 1-8 for the detailed geometry of the C Module for simulation cases 11 and 12 (See Simulation cases 11-15 in Table 5.2)

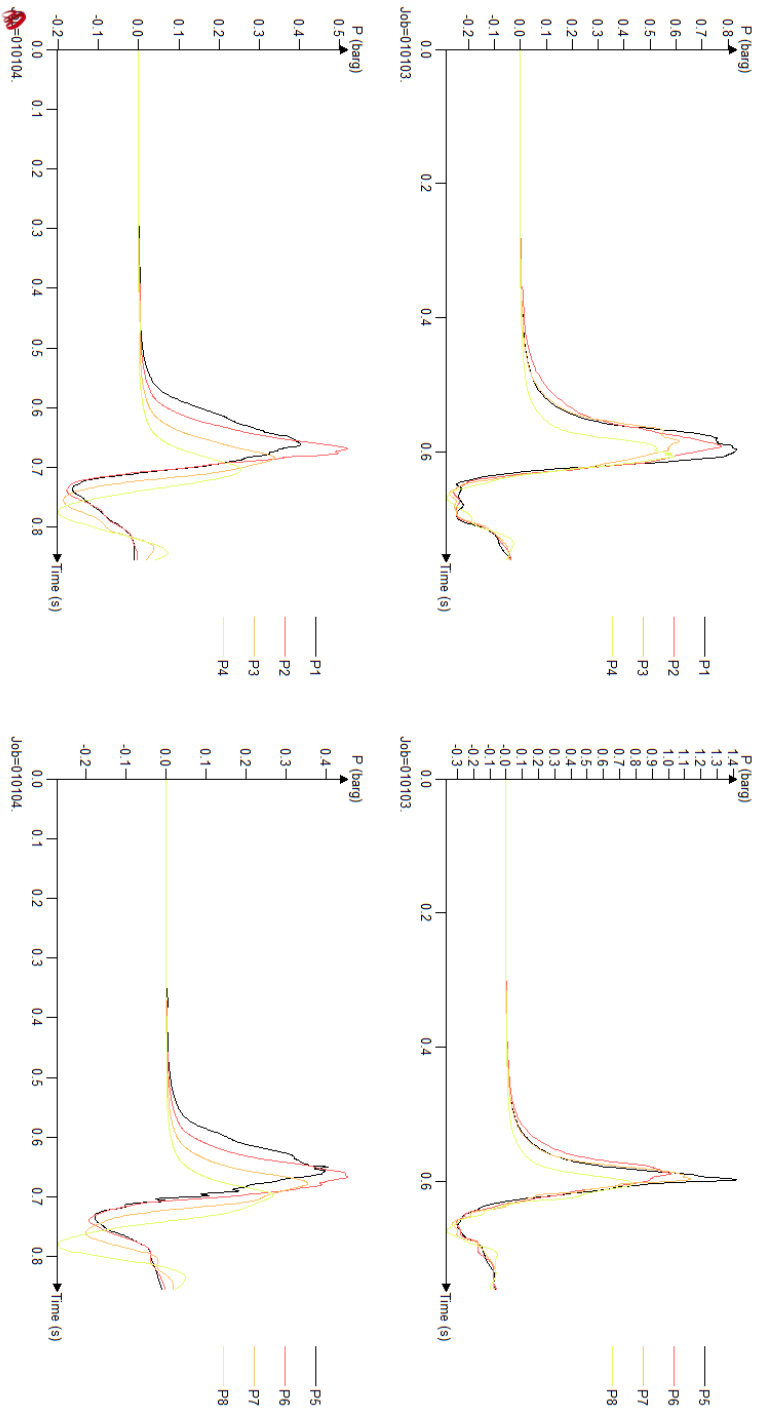


Figure C.4: Maximum pressures at Monitor Points 1-8 for the detailed geometry of the C Module for simulation cases 13 and 14 (See Simulation cases 11-15 in Table 5.2)

The entire platform

The figures below are for simulation cases 16-20, where Job Number 010101, 010102, 010103, 010104 and 010100 refers to simulation cases 16, 17, 18, 19 and 20, respectively.

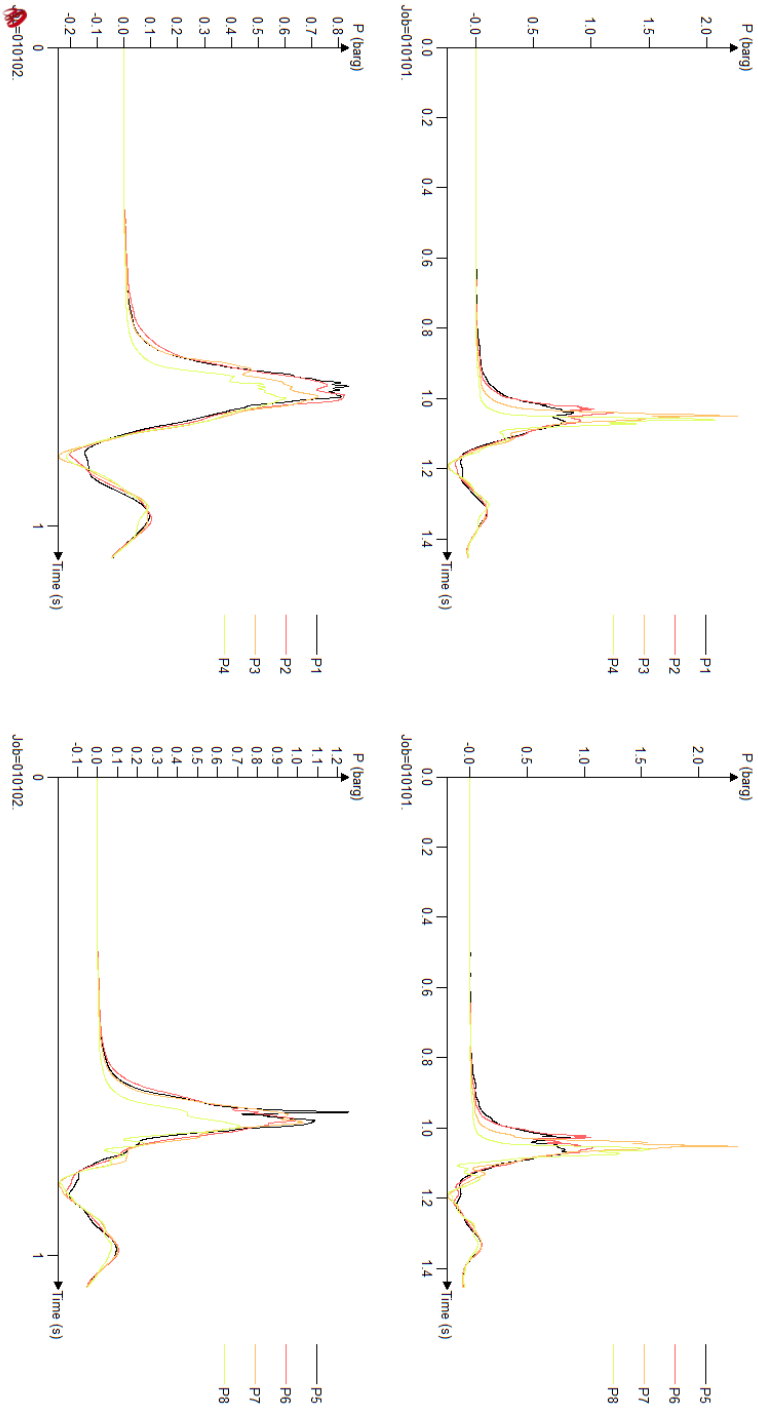


Figure C.5: Maximum pressures at Monitor Points 1-8 for the geometry of the whole platform for simulation cases 16 and 17 (See Simulation cases 16-20 in Table 5.2)

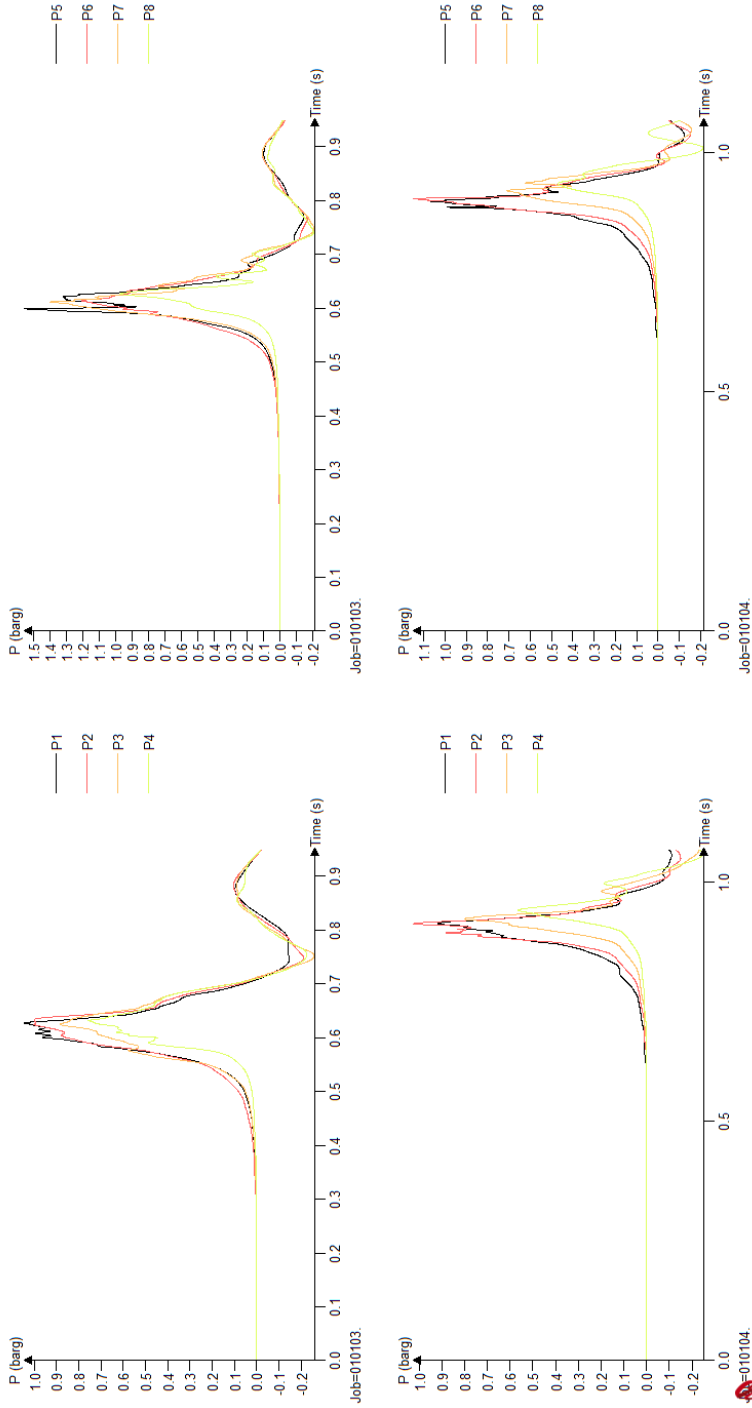


Figure C.6: Maximum pressures at Monitor Points 1-8 for the geometry of the whole platform for simulation cases 18 and 19 (See Simulation cases 16-20 in Table 5.2)

The new simulation cases

The figures below are for simulation cases 21-26, where Job Number 010701, 010702, 010705, 020701 and 020702 refers to simulation cases 21, 22, 23, 24 and 25, respectively. No ignition occurred for Job Number 020705 (Simulation case 26).

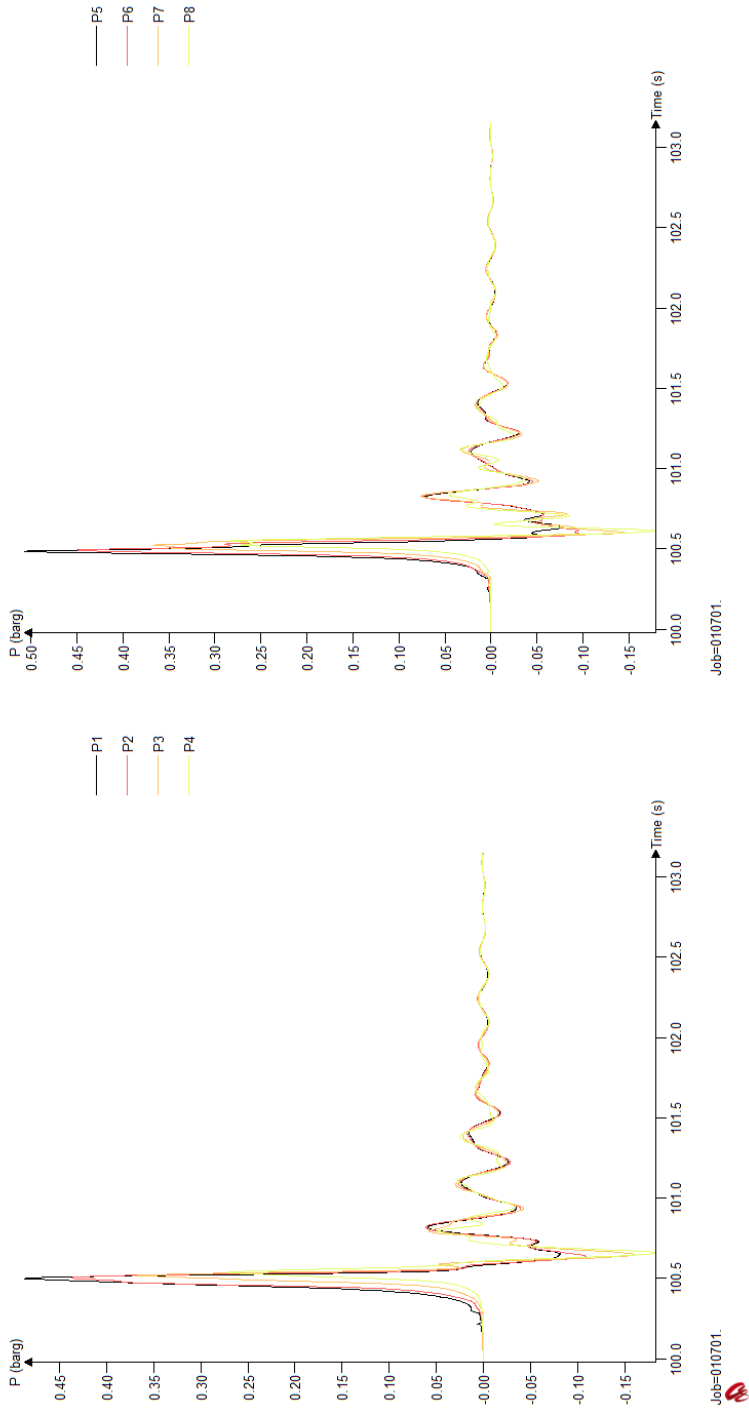


Figure C.7: Maximum pressures at Monitor Points 1-8 for simulation case 21 (Table 5.6).

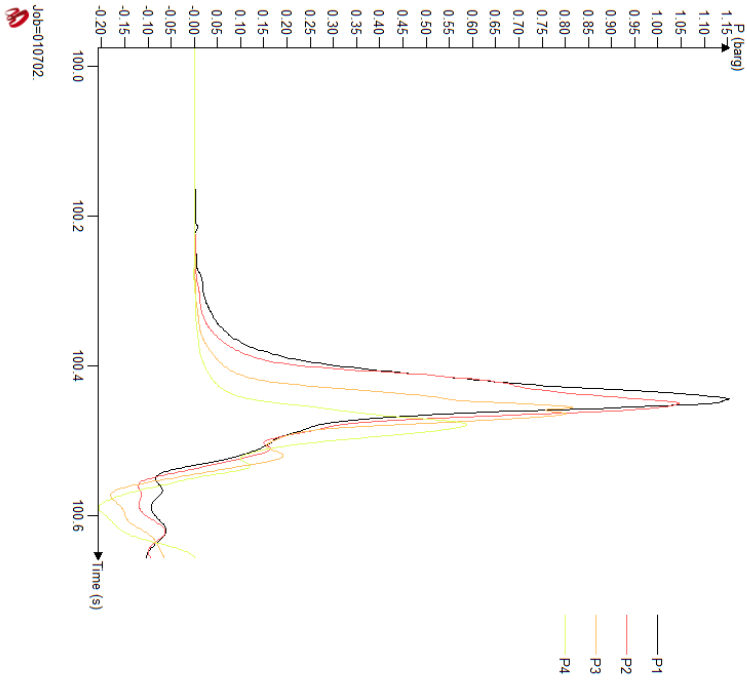
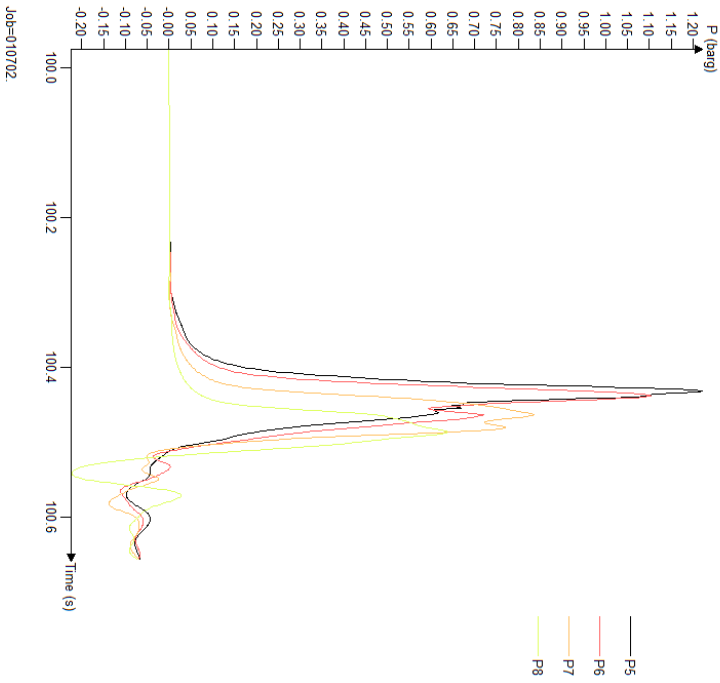


Figure C.8: Maximum pressures at Monitor Points 1-8 for simulation case 22 (Table 5.6).



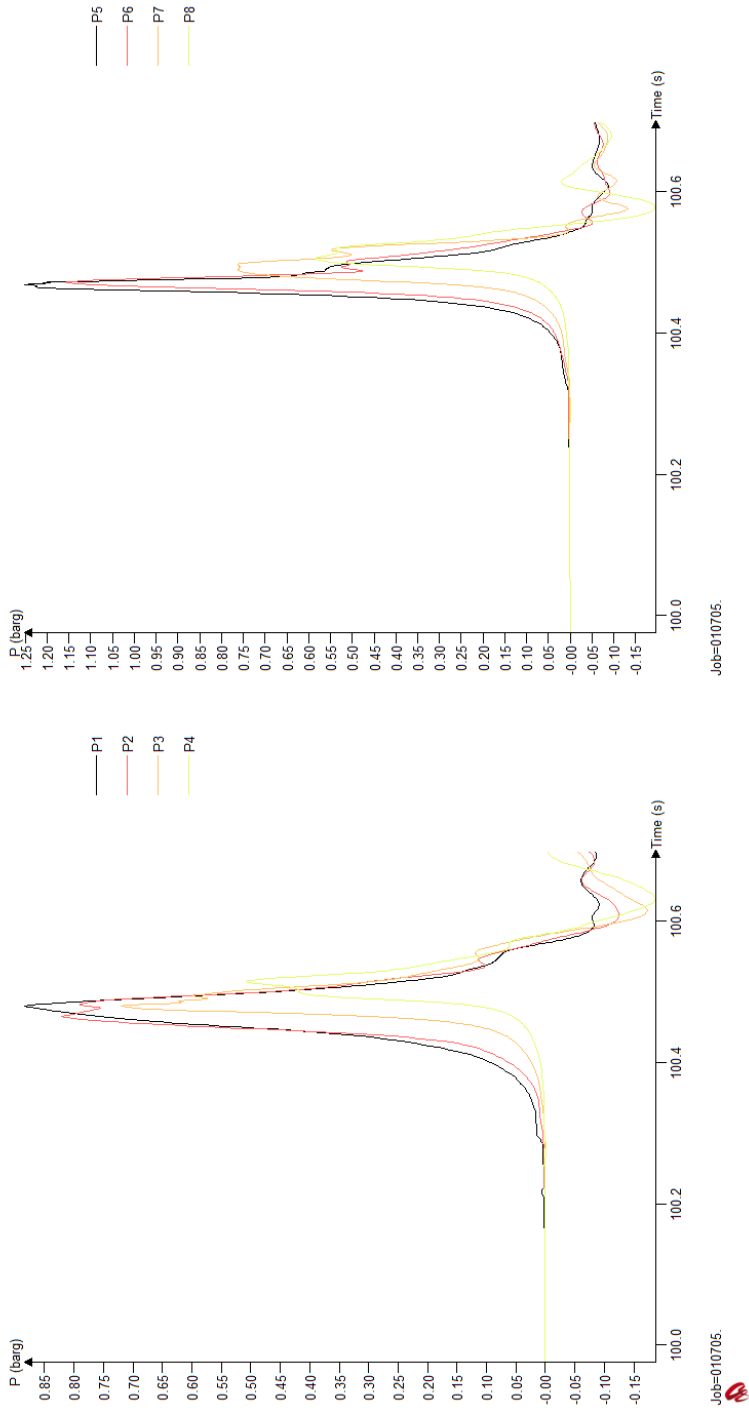


Figure C.9: Maximum pressures at Monitor Points 1-8 for simulation case 23 (Table 5.6).

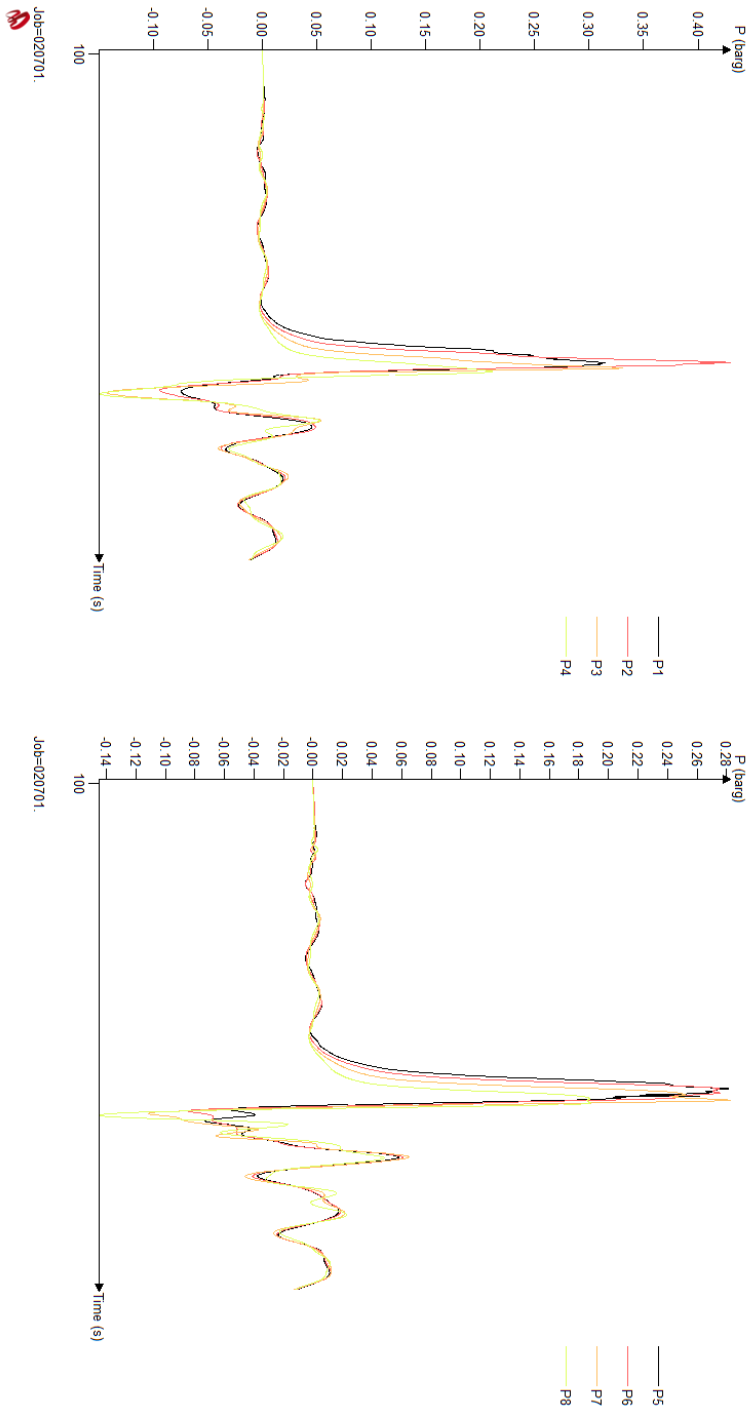


Figure C.10: Maximum pressures at Monitor Points 1-8 for simulation case 24 (Table 5.6).

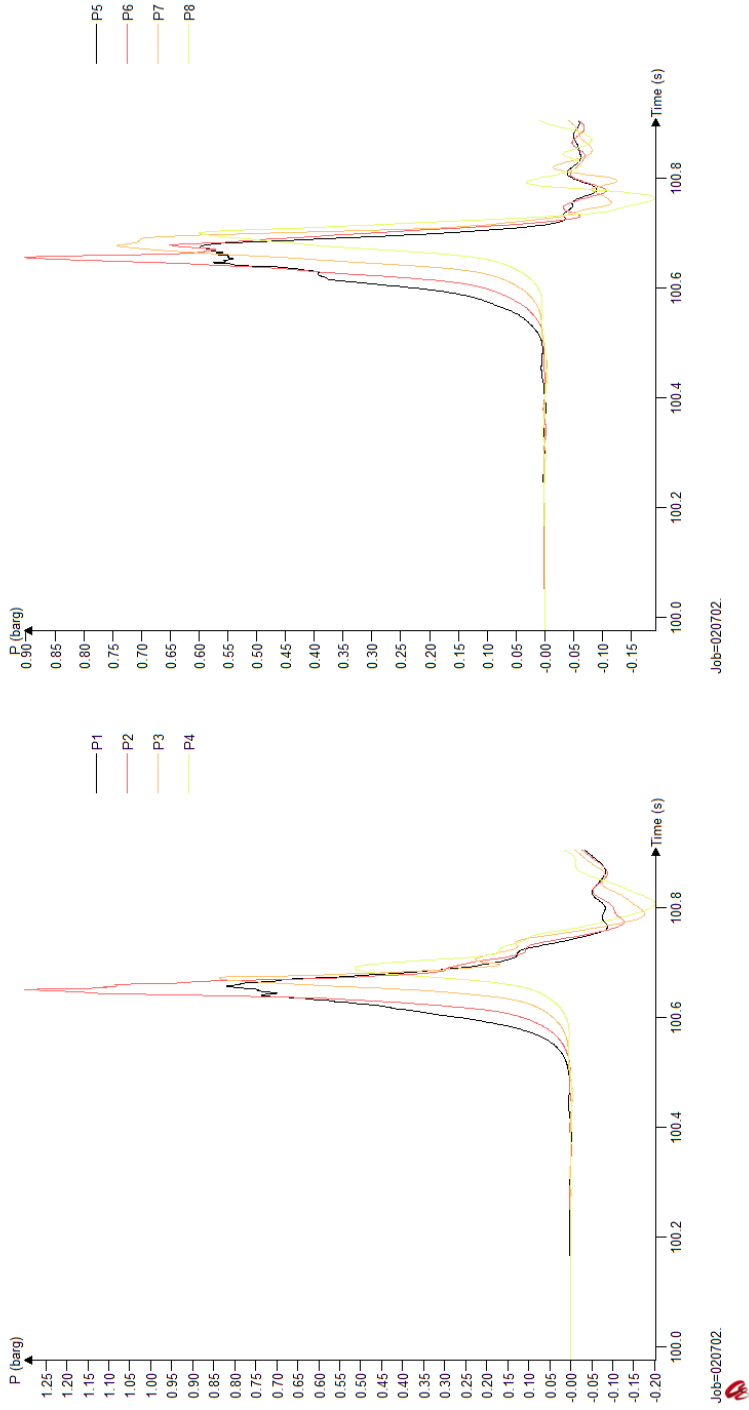


Figure C.11: Maximum pressures at Monitor Points 1-8 for simulation case 25 (Table 5.6).

C.2 Gas cloud sizes

C.2.1 Dispersion

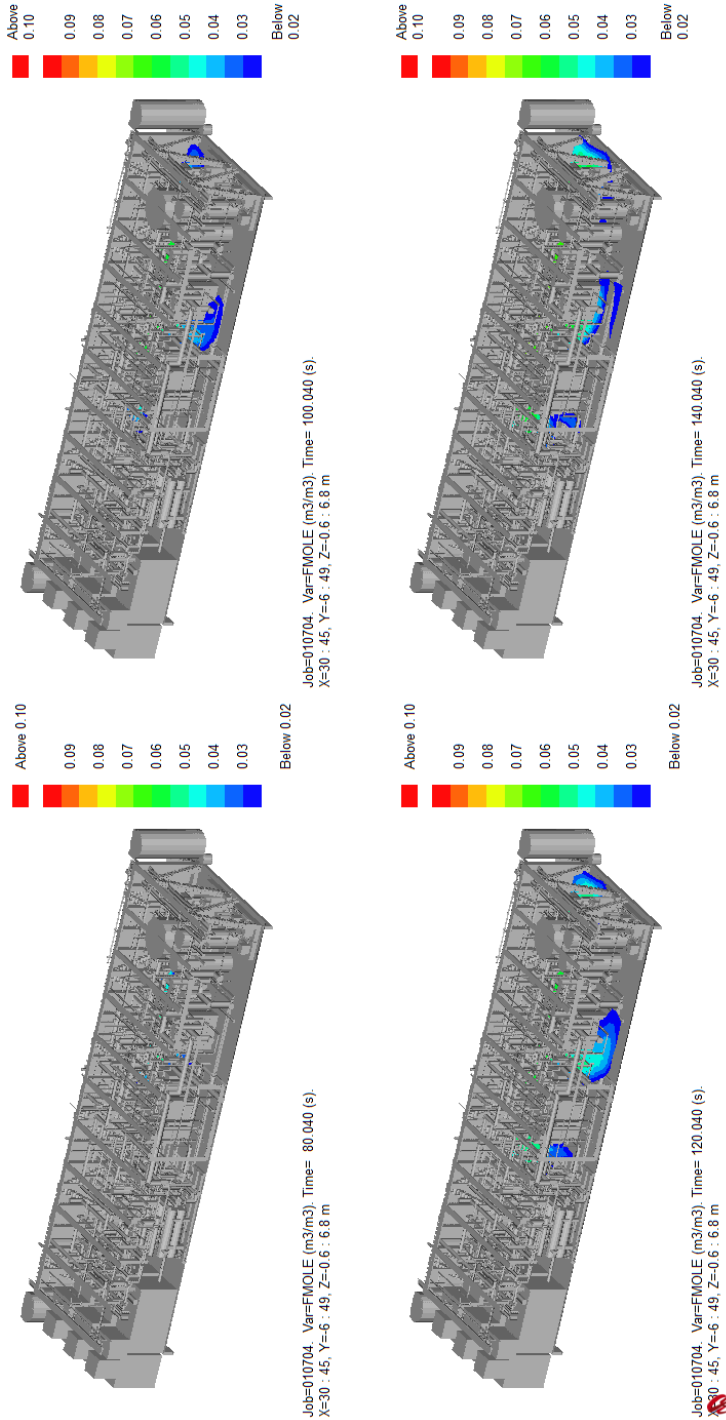


Figure C.12: The gas cloud generation for dispersion simulation case 010704 at 4 different time steps.

Flow pattern

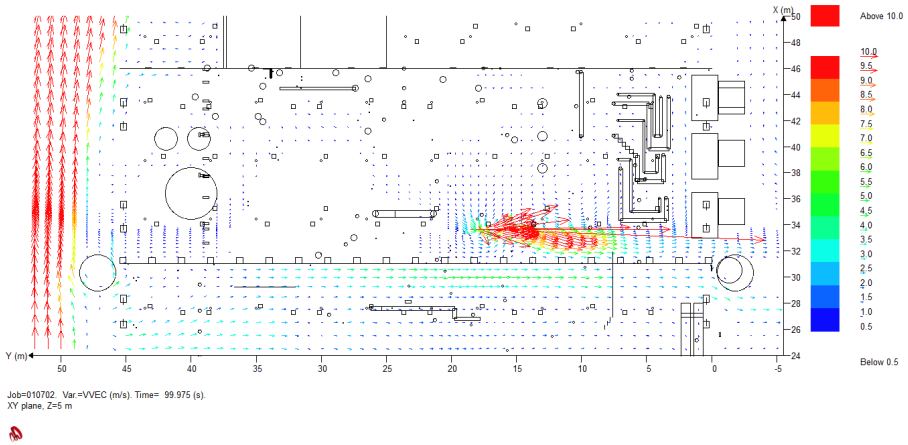


Figure C.13: Vector gradient for the leakage in simulation case 010702 after 40 seconds..

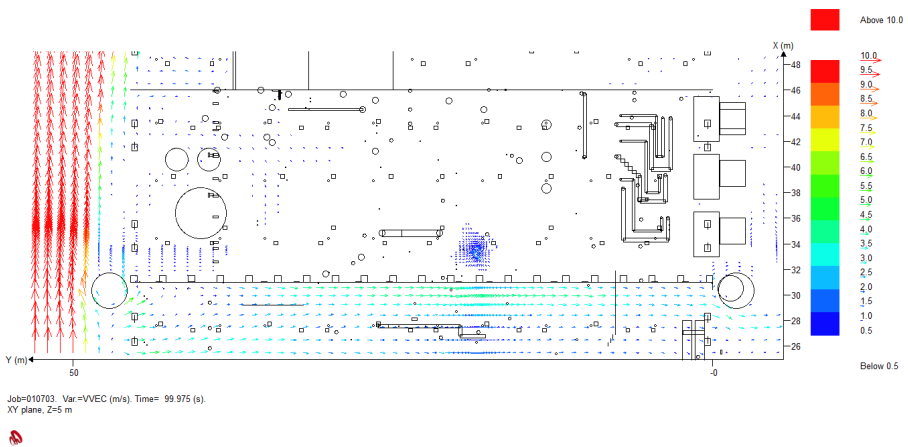


Figure C.14: Vector gradient for the leakage in simulation case 010703 after 40 seconds..

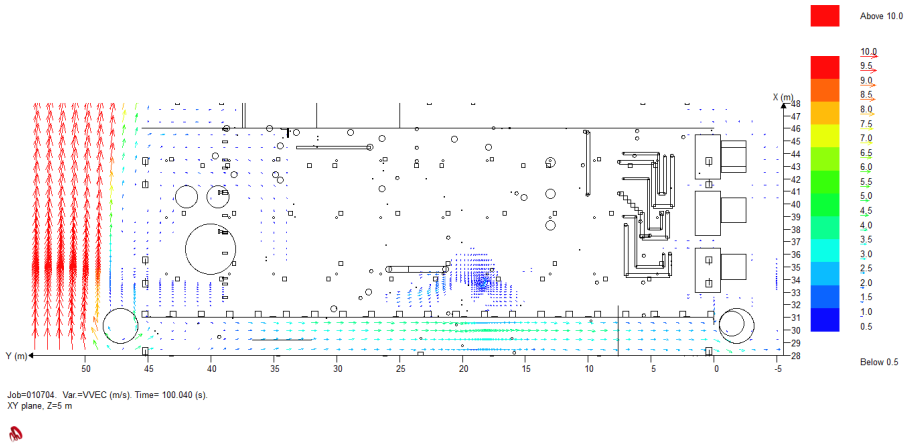


Figure C.15: *Vector gradient for the leakage in simulation case 010704 after 40 seconds..*

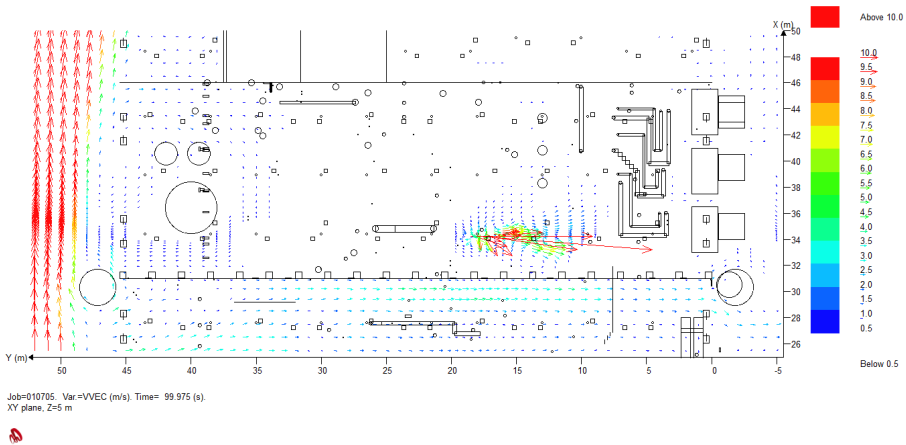


Figure C.16: *Vector gradient for the leakage in simulation case 010705 after 40 seconds..*

C.2.2 Explosion

The entire platform

The figures below are for simulation cases 16-20, where Job Number 010101, 010102, 010103, 010104 and 010100 refers to simulation cases 16, 17, 18, 19 and

20, respectively.

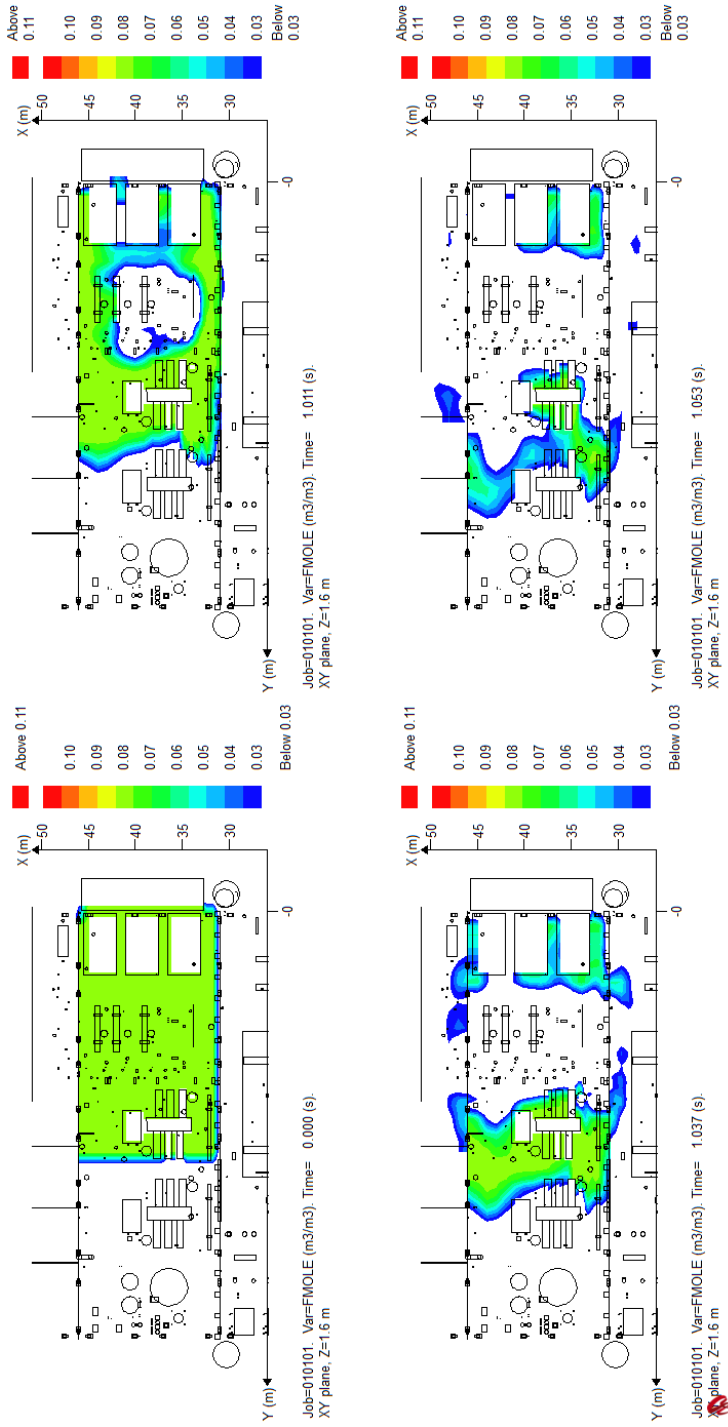


Figure C.17: Generated gas cloud at 4 different time steps for simulation case 16 (Table 5.2).

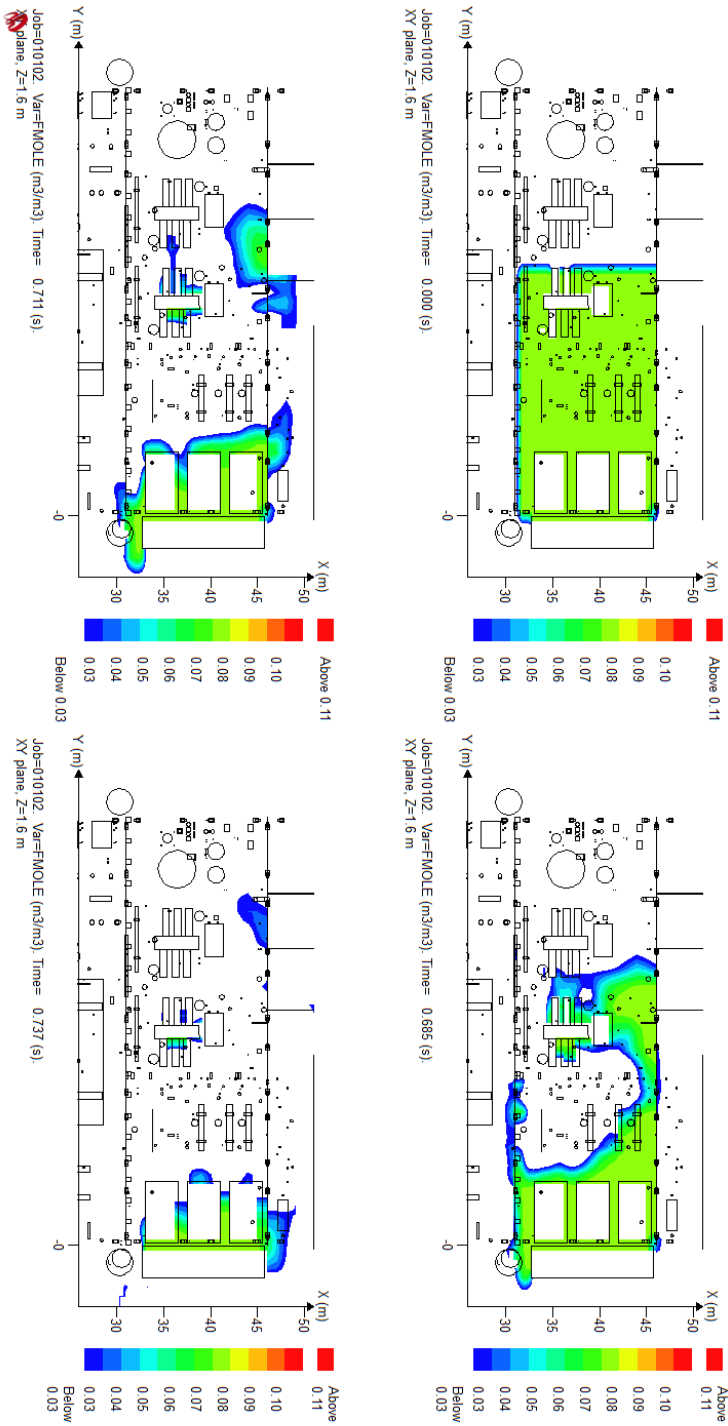


Figure C.18: Generated gas cloud at 4 different time steps for simulation case 16 (Table 5.2).

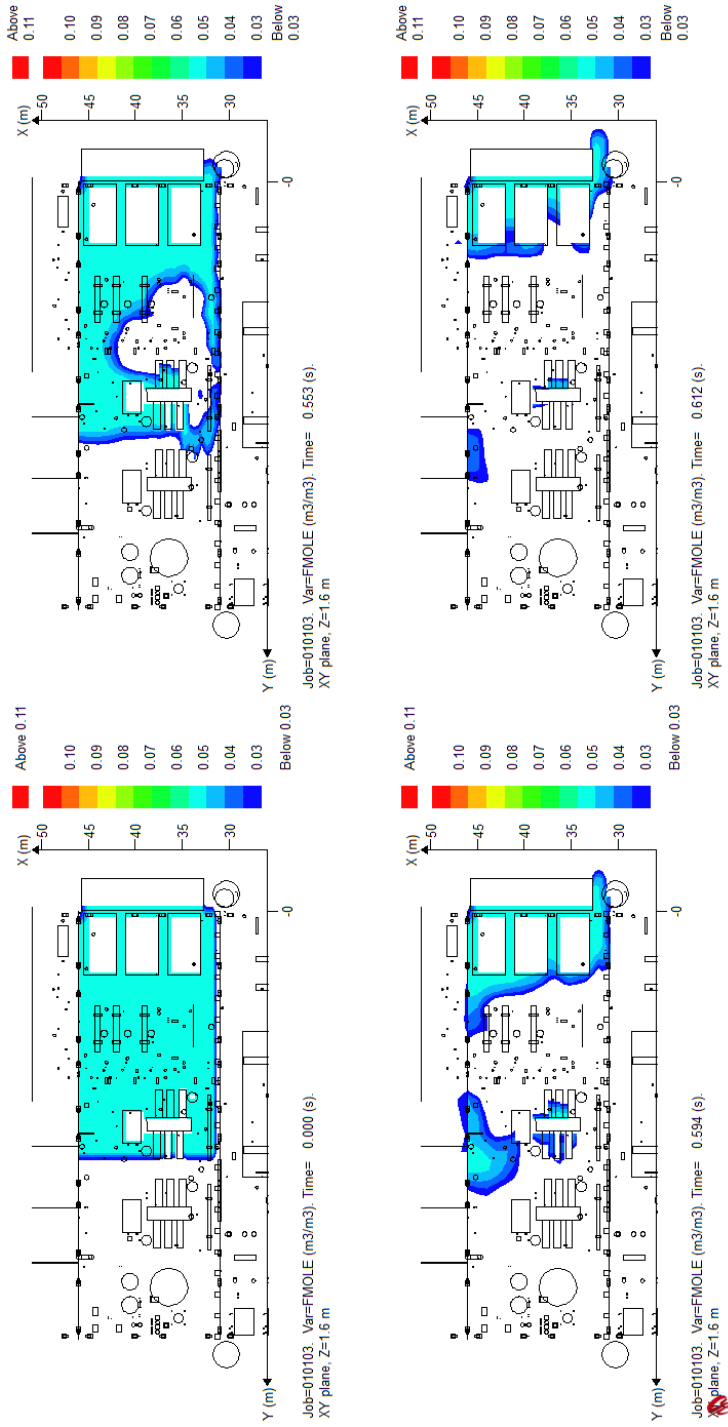


Figure C.19: Generated gas cloud at 4 different time steps for simulation case 18 (Table 5.2).

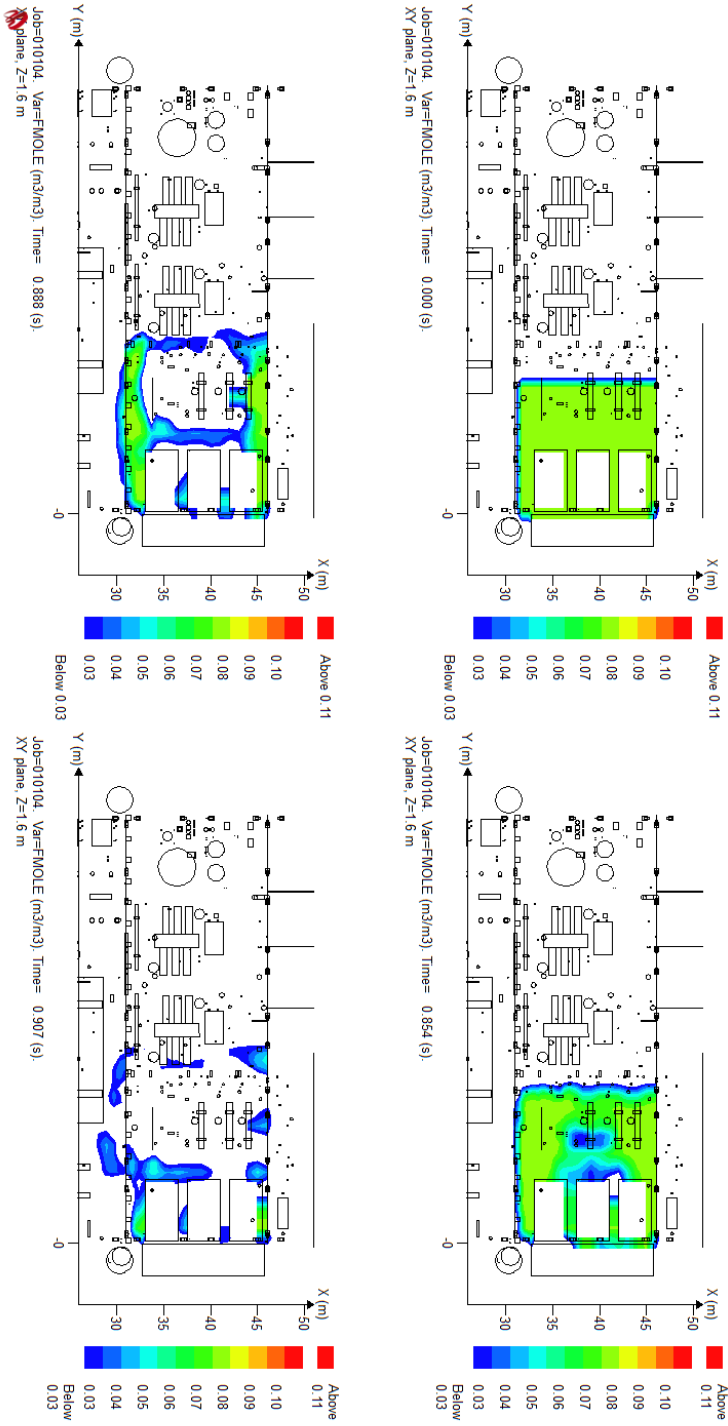


Figure C.20: Generated gas cloud at 4 different time steps for simulation case 19 (Table 5.2).

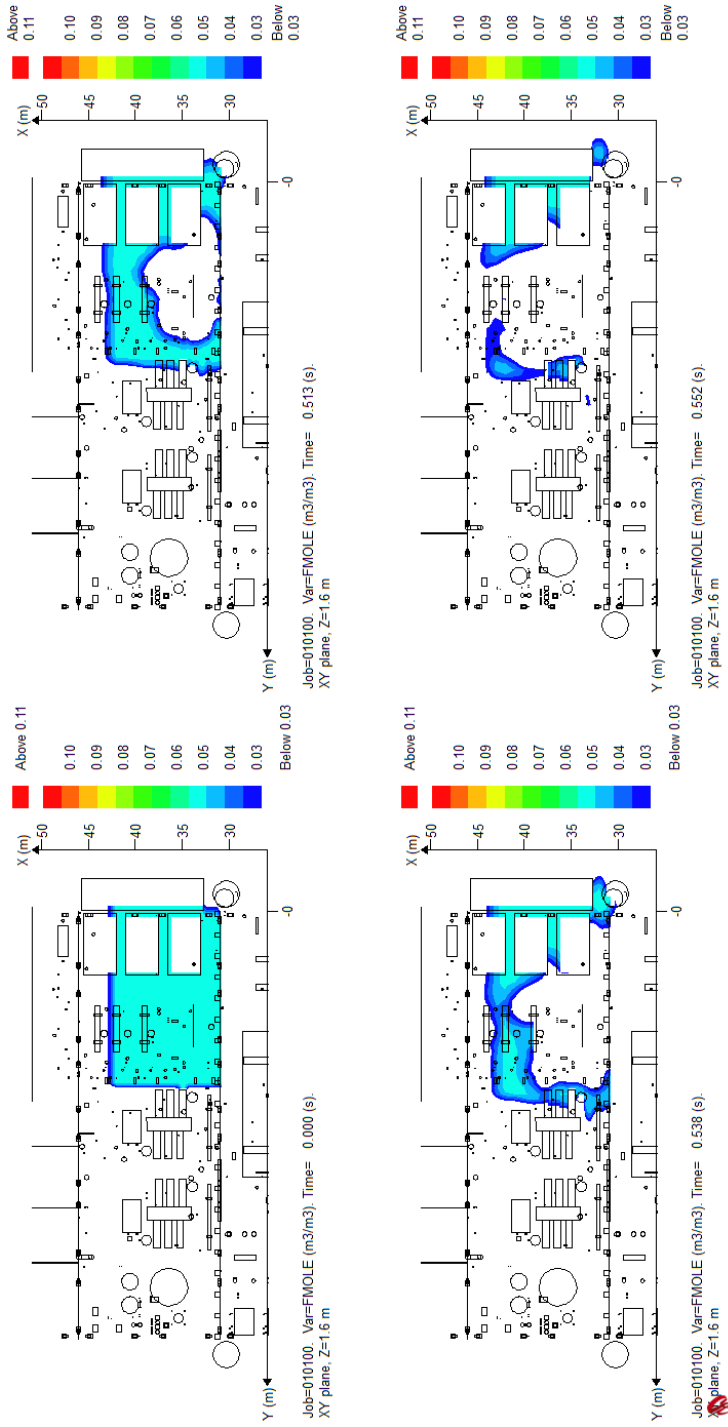


Figure C.21: Generated gas cloud at 4 different time steps for simulation case 20 (Table 5.2).

The new simulation cases

The figures below are for simulation cases 21-26, where Job Number 010701, 010702, 010705, 020701 and 020702 refers to simulation cases 21, 22, 23, 24 and 25, respectively. No ignition occurred for Job Number 020705 (Simulation case 26).

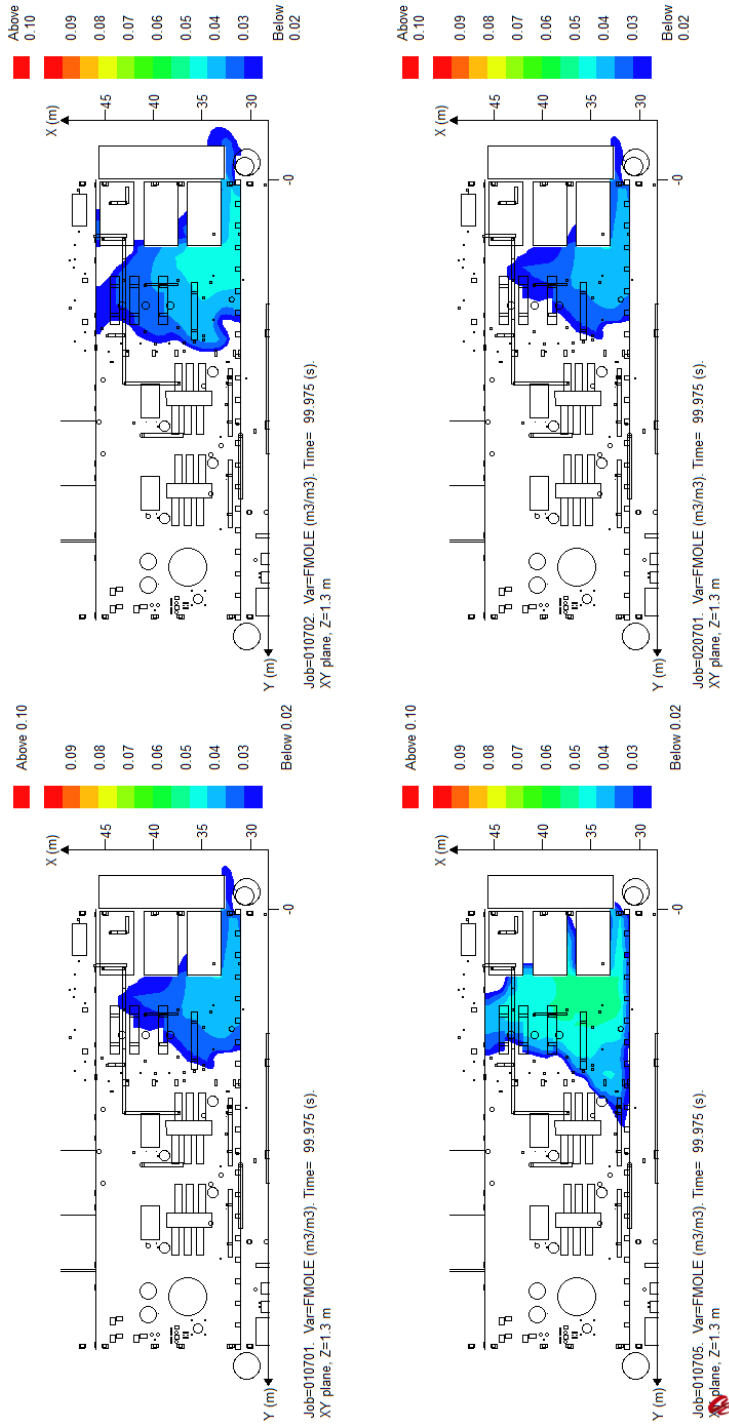


Figure C.22: Generated gas cloud at time of ignition for simulation cases 21-25 (Table 5.6).

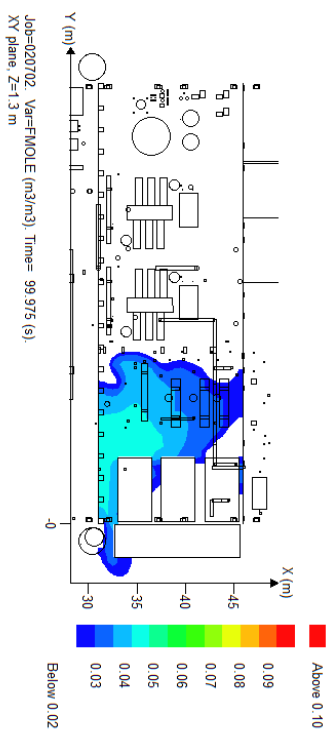


Figure C.23: Generated gas cloud at time of ignition for simulation cases 26 (Table 5.6).

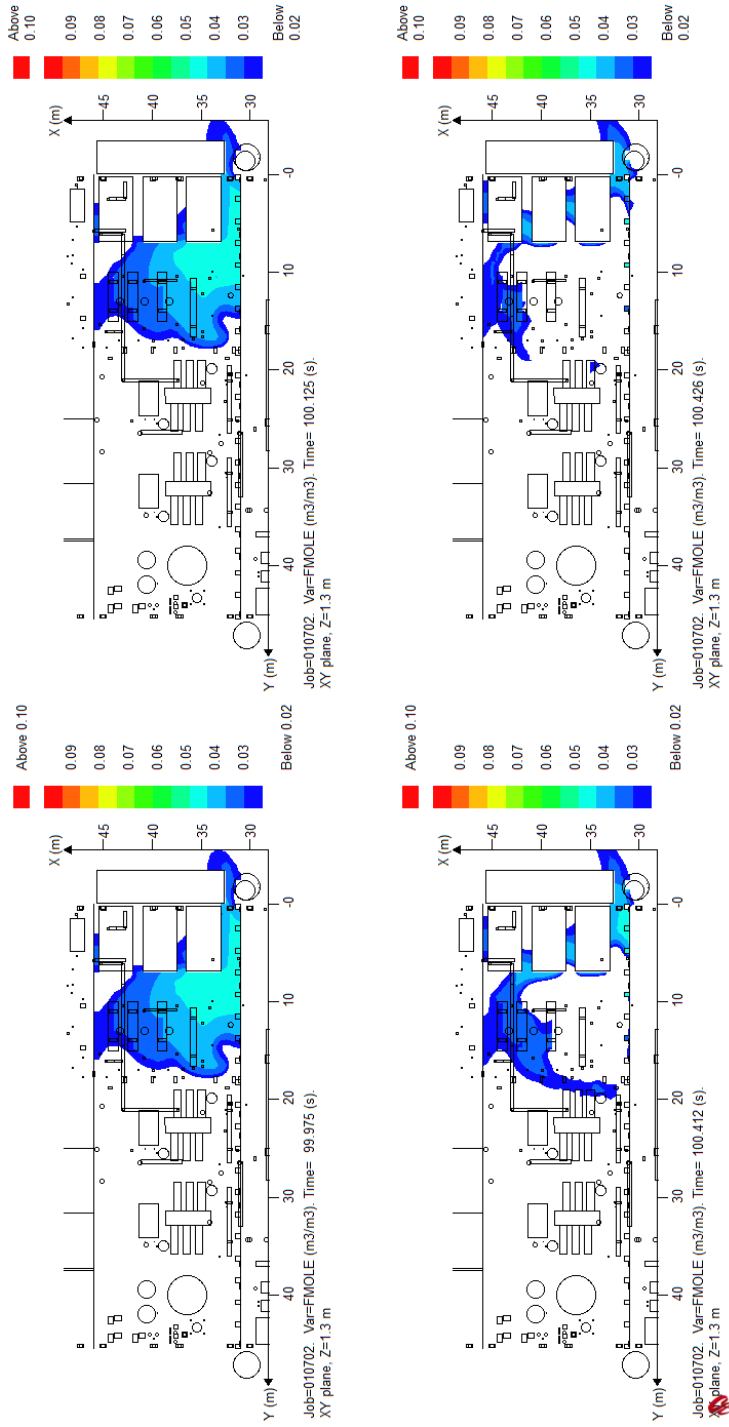


Figure C.24: Generated gas cloud at 4 different time steps for simulation case 22 (Table 5.6).

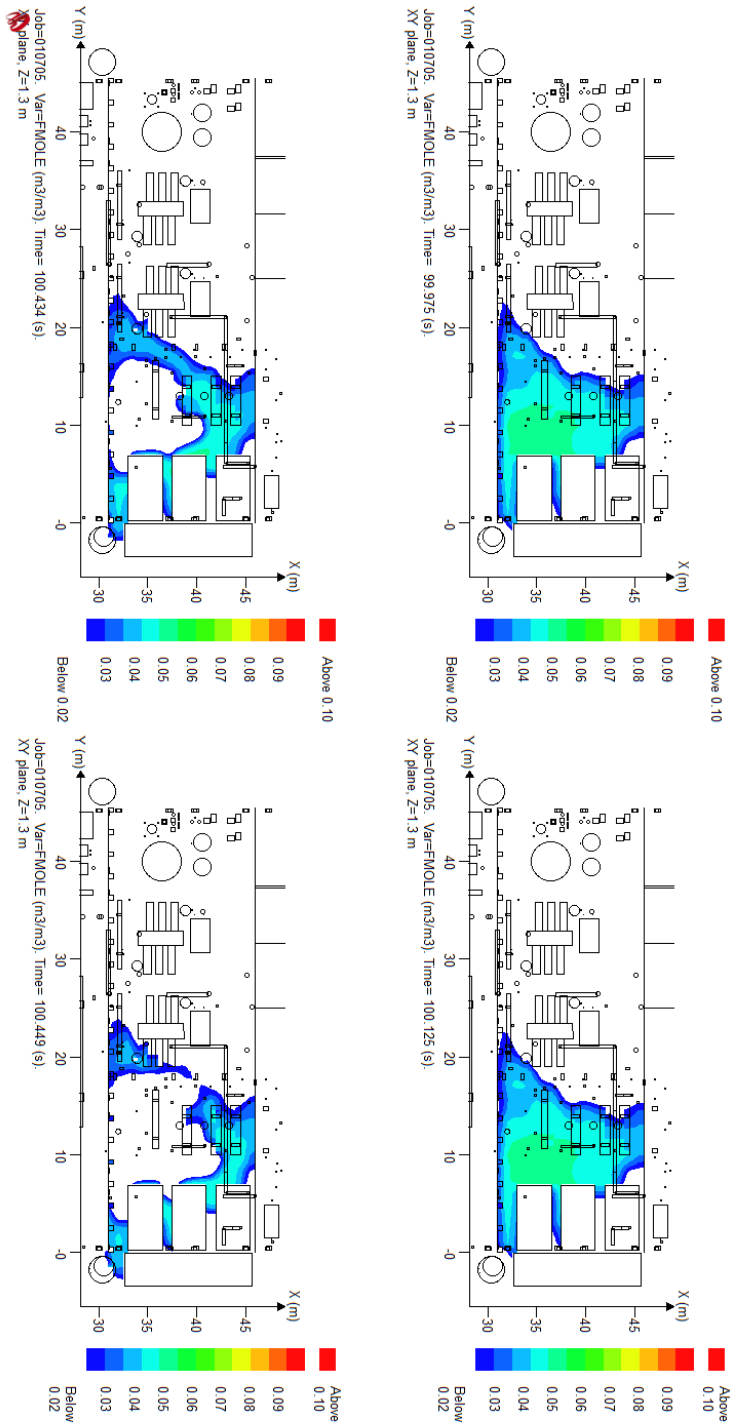


Figure C.25: Generated gas cloud at 4 different time steps for simulation case 23 (Table 5.6).

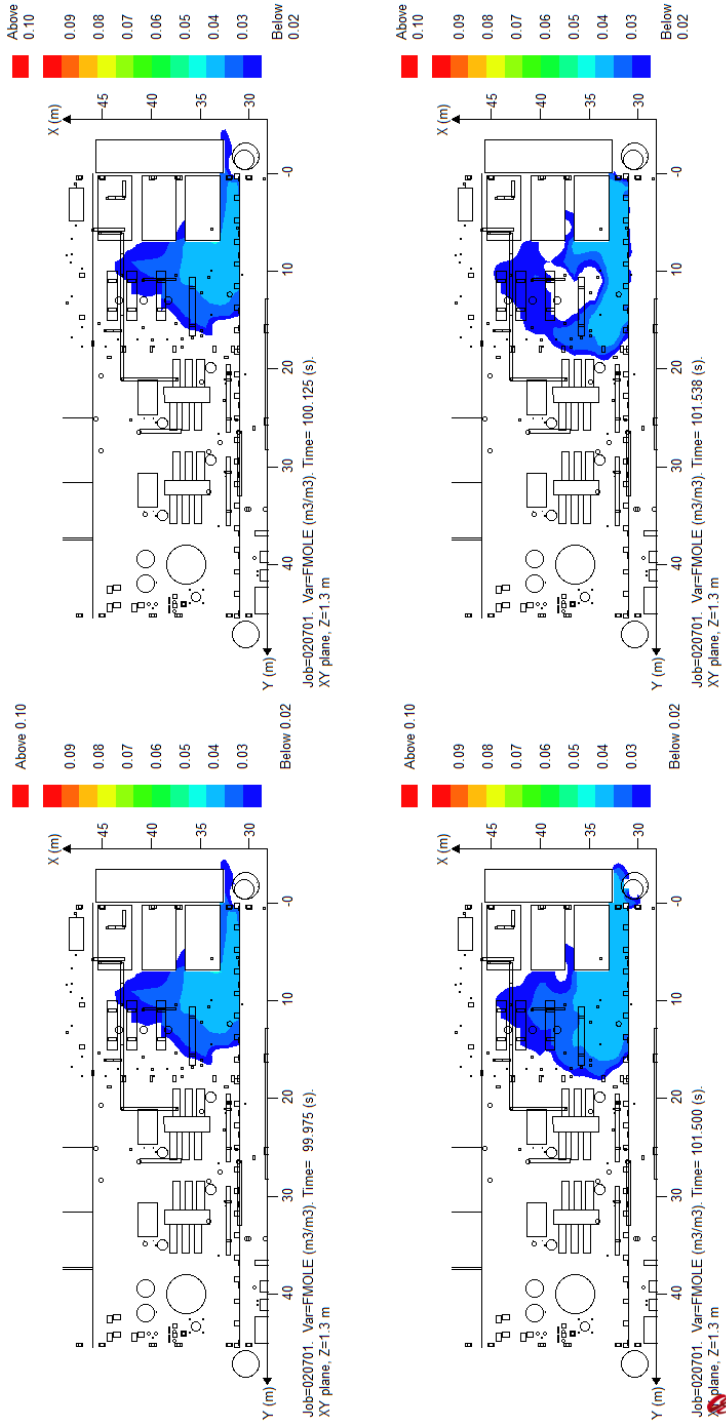


Figure C.26: Generated gas cloud at 4 different time steps for simulation case 24 (Table 5.6).

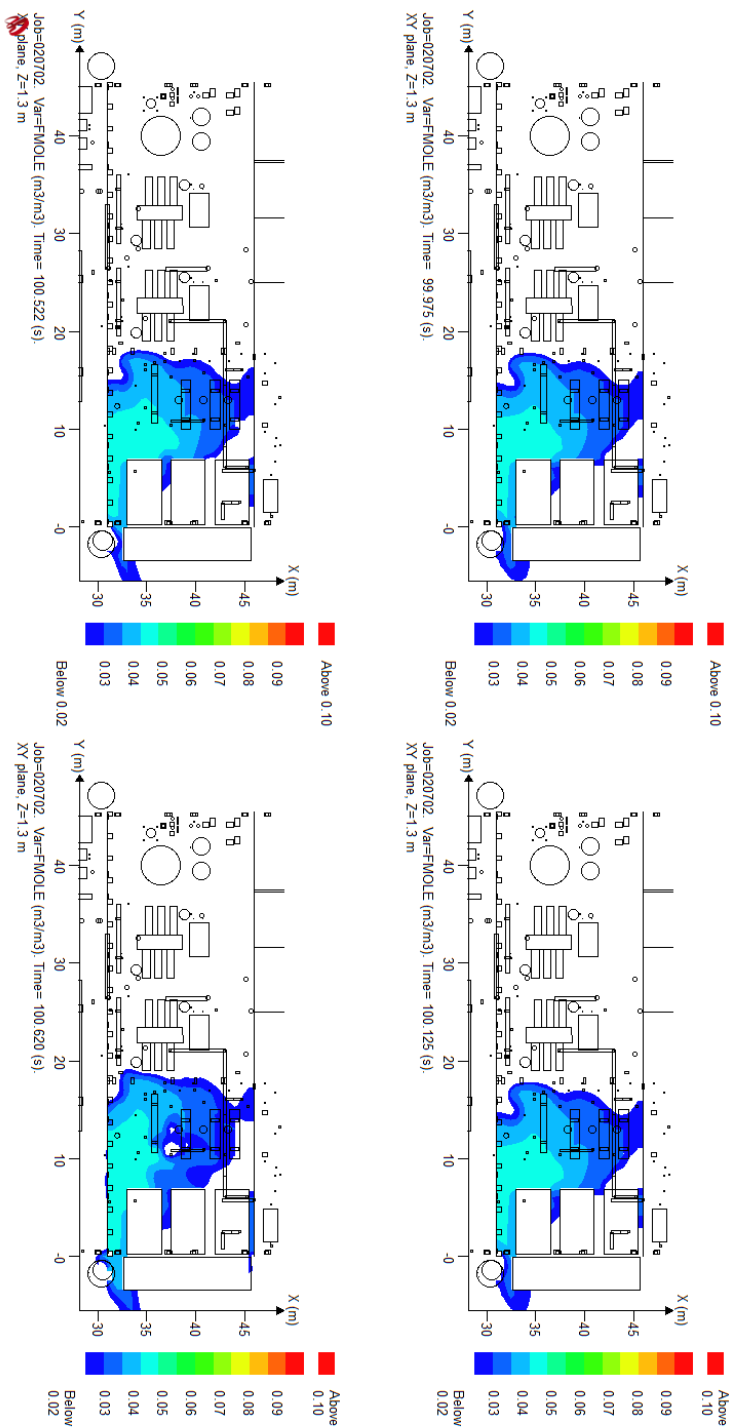


Figure C.27: Generated gas cloud at 4 different time steps for simulation case 25 (Table 5.6).

C.3 Gas detector readings

The figures below are for dispersion simulation cases (010701-010706).

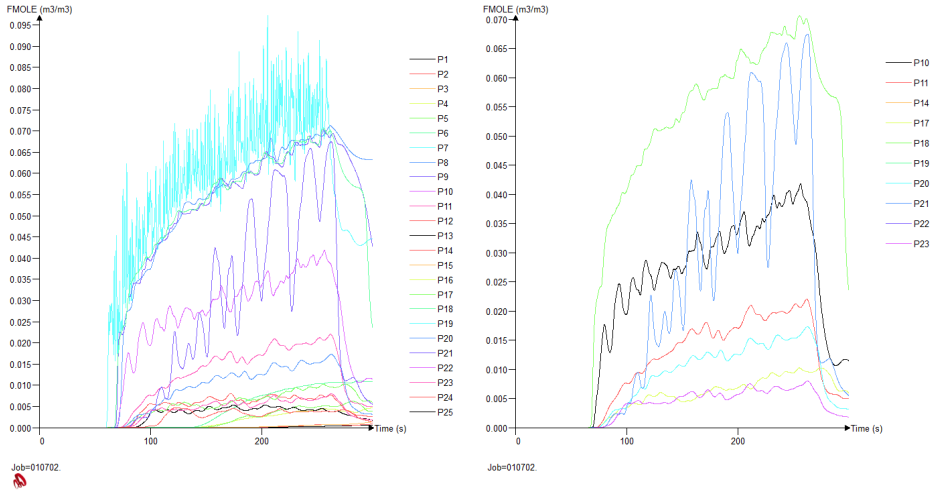


Figure C.28: *Simulation case 010702. Left side: Gas detector pattern for the alarms in the C Module, right side: Gas detector pattern for the alarms in zone C3.*

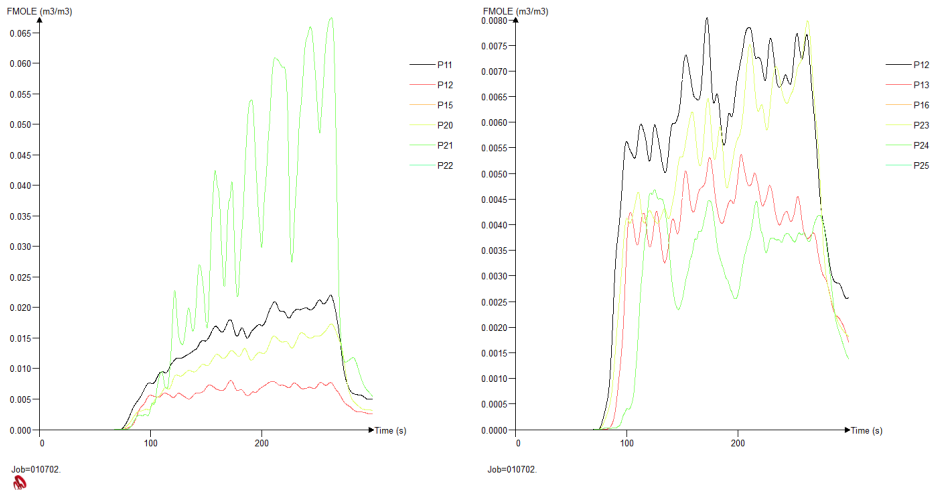


Figure C.29: *Simulation case 010702. Left side: Gas detector pattern for the alarms in zone C4, lower right side: Gas detector pattern for the alarms in zone C5.*

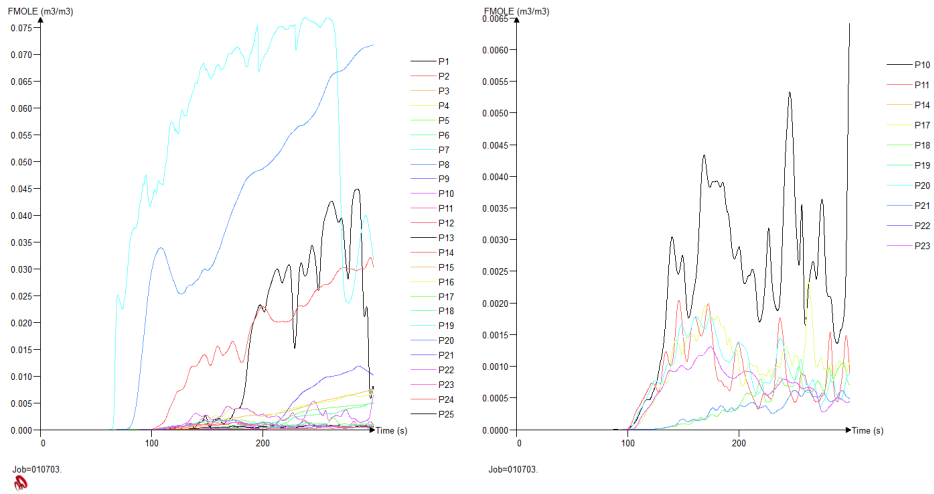


Figure C.30: *Simulation case 010703. Left side: Gas detector pattern for the alarms in the C Module, right side: Gas detector pattern for the alarms in zone C3.*

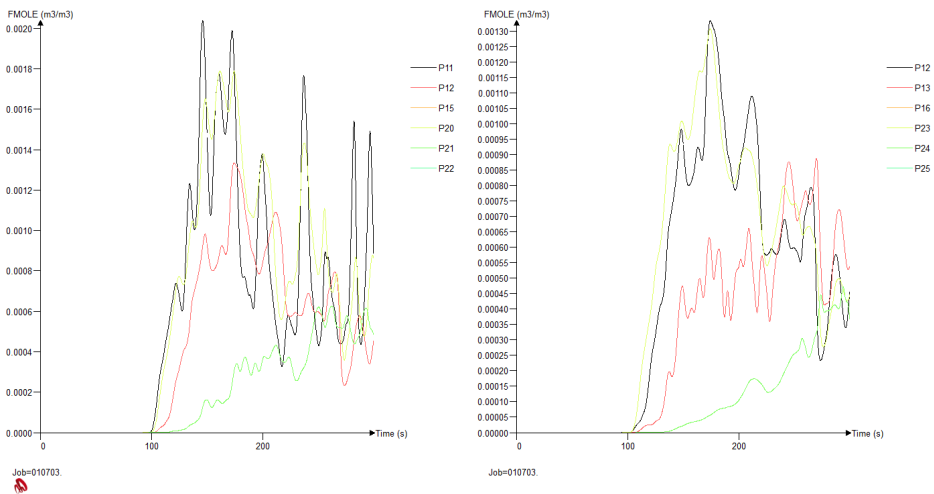


Figure C.31: *Simulation case 010703. Left side: Gas detector pattern for the alarms in zone C4, lower right side: Gas detector pattern for the alarms in zone C5.*

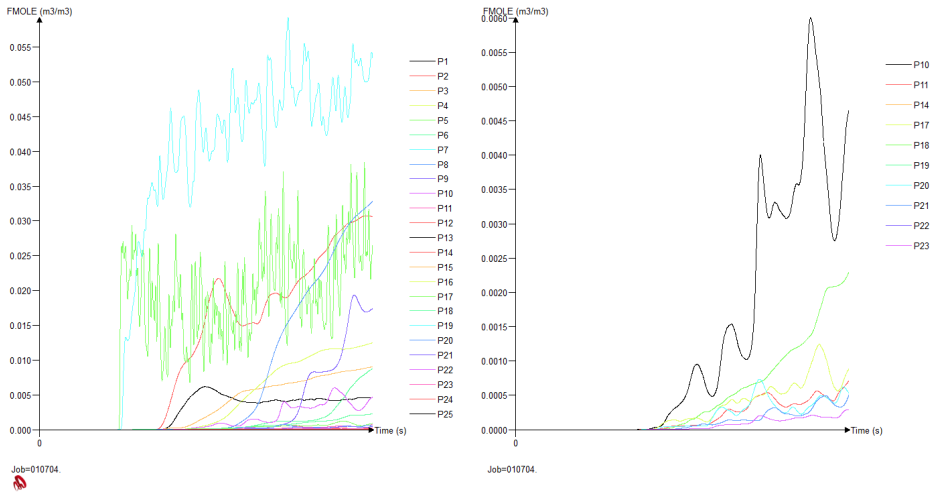


Figure C.32: *Simulation case 010704. Left side: Gas detector pattern for the alarms in the C Module, right side: Gas detector pattern for the alarms in zone C3.*

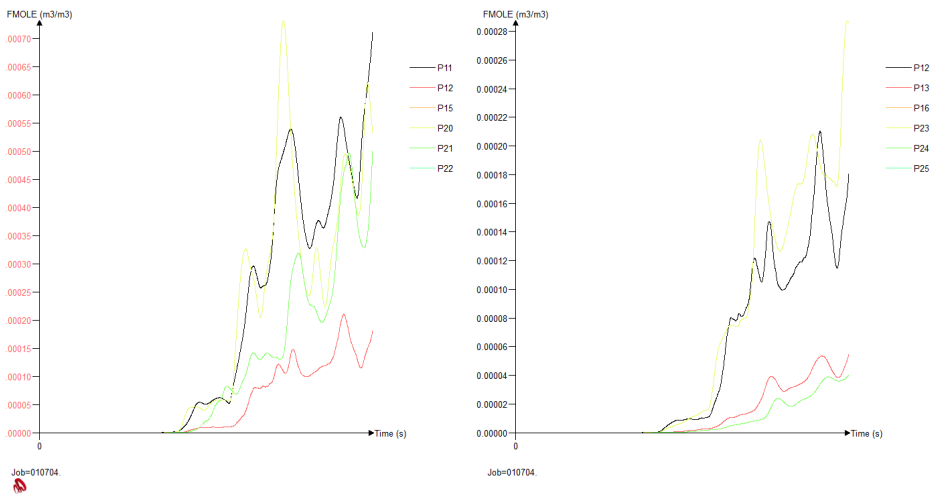


Figure C.33: *Simulation case 010704. Left side: Gas detector pattern for the alarms in zone C4, lower right side: Gas detector pattern for the alarms in zone C5.*

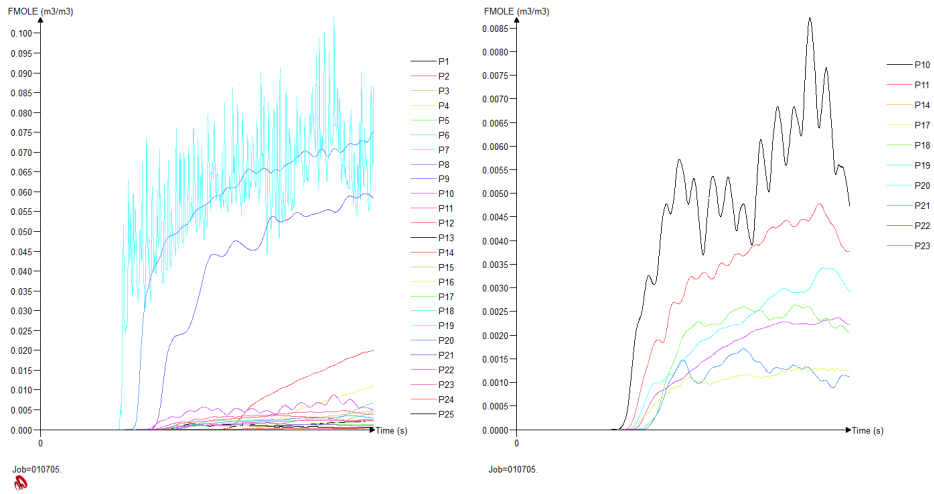


Figure C.34: *Simulation case 010705. Left side: Gas detector pattern for the alarms in the C Module, right side: Gas detector pattern for the alarms in zone C3.*

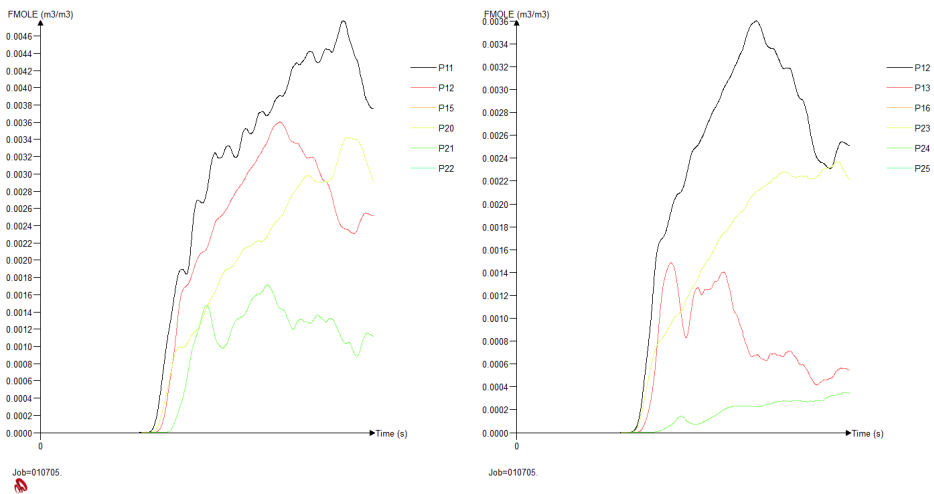


Figure C.35: *Simulation case 010705. Left side: Gas detector pattern for the alarms in zone C4, lower right side: Gas detector pattern for the alarms in zone C5.*

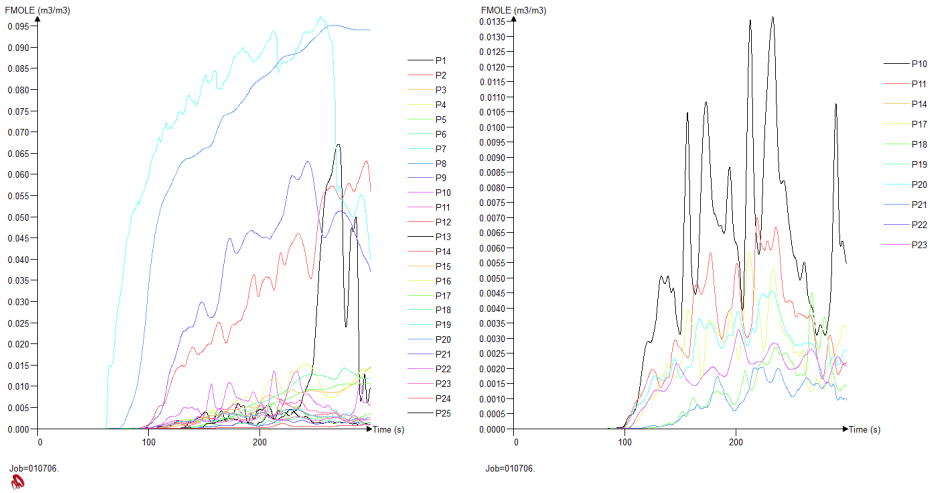


Figure C.36: *Simulation case 010706. Left side: Gas detector pattern for the alarms in the C Module, right side: Gas detector pattern for the alarms in zone C3.*

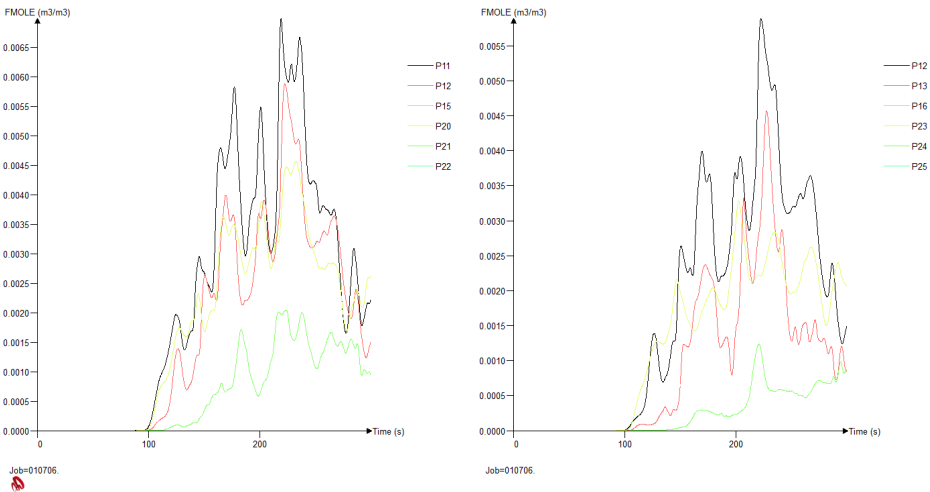


Figure C.37: *Simulation case 010706. Left side: Gas detector pattern for the alarms in zone C4, lower right side: Gas detector pattern for the alarms in zone C5.*

C.4 Firewalls

Simplified Geometry

The figures below are for simulation cases 6-9, where Job Number 010101, 010102, 010103 and 010104 refers to simulation cases 6, 7, 8 and 9, respectively.

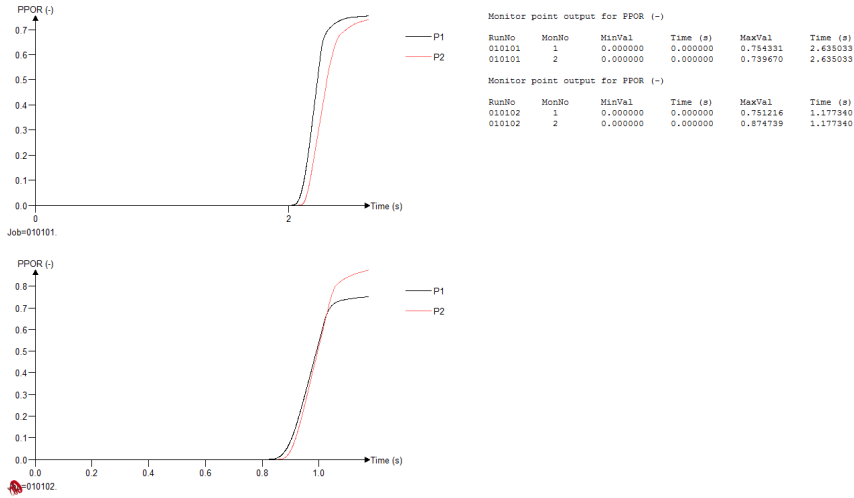


Figure C.38: Panel porosity for simulation cases 6 and 7.

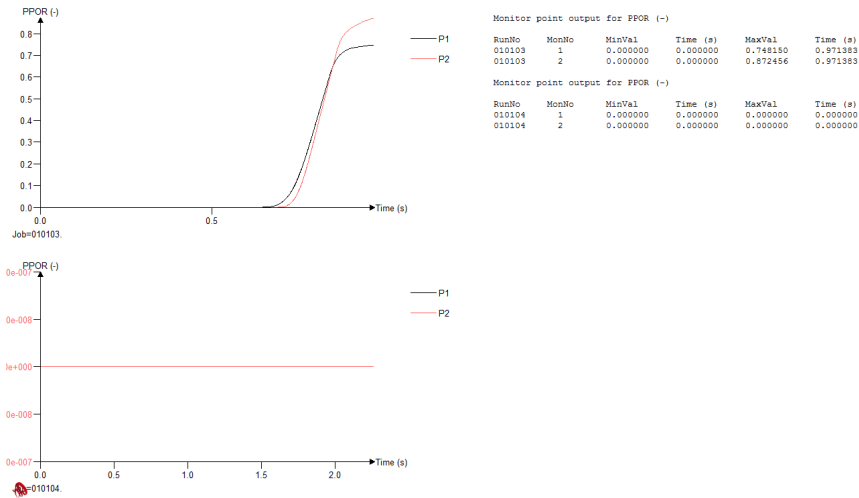


Figure C.39: Panel porosity for simulation cases 8 and 9.

Detailed Geometry

The figures below are for simulation cases 11-14, where Job Number 010101, 010102, 010103 and 010104 refers to simulation cases 11, 12, 13 and 14, respectively.

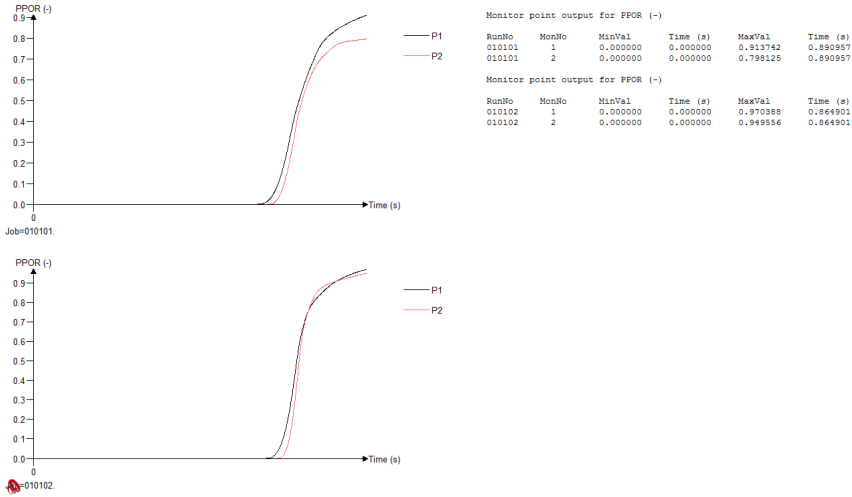


Figure C.40: Panel porosity for simulation cases 11 and 12.

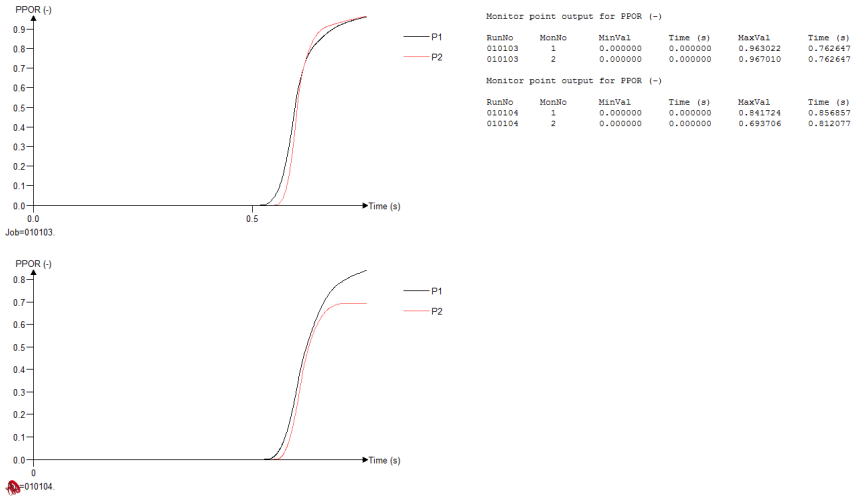


Figure C.41: Panel porosity for simulation cases 13 and 14.

The entire platform

The figures below are for simulation cases 16-19, where Job Number 010101, 010102, 010103 and 010104 refers to simulation cases 16, 17, 18 and 19, respectively.

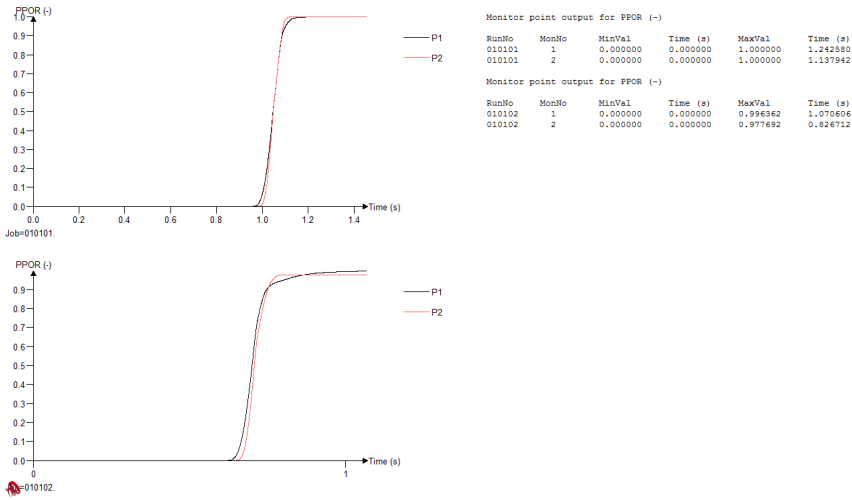


Figure C.42: Panel porosity for simulation cases 16 and 17.

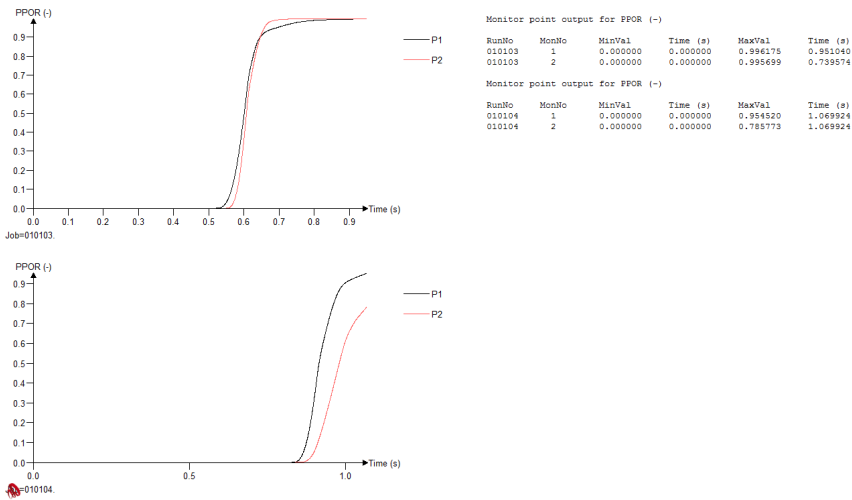


Figure C.43: Panel porosity for simulation cases 18 and 19.

The new simulation cases

The figures below are for simulation cases 21-26, where Job Number 010701, 010702, 010705, 020701 and 020702 refers to simulation cases 21, 22, 23, 24 and 25, respectively. No ignition occurred for Job Number 020705 (Simulation case 26).

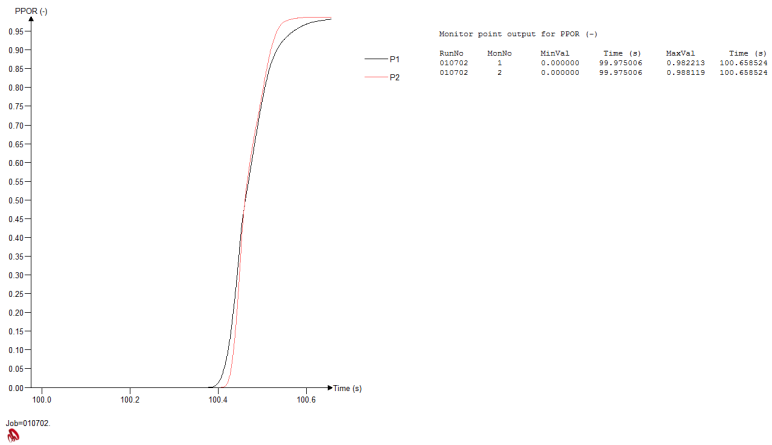


Figure C.44: Panel porosity for simulation case 22.

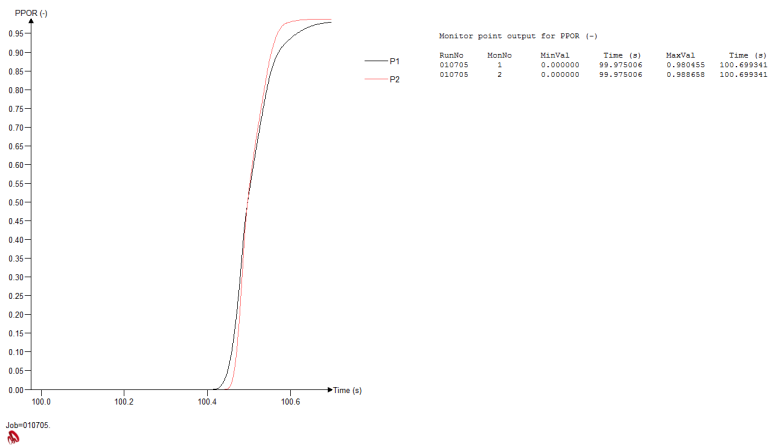


Figure C.45: Panel porosity for simulation case 23.

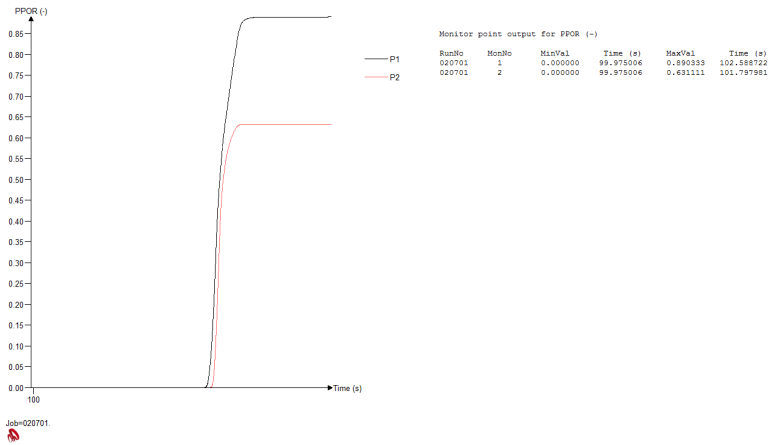


Figure C.46: Panel porosity for simulation case 24.

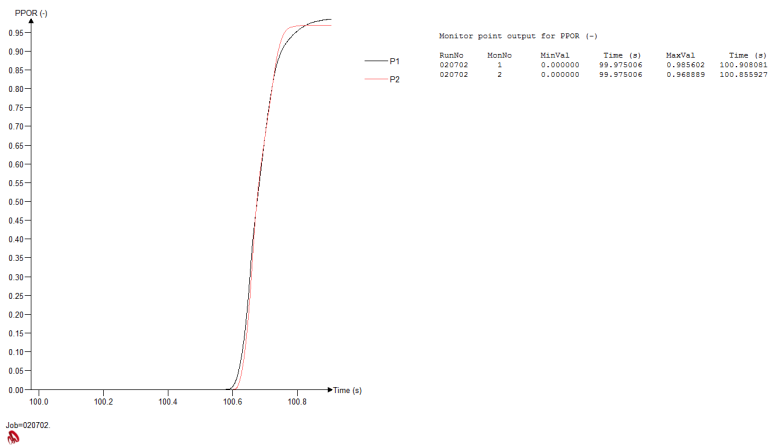


Figure C.47: Panel porosity for simulation case 25.

Bibliography

- [1] J.R. Bakke and I. Storvik. Simulation of gas explosions in module c, piper alpha. Technical report, Department of Science and Technology, CMR, November, 1988.
- [2] Idar Storvik and Jan Roar Bakke. Gas explosion simulation in piper-alpha module c using flacs. Technical report, Department of Science and Technology, CMR, September, 1989.
- [3] CMR GexCon. *FLACS v10.0 User's Manual*, January 2013.
- [4] Oil and Gas Offshore. Piper alpha platform. <http://oilandgasoffshore.wordpress.com/2012/04/05/piper-alpha-platform/>, June 7, 2013.
- [5] Seconds from Disaster. Explosion in the north sea: Piper alpha disaster. <http://secondsfromdisaster.net/s01e10-explosion-in-the-north-sea-piper-alpha-disaster/>, June 7, 2013.
- [6] Model Photographs of Piper Alpha, Unknown publisher.
- [7] Dag Bjerketvedt, Jan Roar Bakke, and Kees van Wingerden. *Gas Explosion Handbook, Version 1.2*. Gas Safety Programme 1990-1992, CMR, 1993.
- [8] The Hon Lord Cullen. *The Public Inquiry into the Piper Alpha Disaster*. November, 1990. Presented to Parliament by the Secretary of State for Energy by Command of Her Majesty.
- [9] Wikipedia. Wikipedia article about piper alpha. http://en.wikipedia.org/wiki/Piper_Alpha, May 16, 2013.
- [10] Jan Roar Bakke. Piper alpha gas explosion simulation. Technical report, Christian Michelsen Research, January, 1993.
- [11] Stephen McGinty. *Fire in the Night - The Piper Alpha Disaster*. Pan Books, June 2009.
- [12] Firebrand International Ltd. A critical review of post piper-alpha developments in explosion science for the offshore industry. Technical report, Prepared by Firebrand International Ltd for the Health and Safety Executive 2004. Research Report 89.

- [13] D. D. Drysdale and R. Sylvester-Evans. The explosion and fire on the piper alpha platform, 6 july 1988. a case study. *The Royal Society*, 1998. Printed in Great Britain.
- [14] M. Elisabeth Pate-Cornell. Learning from the piper alpha accident: A post-mortem analysis of technical and organizational factors. In *Risk Analysis*, volume Vol. 13. 1993.
- [15] M.R. Acton, P. Sutton, and M.J. Wickens. An investigation of the mitigation of gas cloud explosions by water sprays. In Institution of Chemical Engineers, editor, *Piper Alpha - Lessons for Life-Cycle Safety Management*, Symposium Series No. 122, September 1990.
- [16] Yut Art Film & Video. The piper alpha documentary part 1 of 2. A documentary produced by Yut Art in 2008 commemorating the 20th anniversary of the Piper Alpha oil rig disaster in the North Sea, 2008. <http://vimeo.com/43095882>, May 10, 2013.
- [17] Yut Art Film & Video. The piper alpha documentary part 2 of 2. A documentary produced by Yut Art in 2008 commemorating the 20th anniversary of the Piper Alpha oil rig disaster in the North Sea, month 2008. <http://vimeo.com/43097694>, May 10, 2013.
- [18] Joe Shepherd. Explosion dynamics laboratory. <http://www2.galcit.caltech.edu/EDL/projects/JetA/Glossary.html>, June 5, 2013.
- [19] Opinion of lord caplan, vol. 1. <http://www.scotcourts.gov.uk/opinions/Pipervol1.html>, May 10, 2013.
- [20] Opinion of lord caplan, vol. 2. <http://www.scotcourts.gov.uk/opinions/Pipervol2.html>, May 10, 2013.
- [21] Bjørn Johan Arntzen. *Modelling of Turbulence and Combustion for Simulation of Gas Explosions in Complex Geometries*. PhD thesis, NTNU, May 1998.
- [22] H.H. Pedersen, G.A.Enstad, T. Skjold, and R.W. Brewerton. The effect of vegetation with various degrees of foliage on gas explosions in a 1.5 m channel. In *Proc. of the Seventh International Seminar on Fire & Explosion Hazards (ISFEH7)*.
- [23] Kees van Wingerden, Magne Bjørkhaug, and Dag Bjerketvedt. Dispersion experiments in a 1:5 scale offshore module. Technical report, Christian Michelsen Research, Bergen, Norway.